1b 184

ANL-78-65
Part I

177
10-23-79

ANL-78-65
Part I

RADIOLOGICAL AND ENVIRONMENTAL RESEARCH DIVISION ANNUAL REPORT

Fundamental Molecular Physics and Chemistry

October 1977—September 1978

MASTER

ARGONNE NATIONAL LABORATORY, ARGONNE, ILLINOIS

Prepared for the U. S. DEPARTMENT OF ENERGY
under Contract W-31-109-Eng-38

DISTRIBUTION OF THIS DOCUMENT IS UNLIMITED

Distribution Category:
Biology and Medicine (UC-48)

ANL-78-65
Part I

ARGONNE NATIONAL LABORATORY
9700 South Cass Avenue
Argonne, Illinois 60439

RADIOLOGICAL AND ENVIRONMENTAL RESEARCH DIVISION ANNUAL REPORT

Fundamental Molecular Physics and Chemistry

October 1977 through September 1978

R. E. Rowland, Division Director
Mitio Inokuti, Section Head

DISCLAIMER

Preceding Report: ANL-77-65, Part I, October 1976–September 1977

FOREWORD

Following is the eighth Annual Report of our Section's work.

Scientifically, the work belongs to the chemical physics of atoms and molecules. More specifically, we work in three general subfields: electron interactions with molecules, photoabsorption in far and near vacuum ultraviolet regions and its consequences, and theories pertinent to these topics.

Programmatically, the work aims at several of the current DOE needs. First, we generage cross-section data for electron and photon interactions with molecules for the elucidation of radiation action on matter, including biological substances. In addition, we are developing theories that predict in detail the course of the earliest events of radiation action. All these efforts constitute a groundwork for the complete evaluation of the health effects of nuclear fission and fusion energy technologies. Second, we are studying the chemical physics of atmospheric-pollutant molecules (and related molecules) that emerge from coal and other non-nuclear energy technologies. These studies are supported by the Office of Environment, DOE. Third, some of our studies address themselves to the feasibility of fusion energy technologies; specifically, these studies concern spectral and collisional properties of highly stripped ions and their relations to plasma diagnostics and modeling. These studies are supported by the Office of Basic Energy Sciences, DOE. Finally, other of our studies concern basic aspects of the magnetohydrodynamic power-generation technology.

The articles in the present volume are loosely arranged according to the subject they treat. Papers 1–11 concern photoabsorption processes and their immediate consequences. Papers 12–15 concern interactions of high-energy electrons with atoms and molecules. Papers 16–30 concern theories of low-energy electron interactions with molecules and of molecular photoionization. Papers 31–41 concern experiments on interactions of low-energy electrons with atoms and molecules. Papers 42–47 concern basic radiation physics. Finally, papers 48–54 concern the theoretical physics of atoms and atomic ions, pertinent to fusion energy technology.

We take this opportunity to thank our many collaborators all around the world. Among them, U. Fano (University of Chicago) and W. R. Johnson (University of Notre Dame) hold Faculty Research appointments as Participants through Argonne Center for Educational Affairs. Others are appointed as our official consultants; they are P. D. Burrow (University of Nebraska), J. P. Desclaux (Centre d'Etudes Nucleaires de Grenoble), D. Dill (Boston University), D. A. Douthat (Kennedy-King College), J. H. Macek (University of Nebraska), S. T. Manson (Georgia State University), C. J. Roothaan (University of Chicago) and S. Tani (Marquette University). We than them all for providing valuable ideas and information and hope that they will feel it worthwhile to work with us for years to come.

It is also a pleasure to announce a new staff appointment: Michael A.Dillon from Carnegie-Mellon University, where he was an associate of Professor Edwin N. Lassettre. Dr. Dillon came to join us in April 1978 and took charge of an electron-collision program, which had been conducted by Russell H. Huebner. Dr. Huebner left us to become the Coordinator of Biomedical and Environmental Programs under Dr. W. K. Sinclair, Associate Laboratory Director.

We have participated in many scientific affairs besides the normal work in the Laboratory. Some examples may be mentioned here: We hosted the Workshop on Electron Degradation in Matter, November 1977, which was attended by some forty experts. Also, we have been working for the Radiation Research Society in many functions, including those of Inokuti as an Associate Editor and a Councilor. In addition, we have been working with the International Commission on Radiation Units and Measurements. Further, a report on the W value resulting from the work is forthcoming; and another report, this time on stopping powers, is now being written.

Mitio Inokuti

TABLE OF CONTENTS

Fundamental Molecular Physics and Chemistry

MOLECULAR PROPERTIES OF GAS PHASE CLUSTERS — A MICROSCOPIC APPROACH TO THE STUDY OF NUCLEATION — A NEW EXPERIMENTAL PROGRAM

P. M. Dehmer

A new experimental program has been introduced to study the physical properties and the chemical reactions of atmospheric constituents, with emphasis on the role of pollutants arising from the use of fossil fuels. Special effort is being placed on understanding nucleation phenomena through the study of the molecular properties of gas phase clusters. A new apparatus to be used in this work is under construction and nearing completion.

Many non-nuclear power generation technologies are accompanied by the production of an enormous variety of gaseous pollutants which may enter into the chemistry of the lower atmosphere through photochemical, and homogeneous and heterogeneous neutral molecule reactions. In order to assess the environmental effects of these technologies, which are primarily fossil fuel based, it is necessary to characterize these pollutant molecules thoroughly and to determine their chemical transformations in the atmosphere. In the present program, two experimental efforts which utilize a single laboratory detection apparatus, but which differ in source technology, are being developed together. The basic apparatus consists of a variable wavelength photoionization mass-spectrometer detection system, which may be used with a variety of different types of molecular beam sources. The most important sources for the present work will be a supersonic molecular beam source used to produce cluster species, and a free radical discharge source used to produce and react free radicals of atmospheric importance. Both molecular beam sources have been developed and tested already.

The primary area of investigation will concern the study of the mechanisms and kinetics of homonuclear and heteronuclear cluster formation in atmospheric systems. Initial experiments will study both the kinetics of the nucleation process and the energy level structures of cluster species as a function of the cluster size. Such experiments will provide information on the internal structure of cluster species which are in the transition region between the gas and solid phases. A secondary area of investigation will be the

production and subsequent study of free radicals present in the atmosphere as reaction intermediates. The gas-phase reactions of free radicals such as O, OH, and HO_2 with aliphatic and aromatic hydrocarbons, and with sulfur, nitrogen, and halogen-containing compounds will be studied.

The variable wavelength photoionization mass spectrometer detection apparatus has been under construction for nearly two years and is expected to be operational within the next few months. The major components of this apparatus are (1) a high-intensity capillary discharge lamp used for the production of the rare-gas continua or the hydrogen many-line spectrum (which together cover the wavelength range from approximately 600 to 1700 Å with good intensity); (2) a 1-meter near-normal incidence McPherson Model 225 monochromator* used to disperse the continuum light; (3) separately pumped reaction and detection chambers; and (4) an Extranuclear Model 324-9 quadrupole mass filter† used to detect the photoions. As mentioned previously, several types of molecular beam sources may be used in the reaction chamber to produce the target beam. These sources are easily interchangeable. In addition, the reaction chamber has been fitted with two layers of high quality mu-metal magnetic shielding to eliminate the effects of the earth's magnetic fields. This gives us the option of using a photoelectron spectrometer to detect photoelectrons in future experiments. The rather complex vacuum system for this instrument has been completely safety interlocked, using several specially designed relay-logic protection circuits. A dedicated PDP-11/03 on-line microcomputer‡ will serve to control the experiment and collect the data. The PDP-11/03 is interfaced to (1) a CAMAC crate, which houses scalers, timers, a stepping-motor controller for the monochromator grating drive, and other general purpose laboratory interfaces; (2) a Tektronix 4006 video terminal; (3) a DEC writer II hard copy terminal; and (4) a modem for coupling a telephone line to the computer. The microcomputer will control

---

*GCA/McPherson Instrument Company, 530 Main Street, Acton, Mass. 01720.
†Extranuclear Laboratories, Inc., P.O. Box 11512, Pittsburgh, Pa. 15238.
‡Digital Equipment Corporation, Maynard, Mass. 01752.

the experiment, store the data, and make data reduction calculations, plot the data on the graphics (video) terminal, and send the data (via a dial-up telephone line) to ANL's central computing facility.* This last feature is a very powerful capability that allows access to all of the features of Argonne's IBM 370/195 computer facility from the laboratory.

---

*The program to send data between the PDP-11/03 and Argonne's IBM 370/195 was written by Professor Dan Dill of Boston University and was very kindly provided by him.

PHOTOIONIZATION OF H_2O AT HIGH RESOLUTION

P. M. Dehmer and W. A. Chupka*

The relative photoionization cross sections for the formation of H_2O^+, OH^+, and H^+ from H_2O have been measured at high wavelength resolution using a 3-meter photoionization mass spectrometer equipped with a quadrupole mass filter and a 1-meter photoionization mass spectrometer equipped with a 12-inch radius, 60° sector magnetic mass spectrometer. Discrete structure in the parent ion photoionization efficiency curve is interpreted in terms of Rydberg series converging to excited states of the H_2O^+ ion.

Introduction

In spite of considerable effort, the vacuum UV absorption spectrum of H_2O in the region of the ionization continuum is still not well understood. In particular, the discrete structure in the absorption and ionization efficiency curves has not yet been quantitatively assigned to specific Rydberg states. The ground state configuration of H_2O is $(1a_1)^2(2a_1)^2(1b_2)^2(3a_1)^2(1b_1)^2\ ^1A_1$. The He I 584 Å photoelectron spectrum consists of the states produced by ionization from the outermost three orbitals (see for example, Refs. 1 and 2). The ionization processes studied in this work consist of the corresponding three direct ionization processes as well as autoionization of Rydberg series converging to these limits. The absorption and photoionization cross sections for H_2O have previously been studied at low wavelength resolution (0.5 Å, FWHM) by Katayama et al.,[3] and the absorption cross section at very high resolution (0.03 Å) has recently been reported by Gürtler et al.[4] In the present work we report the high resolution (0.07 Å) relative photoionization cross section for H_2O, and in addition we also report the photoionization efficiency curves for OH^+ and H^+ formation, which have not been given previously at high resolution.

Experimental

The high resolution photoionization mass spectrometer used to measure the relative photoionization cross sections for the H_2O^+ parent ion and for the

*Department of Chemistry, Yale University, New Haven, Connecticut 06520

OH^+ fragment ion has been described in detail previously.[5] Briefly, the apparatus consists of a helium continuum light source, a McPherson 3-meter near-normal incidence monochromator, which disperses and then refocusses the selected light into an ionization chamber, a set of ion extraction and focussing lenses, and a quadrupole mass filter for ion detection. The spectra were taken at room temperature and at wavelength resolutions of 0.07 Å for H_2O^+ and 0.15 Å for OH^+.

The ion collection and detection system of this apparatus discriminates somewhat against particles formed with kinetic energy. In the case of photofragmentation of H_2O to produce $H^+ + OH + e^-$ at photon energies above the threshold for formation, the excess kinetic energy appears to a large extent as kinetic energy of the H^+ fragment. Measurements of the energy distribution of H^+ ions from dissociative photoionization at 508, 554, and 630 Å show that the distribution peaks at ~0.1 eV and has a high energy tail extending to > 0.4 eV.[6] The relative photoionization cross section for the H^+ fragment was measured, using a photoionization mass spectrometer which collects a larger fraction (although still not all) of the ions with kinetic energy. This apparatus, which has been described previously,[7] employs a magnetic sector mass spectrometer and uses an ion extraction potential of 4 to 5 kV. It has a 1-meter rather than a 3-meter monochromator and hence operates at lower wavelength resolution than the quadrupole instrument; however, this is not a disadvantage for the present measurement since the H^+ fragment ion photoionization efficiency curve shows no sharp structure. The H^+ cross section reported here was measured at a wavelength resolution of 0.83 Å. Measurements were also performed at higher resolution, and no additional syructure was observed. The cross section for the OH^+ fragment ion was also measured, using this apparatus; and the overall shape of the cross section agrees with that determined with the high resolution instrument, indicating that there was probably little kinetic energy discrimination, in accord with the expectation, based on energy and momentum conservation, that the OH^+ fragment is formed with only minimal kinetic energy.

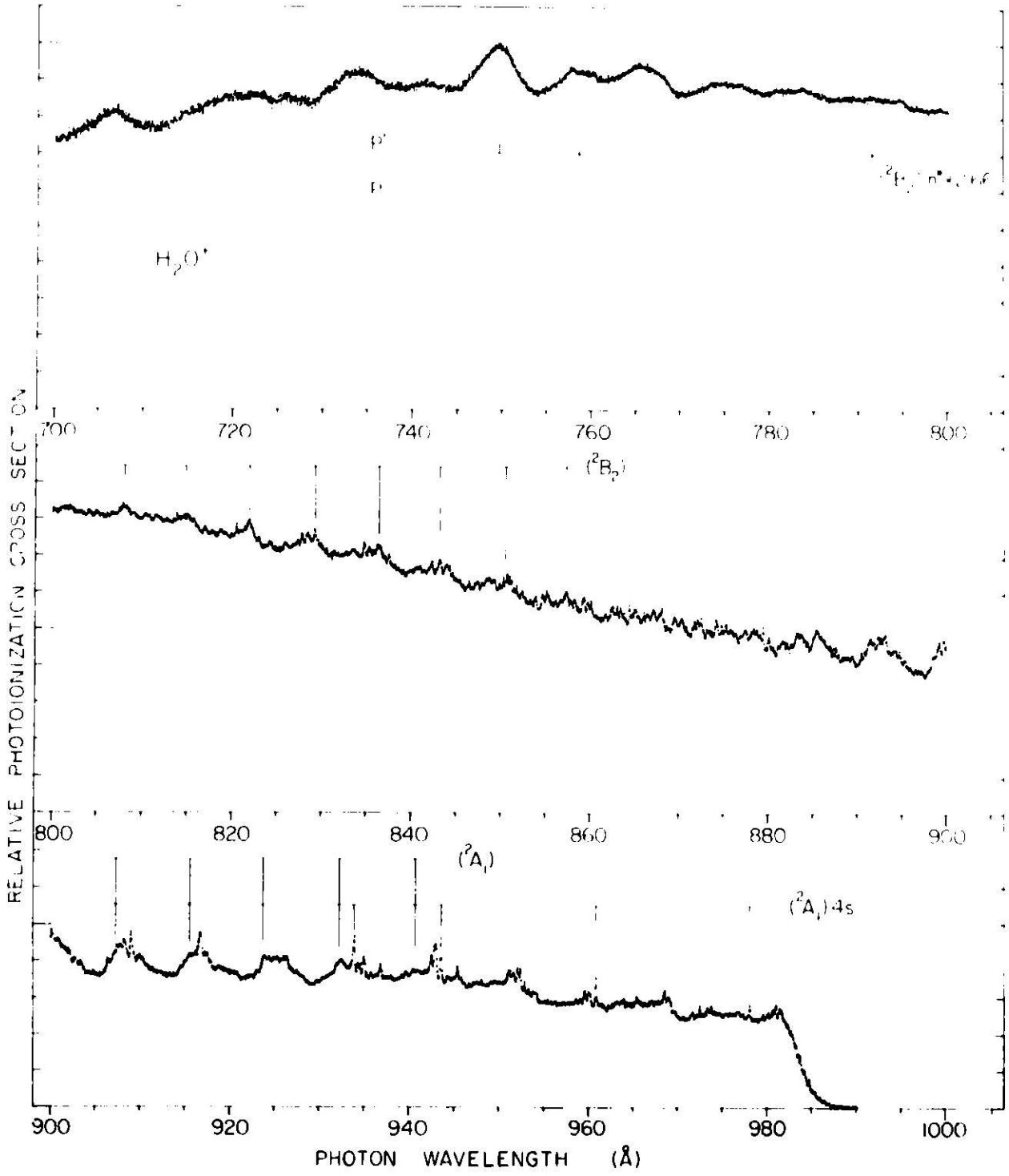

FIG. 1.--Relative photoionization cross section for H_2O measured at room temperature with a wavelength resolution of 0.07 Å (FWHM).

H_2O^+ Parent Ion Formation

Figure 1 shows the relative photoionization cross section for the formation of the H_2O^+ ion from H_2O at room temperature. While the major part of the photoionization occurs by the direct process, significant structure due to autoionization of Rydberg states is also present. These Rydberg states undergo simultaneous competitive decay to neutral products, as is readily seen from the data of Katayama et al.,[3] who measured separately the absolute cross sections for absorption and ionization. Predissociation is the most likely competing process, although fluorescence can be dominant in certain cases.[8]

Steplike structure is observed in the region of the $X\ ^2B_1$ ionization threshold corresponding to the formation of the H_2O^+ ion in the (0,0,0), (0,1,0), and (1,0,0) vibrational levels of the $X\ ^2B_1$ state, and Katayama et al.[3] have compared the relative intensities of these steps to the corresponding photoelectron intensities. The fact that these steps are clearly displayed at the vibrational limits is proof that the major fraction of the Rydberg states converging to these thresholds decay by processes other than autoionization, since the principle of continuity of oscillator strength through a convergence limit demands that no steps appear in the ionization efficiency curve if these Rydberg states were totally autoionized.

There is considerable structure in the region from the ionization threshold to 700 Å. Identification of the structure is suggested based on quantum defects and on the similarity to the band shapes in the photoelectron spectrum. The structure in the region from threshold to about 880 Å consists of two Rydberg states converging to the $^2A_1$ (the first excited) state of H_2O^+. A weak, sharp Rydberg state is observed in the region from 980 to 920 Å, which we assign as the 4s state. Another stronger and broader state is observed at slightly shorter wavelength and may be the 3d or the 4p state.[4] A vibrational progression is observed in the region from 860 to 800 Å, which is probably the 3s Rydberg state converging to the $^2B_2$ (the second excited) state of H_2O^+. A pair of vibrational progressions are observed in the region from 800 to 700 Å which have $n^* = 2.66$ and which also converge to $H_2O^+\ ^2B_2$; P is a progression in $n\nu_1'$ and P' is a progression in $\nu_3' + n\nu_1'$.[1]

OH^+ and H^+ Fragment Ion Formation

The relative photoionization cross sections for the formation of OH^+ and H^+ are shown in Fig. 2. The fragment ion cross sections show a steplike structure which may be correlated to some extent with the vibrational thresholds of the $^2B_2$ state of H_2O^+. In order to compare the spacings between the steps with the photoelectron spectrum of H_2O in this region, the derivatives of the

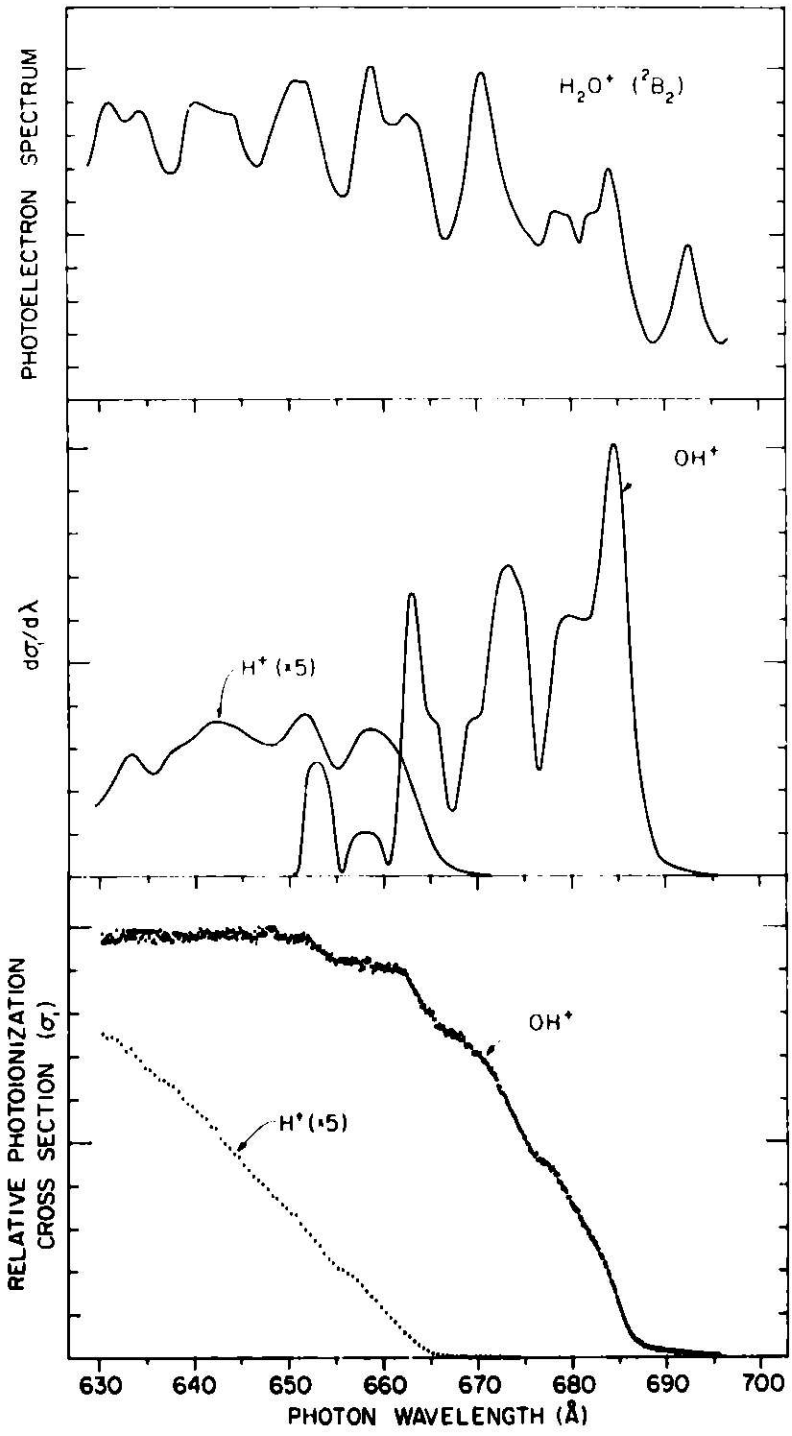

FIG. 2.--Relative photoionization cross sections for the formation of OH^+ and H^+ from H_2O measured at room temperature and with wavelength resolutions of 0.15 Å for OH^+ and 0.83 Å for H^+ (lower trace). The steplike structure in the cross sections may be compared to the vibrational thresholds of the $^2B_2$ state of H_2O^+ shown in the photoelectron spectrum (upper trace). For ease of comparison, the derivatives of the cross sections are shown in the middle trace. (ANL Neg. 209-76-352)

photoionization efficiency curves were taken after first smoothing the raw data. The derivatives are shown in the middle section of Fig. 2, and the high resolution photoelectron spectrum of Dixon et al.[1] is shown in the upper section of the figure.

The relative ionization yields for H_2O^+:OH^+:H^+ are 1.00:0.33:0.02 at 650 Å. The H_2O^+:HO^+ ratio is in good agreement with the results of Dibeler et al.[9] who determined a relative abundance of 1.0:0.4 at 584 Å. Cairns et al.[6] determined a somewhat larger value for this ratio of 1:0.47 at 630 Å. Since kinetic energy effects are probably present in our data for H^+, our H_2O^+:H^+ ratios should be taken as lower limits to the true values.

References

1. R. N. Dixon, G. Duxbury, J. W. Rabalais, and L. Åsbrink, Mol. Phys. 31, 423 (1976).
2. L. Karlsson, L. Mattsson, R. Jadrny, R. B. Albridge, S. Pinchas, T. Bergmark, and K. Siegbahn, J. Chem. Phys. 62, 4743 (1975).
3. D. H. Katayama, R. E. Huffman, and C. L. O'Bryan, J. Chem. Phys. 59, 4309 (1973).
4. P. Gürtler, V. Saile, and E. E. Koch, Chem. Phys. Lett. 51, 386 (1977).
5. W. A. Chupka, P. M. Dehmer, and W. T. Jivery, J. Chem. Phys. 63, 3929 (1975).
6. R. B. Cairns, H. Harrison, and R. I. Schoen, J. Chem. Phys. 55, 4886 (1971).
7. W. A. Chupka and J. Berkowitz, J. Chem. Phys. 47, 2921 (1967).
8. P. M. Dehmer and W. A. Chupka, J. Chem. Phys. 65, 2243 (1976).
9. V. H. Dibeler, J. A. Walker, and H. M. Rosenstock, J. Res. Nat. Bur. Std. 70A, 459 (1966).

PHOTOIONIZATION OF CO

P. M. Dehmer and W. A. Chupka*

The relative photoionization cross section for CO taken at liquid nitrogen temperature and a wavelength resolution of 0.07 Å (FWHM) is presented in the wavelength region between the ionization threshold at 884.73 Å and 600 Å.

The relative photoionization cross section for CO has been determined using the high-resolution 3-meter photoionization mass spectrometer described in detail previously.[1] The data taken at 77°K and at a wavelength resolution of 0.07 Å (FWHM) are shown in Fig. 1. The Rydberg series shown in Fig. 1 are taken from the work of Ogawa and Ogawa,[2] who have most recently investigated the absorption spectrum of CO in the region of the ionization continuum.

Rydberg series converging to the $A\,^2\Pi$ state of CO^+ are located mainly in the wavelength region from 880 to 690 Å and show complex patterns owing to the overlapping of many series consisting of several vibrational series each. Ogawa and Ogawa[2] have studied this region of the spectrum and have reclassified the bands into five Rydberg series. The high intensity R_A-I series consisting of eight vibrational series is shown in part in Fig. 1a. The band with m = 3 has a quantum defect of either 0.05 or 1.05, and thus, the possible electron configurations of the upper state are $(\sigma_u 2s)^2(\pi_u 2p)^3(\sigma_g 2p)^2$ nd or ns.

The bands in the wavelength region from 720 to 620 Å are shown in Fig. 1b and have been classified into five Rydberg series (Sharp, Diffuse, III, IV, and V) converging to the $B\,^2\Sigma$ state of CO^+. The running number m of each Rydberg state is defined by $\mu = m - n^*$, so that it gives a minimum positive value of μ, where n^* is the effective quantum number. The Sharp Series and Series V have quantum defects of 0.67 and 0.61, respectively, and are probably the singlet and triplet Π states arising from the electron configuration $(\sigma_u 2s)(\pi_u 2p)^4(\sigma_g 2p)^2$ np π. The Diffuse series has a quantum defect of 0.55 and is tentatively assigned as np σ. Series III and IV have quantum defects of 0.93 and 0.19,

*Department of Chemistry, Yale University, New Haven, Connecticut 06520.

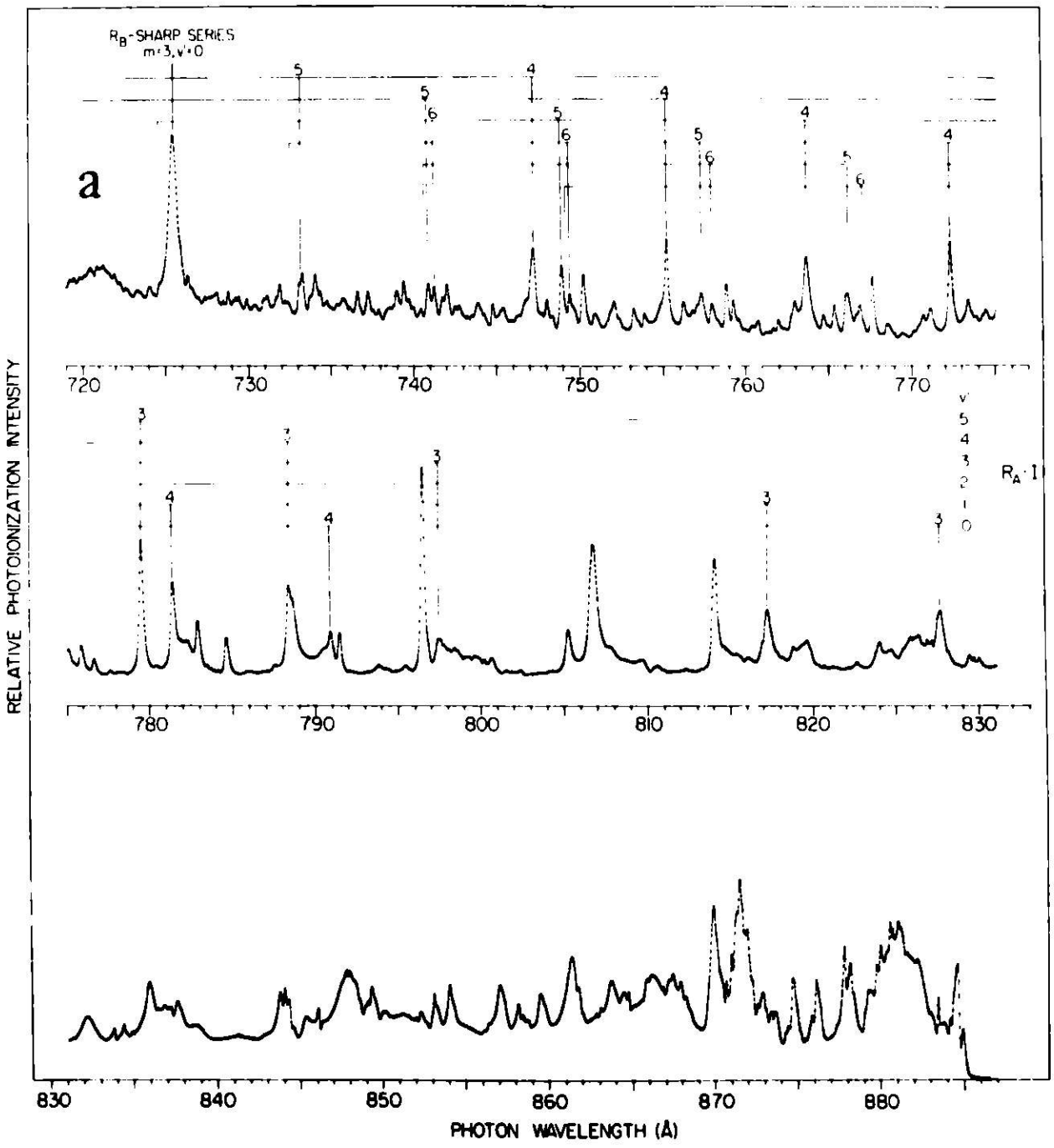

Fig. 1.--Relative photoionization cross section for CO measured at 77°K and at a wavelength resolution of 0.07 Å (FWHM). (ANL Neg. 149-79-3)

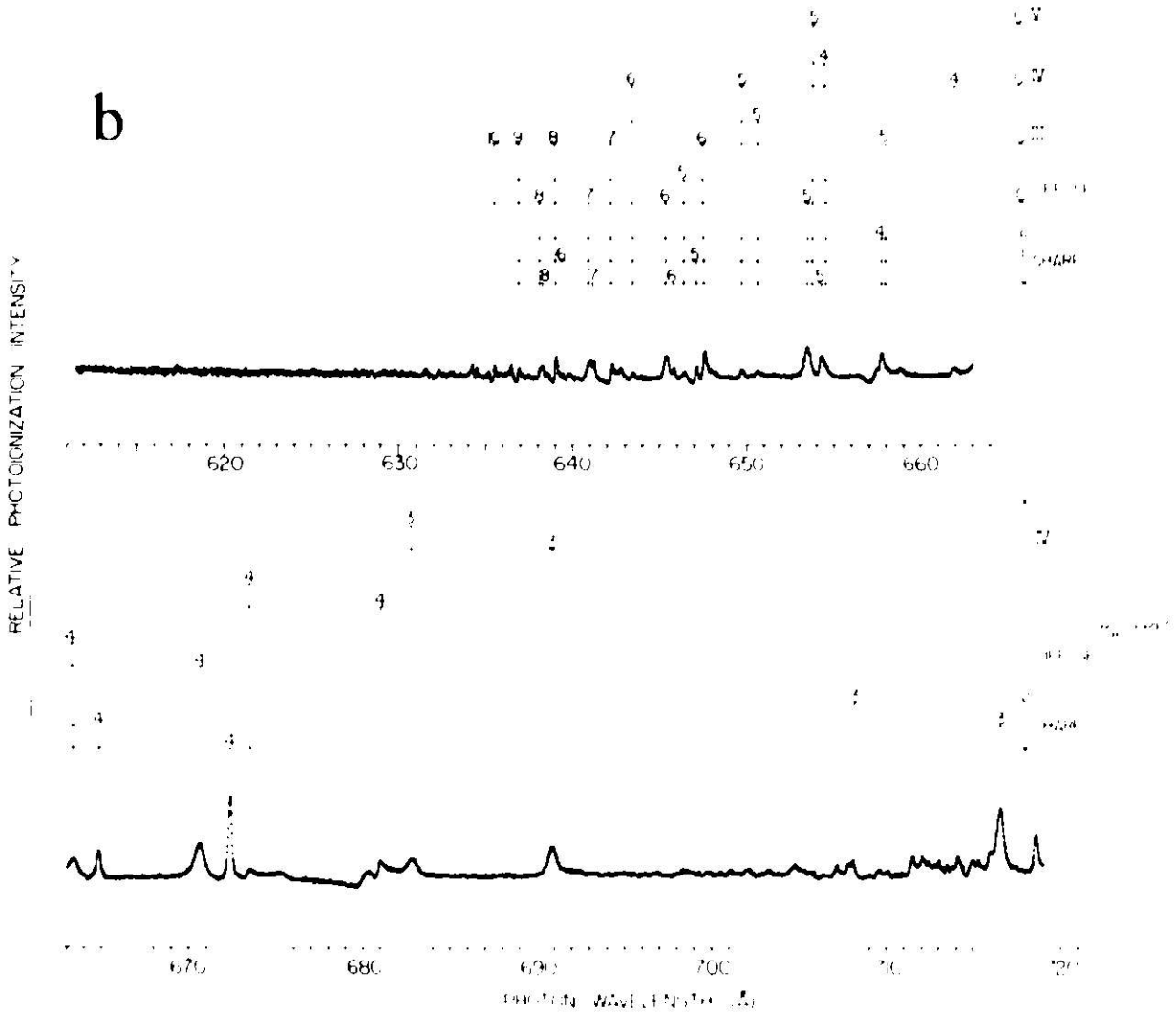

FIG. 1.--(continued). (ANL Neg. 149-79-2).

respectively, and are assigned nsσ and ndσ or ndπ.

The ionization yield of these Rydberg states, which is less than unity, has been investigated in detail by Cook et al.,[3] who measured separately the photoionization and absorption coefficients for CO in the wavelength region from 1000 to 600 Å.

References

1. W. A. Chupka, P.M. Dehmer, and W.T. Jivery, J. Chem. Phys. 63, 3929 (1975).
2. M. Ogawa and S. Ogawa, J. Mol. Spectrosc. 41, 393 (1972).
3. G. R. Cook, P. H. Metzger, and M. Ogawa, Can. J. Phys. 43, 1706 (1965).

PHOTOIONIZATION OF THE HYDROGEN HALIDES–RYDBERG SERIES CONVERGING TO THE $A^2\Sigma^+$ STATE OF THE HX^+ ION (X = Cl, Br, I).

P. M. Dehmer and W. A. Chupka

Relative photoionization cross sections were determined for HCl, HBr, and HI at high wavelength resolution using a cooled ionization chamber. Spectra are presented in the wavelength region from the ionization threshold to approximately the convergence limit of the $HX^+A^2\Sigma^+$ state for each molecule. Rydberg state structure converging to the A state of the HX^+ ions is shown.

Introduction

The electronic configuration of the ground state of HX is $(ns\sigma)^2(np\sigma)^2(np\pi)^4\,{}^1\Sigma^+$, where n = 3 for HCl, 4 for HBr, and 5 for HI.[1] The ground state of HX^+ is formed by the removal of an $np\pi$ electron giving $^2\Pi_{\frac{3}{2}}$ and $^2\Pi_{\frac{1}{2}}$ ionic states. The spin orbit splitting of the $^2\Pi$ components increases from 0.08 eV for HCl^+ to 0.66 eV for HI^+.[2] The region between these two limits contains complex autoionization structure, which has only been partially analyzed for HI^+ [3,4] This part of the spectrum will be discussed elsewhere.[5] The first excited state of HX^+ is formed by the removal of an $np\sigma$ electron, giving the $A^2\Sigma^+$ state. Since the internuclear separation of the ground state of HX differs appreciably from that of the A state of HX^+, transitions from the ground state of HX to the A state of HX^+ (or to Rydberg states converging to the A state) will show a long vibrational progression. Terwilliger and Smith[6–8] have studied the Rydberg series in the absorption spectra converging to the A state of HCl^+ and HBr^+ in great detail and have assigned nearly all of the prominent structures converging to this limit. The HI spectrum shows only one broad peak in the relevant region of the spectrum. The lack of vibrational structure indicates that HI^+ $A^2\Sigma^+$ is strongly predissociated, with a predissociation lifetime shorter than one vibrational period.

Experimental

The relative photoionization cross sections for HCl, HBr, and HI were

*Department of Chemistry, Yale University, New Haven, Connecticut 06520.

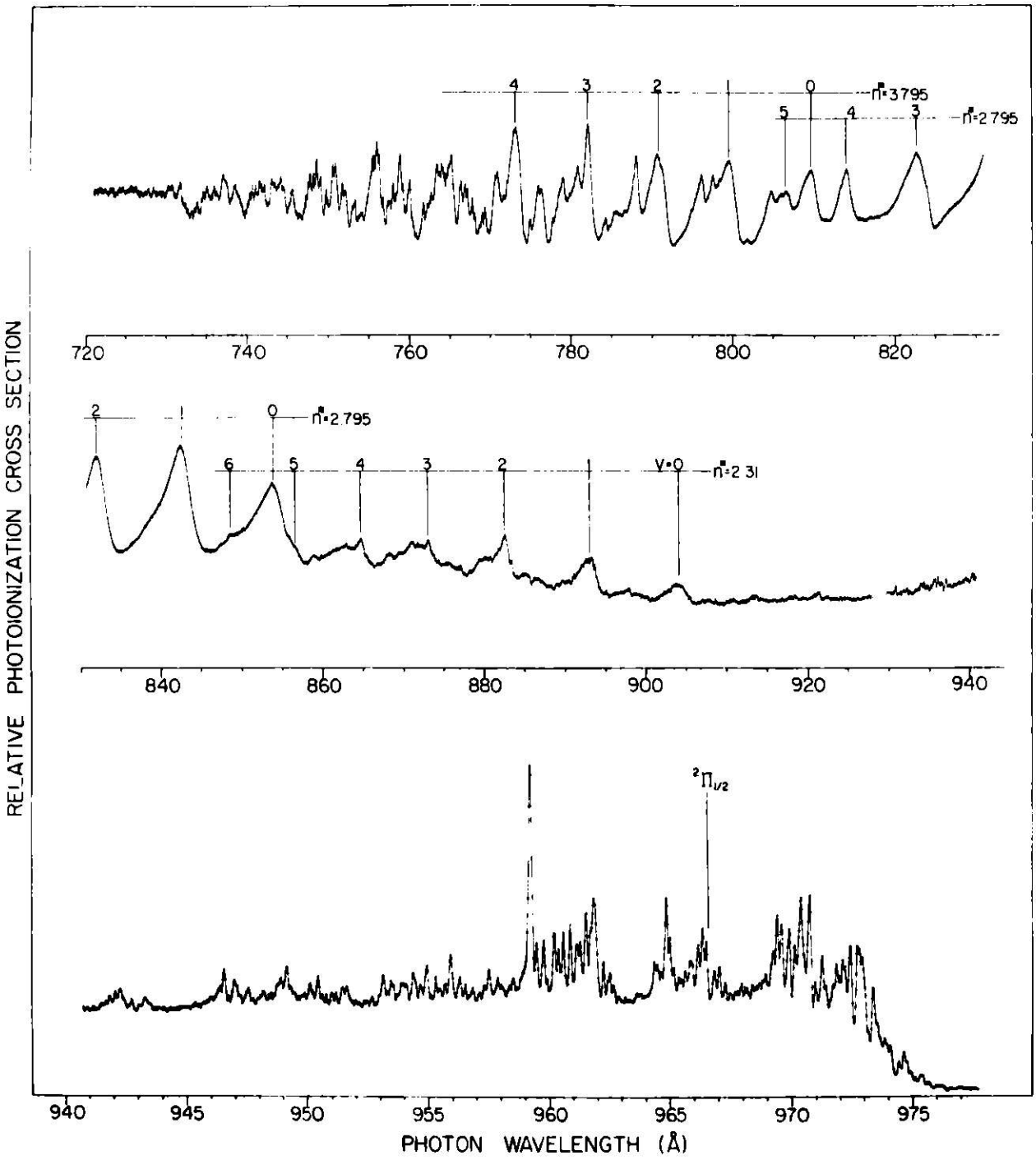

FIG. 1.--Relative photoionization cross section for HCl taken at a wavelength resolution of 0.07 Å (FWHM) and a temperature of approximately -150°C.

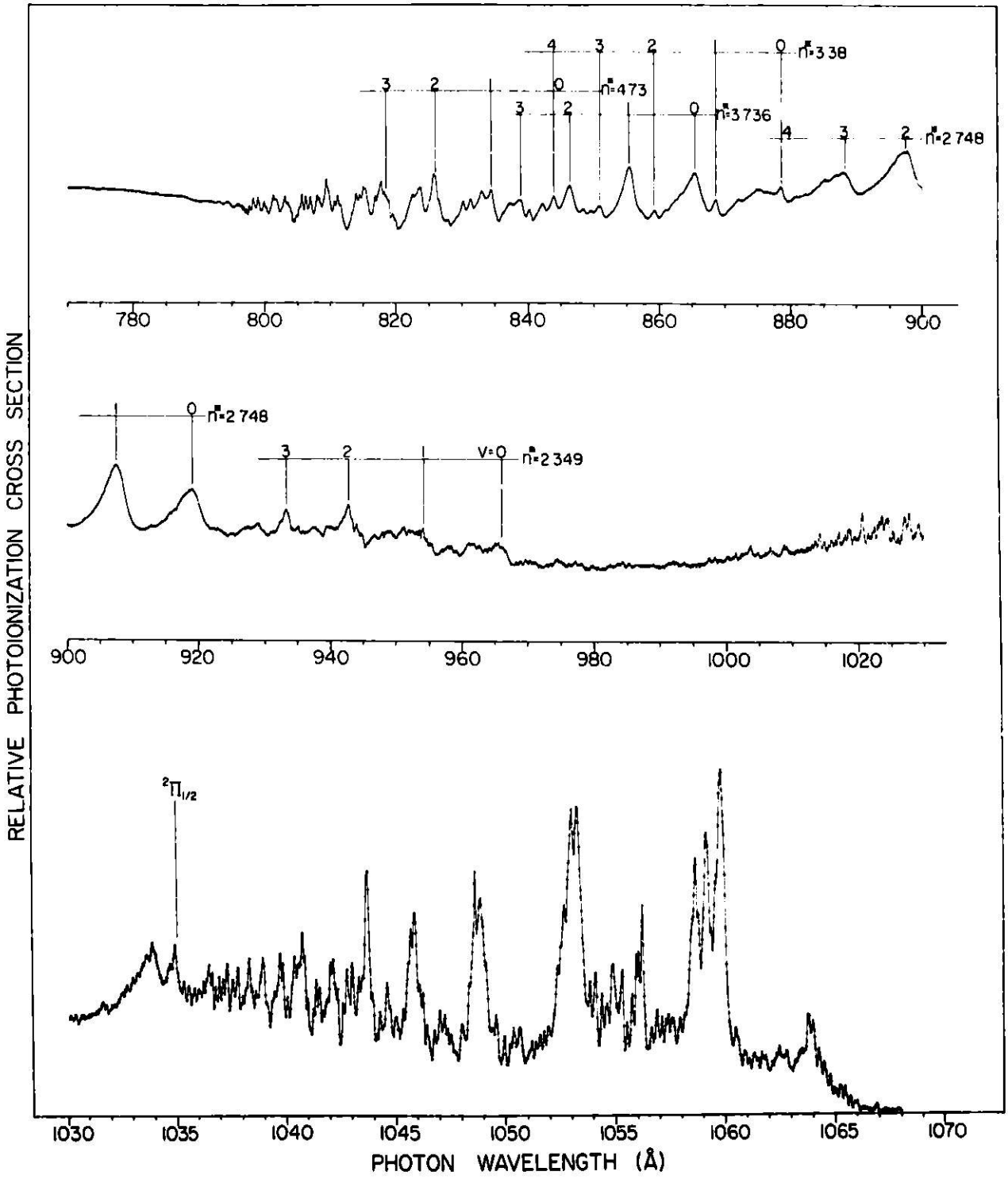

FIG. 2.--Relative photoionization cross section for HBr taken at a wavelength resolution of 0.15 Å (FWHM) and a temperature of approximately -120°C.

determined, using the high-resolution 3-meter photoionization mass spectrometer previously described in detail.[9] The wavelength resolution was 0.07 Å (FWHM) for HCl and 0.15 Å (FWHM) for HBr and HI. The spectra (Figs. 1–3) were taken at temperatures slightly above the condensation temperature for each gas. These temperatures were ~-150°C for HCl, ~-120°C for HBr, and ~-70°C for HI.

Results and Discussion

Terwilliger and Smith have assigned the bands converging to $HX^+ A^2\Sigma^+$ to several vibrational progressions. The most intense progression in HCl has an $n^* = 2.795$, and the corresponding progression in HBr has $n^* = 2.748$. In both cases, higher members of the series are also observed. Terwilliger and Smith originally assigned these states as $^1\Sigma^+$, with the configuration $(ns\sigma)^2 (np\sigma)(np\pi)^4((n+2)s\sigma)$; however, this assignment is uncertain, since the quantum defect for a d Rydberg electron is almost exactly one unit different from that of an s Rydberg electron. In the united atom limit the transition $np^6 \rightarrow np^5(n+1)d$ should be much more intense than the transition $np^6 \rightarrow np^5(n+2)s$, making the probability of an nd transition more likely in the present case.

Another weaker vibrational progression is observed in both HCl and HBr, with the lowest member of the series having $n^* = 2.31$ in HCl and 2.349 in HBr. A higher member of the series is observed only in HBr. Terwilliger and Smith assign these states to a partially resolved p-complex with configuration $(ns\sigma)^2(np\sigma)(np\pi)^4(n+1)p_{\sigma,\pi}$.

In the case of HI only one broad peak with a value of $n^* = 2.78$ is observed. This is in good agreement with the n^* values obtained in the intense progressions in HCl and HBr. No higher members of this series could be identified.

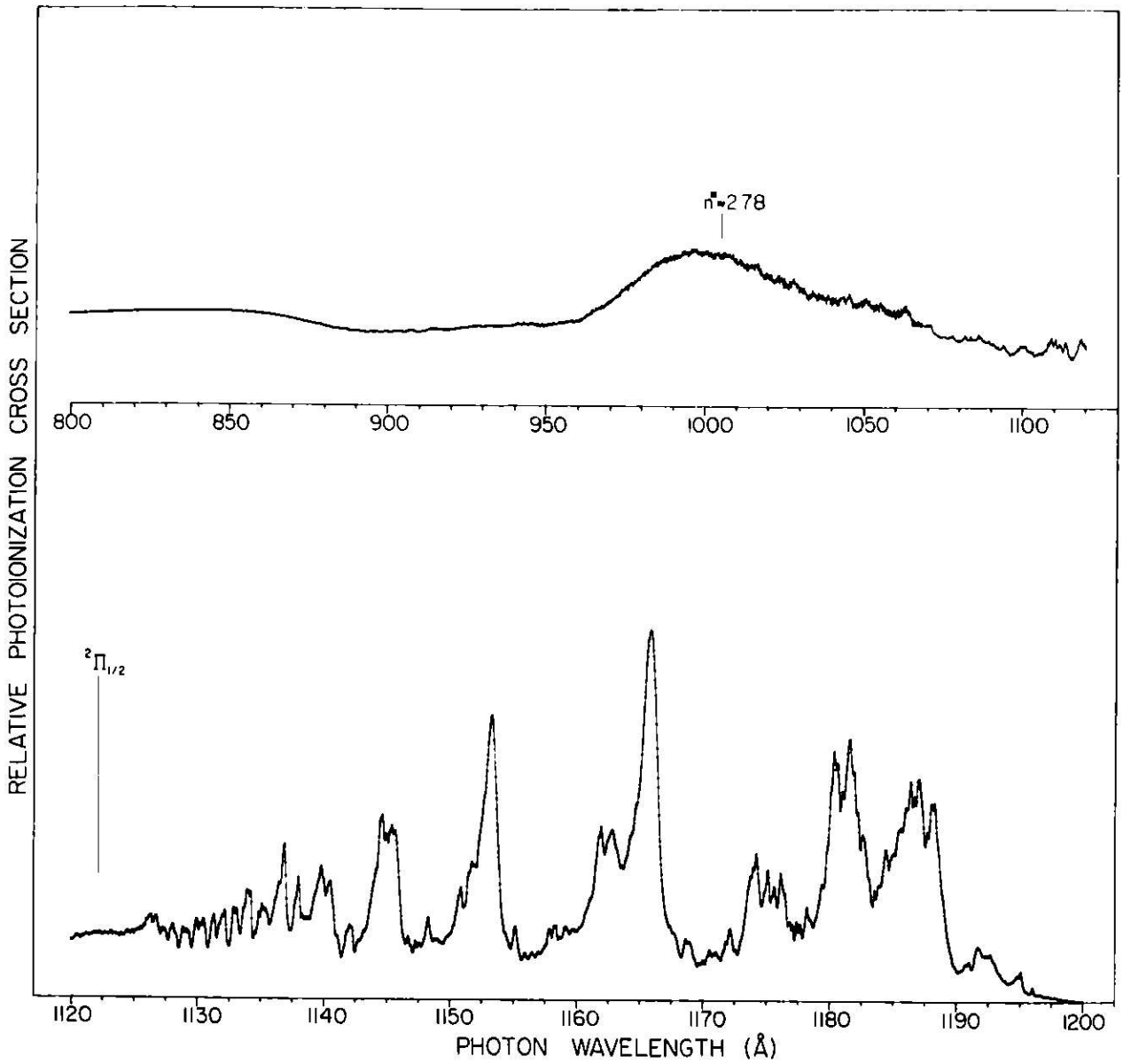

FIG. 3.--Relative photoionization cross section for HI taken at a wavelength resolution of 0.15 Å (FWHM) and a temperature of approximately -70°C.

References

1. G. Herzberg, Spectra of Diatomic Molecules, Van Nostrand, Princeton, p. 341 (1950).
2. D. W. Turner, C. Baker, A. D. Baker, and C. R. Brundle, Molecular Photoelectron Spectroscopy, Wiley, New York, p. 39 (1970).
3. H. T. Wang, W. S. Felps, G. L. Findley, A.R.P. Rau, and S. P. McGlynn, J. Chem. Phys. 67, 3940 (1977).
4. J.H.D. Eland and J. Berkowitz, J. Chem. Phys. 67, 5034 (1977).
5. P. M. Dehmer and W. A. Chupka, "Photoionization of Xe, HI, and CH_3I-anologies between atomic and molecular Rydberg states," this report.
6. D. T. Terwilliger and A. L. Smith, J. Mol. Spectrosc. 45, 366 (1973).

7. D. T. Terwilliger and A. L. Smith, J. Mol. Spectrosc. 50, 30 (1974).
8. D. T. Terwilliger and A. L. Smith, J. Chem. Phys. 63, 1008 (1975).
9. W. A. Chupka, P. M. Dehmer, and W. T. Jivery, J. Chem. Phys. 63, 3929 (1975).

PHOTOIONIZATION OF Xe, HI, AND CH_3I-ANALOGIES BETWEEN ATOMIC AND MOLECULAR RYDBERG STATES

P. M. Dehmer and W. A. Chupka*

Relative photoionization cross sections are presented for Xe, HI, and CH_3I in the wavelength region between the $^2P_{\frac{3}{2}}$ and $^2P_{\frac{1}{2}}$ limits in Xe^+, the $^2\Pi_{\frac{3}{2}}$ and $^2\Pi_{\frac{1}{2}}$ limits in HI^+, and the $^2E_{\frac{3}{2}}$ and $^2E_{\frac{1}{2}}$ limits in CH_3I^+. The analogies between the rare gas spectrum and the molecular spectra are discussed.

Introduction

The ground ionic states of Xe, HI, and CH_3I are all obtained by the removal of a 5p electron, resulting in ^2P, $^2\Pi$, and ^2E electronic states, respectively. Each of these doublet states is split by spin-orbit coupling into two states with total angular momentum of $\frac{3}{2}$ (the lower energy state) and $\frac{1}{2}$. In the case of atomic Xe, two Rydberg series, the ns and the nd series, converge on the higher ionic limit. To a first approximation, the molecules HI and CH_3I should have analogous ns and nd series, and in addition should have an np series which is forbidden in the sphere group but allowed in the molecular point groups.

The similarity among the spectra in this energy region has been the subject of several previous investigations. Tsai and Baer[1] have measured the photoionization spectra of HI and CH_3I at low wavelength resolution and have assigned the low-lying Rydberg states of the ns', nd', and np' series. (The primes indicate Rydberg states converging to the spin-orbit limit with total angular momentum of $\frac{1}{2}$.) Wang et al.[2] presented low resolution absorption spectra for Xe, HI, and CH_3I and extended the Rydberg state assignments made earlier. About the same time, Eland and Berkowitz[3] presented high resolution spectra for HI and DI and assigned Rydberg states belonging to five Rydberg series converging to the $^2\Pi_{\frac{1}{2}}$ ionic state. In the present work we present high resolution spectra for Xe, HI, and CH_3I in the wavelength region between

*Department of Chemistry, Yale University, New Haven, Connecticut 06520.

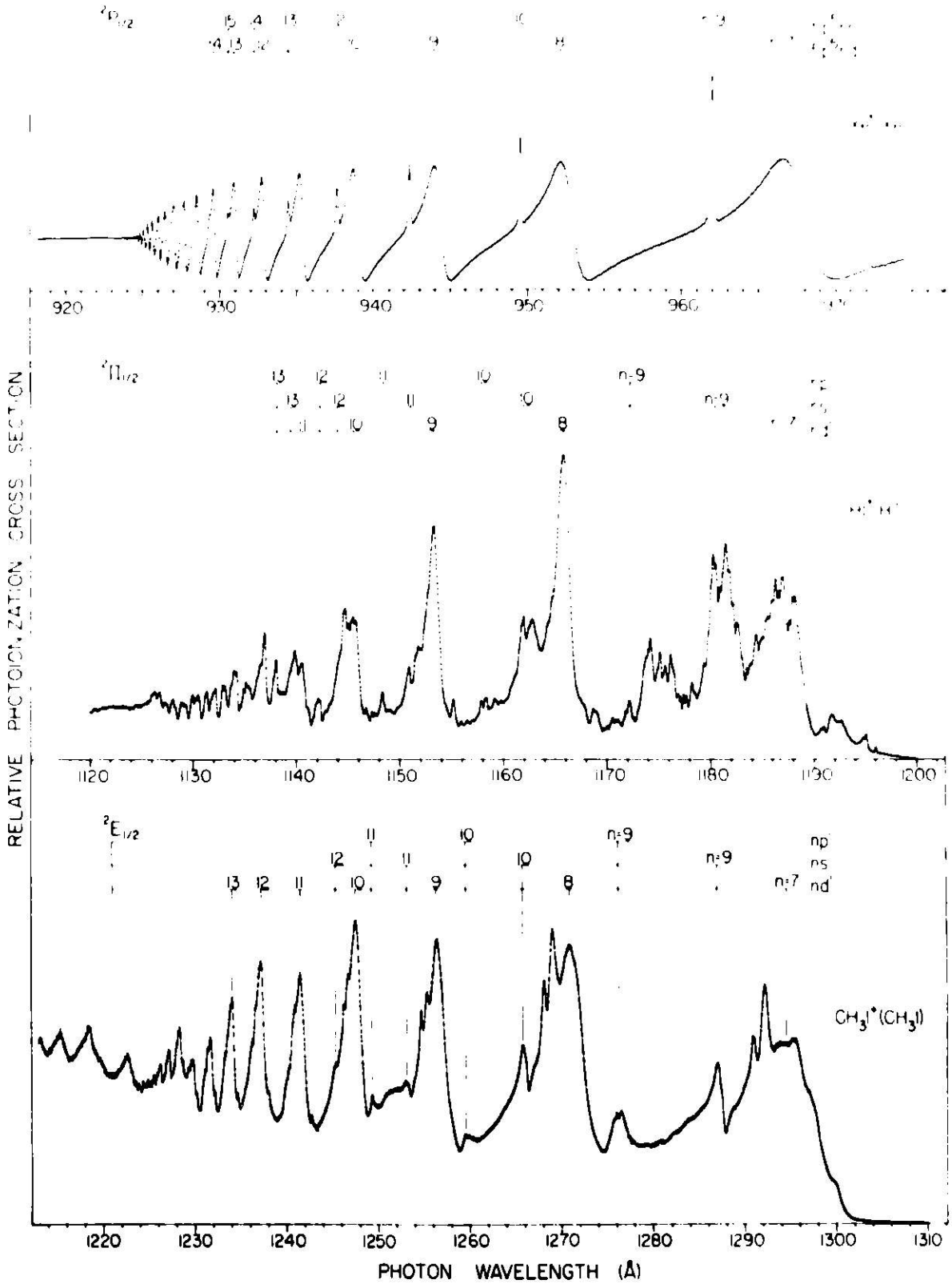

FIG. 1.--Relative photoionization cross sections for Xe, HI, and CH_3I. (ANL Neg. 149-79-57)

the spin-orbit thresholds. The data are presented in such a way as to make the analogy between the atomic and molecular Rydberg states very obvious.

Experimental

The relative photoionization cross sections were measured using the 3-meter photoionization mass spectrometer previously described in detail.[4] The wavelength resolution was 0.07 Å (FWHM) for CH_3I and 0.15 Å (FWHM) for Xe and HI. The HI spectrum was taken at a temperature of -70°C and the Xe and CH_3I spectra were taken at room temperature. The data are shown in Fig. 1 and are plotted so that the 7d' Rydberg states of all three systems line up as do the $\Omega=\frac{1}{2}$ convergence limits. In this way all the intermediate Rydberg states should also line up, assuming that the quantum defects are approximately the same for each system.

Discussion

Assignments for HI and CH_3I are made primarily by analogy with Xe and by the quantum defect of the Rydberg series. It must be stressed that since rotational structure is not observed for any of these bands, the exact nature of the upper electronic states cannot be guaranteed. The series which we label nd', ns', and np' in HI correspond to Series I, III, and IV, respectively, of Eland and Berkowitz.[3] They assign Series I as nd'δ or nd'σ, Series III as ns'σ, and Series IV as nd'π. Both Tsai and Baer[1] and Wang et al.[2] prefer the assignment np' over nd'π for the latter series; however, the assignments for series which are not in direct correspondence with the rare gas series must be taken as speculative. There is good agreement between the HI and CH_3I series as seen from the figure.

References

1. B. P. Tsai and T. Baer, J. Chem. Phys. 61, 203 (1974).
2. H. T. Wang, W. S. Felps, G. L. Findley, A.R.P. Rau, and S. P. McGlynn, J. Chem. Phys. 67, 3940 (1977).
3. J.H.D. Eland and J. Berkowitz, J. Chem. Phys. 67, 5034 (1977).
4. W. A. Chupka, P. M. Dehmer, and W. T. Jivery, J. Chem. Phys. 63, 3929 (1975).

PHOTOELECTRON SPECTROSCOPY OF THE $^2B_{3u} + e^- \leftarrow {}^1A_g$ TRANSITION IN ETHYLENE

P. M. Dehmer and J. L. Dehmer

Introduction

We have previously shown that high resolution photoelectron spectra of molecules are nearly always limited by the rotational, vibrational, and Doppler broadening of the target gas, and that all of these forms of broadening can be substantially reduced by lowering the temperature of the target gas through the use of a supersonic molecular beam source.[1] We report here the He I 584 Å photoelectron spectrum of the $C_2H_4^+ {}^2B_{3u} + e^- \leftarrow C_2H_4 {}^1A_g$ transition in ethylene taken at a spectrometer resolution of 23 meV using a supersonic molecular beam source to cool the target gas. Although the present resolution is worse than reported in previous measurements,[2-5] the present spectrum shows more detail than the others owing to the reduction in Doppler and rotational broadening. Previous analyses of the major vibrational structure in this electronic band were made by analogy with the vibrational assignments for the 3s Rydberg state[6] and were based on the C-C stretching mode ν'_2, and the torsional mode $2\nu'_4$. A broadening of the second peak in the photoelectron band suggested that the HCH bending mode ν'_3 was also excited in the ion; however, this structure was never resolved in any of the previously reported He I photoelectron spectra taken at spectrometer resolutions of 18 to 20 meV.[2-4] This structure is partially resolved in the threshold photoelectron spectrum of Stockbauer and Inghram,[5] which was taken at a resolution of 15 meV; however, the present 23-meV spectrum is both better resolved and free from the extraneous peaks which occur in the threshold photoelectron spectrum.

Recently it was suggested that the vibrational structure in the 3s Rydberg state is not due to the optically-allowed excitations in ν'_2, ν'_3, and $2\nu'_4$, but is actually due to dipole-forbidden excitations that steal intensity from the underlying $\pi^* \leftarrow \pi$ band via vibronic coupling.[7] In the present work we show that this is an unlikely interpretation based on a comparison of the

structure of the VUV spectrum and the photoelectron spectrum.

Experimental

The molecular beam source and photoelectron spectrometer have been described previously.[8-11] The present ethylene data were taken with a 12.5 micron diameter nozzle aperture and stagnation pressures ranging from 3.5 to 4.75 atmospheres. The data shown in Fig. 1 are representative of all of the data taken in this pressure range. The resolution is about 23 meV. Note that the first doublet is split nearly to the baseline. In the spectrum of Branton et al.,[3] which was taken with a spectrometer resolution of 20 meV, this doublet is only split about 30 percent of the way to the baseline, and, in addition, this doublet is not completely resolved from the second peak. In the threshold photoelectron spectrum of Stockbauer and Inghram[5] taken with a resolution of 15 meV, the first doublet is split about 60 percent of the way to the baseline, and, again, it is not completely resolved from the second peak in the spectrum. In addition, several unidentified peaks are observed in the threshold photoelectron spectrum that are not observed in the present He I photoelectron spectrum. This structure may be due to autoionizing states near the ionization threshold which produce low energy electrons. The present data also show more detail in the second and third peaks than do the previously reported measurements.

Assignment of Vibrational Bands in the Photoelectron Spectrum of Ethylene

Traditionally, the assignment of the vibrational bands in the photoelectron spectrum of ethylene has been made by noting the similarity between the vibrational structure of the photoelectron spectrum and that of the Rydberg transitions, particulary the 3s Rydberg transition at 1744 Å. In D_{2h} symmetry, with the z-axis along the carbon double bond and the x-axis perpendicular to the molecular plane, the 3s Rydberg transition is $^1B_{3u}\{(1b_{3u})(4a_g)\} \leftarrow {}^1A_g\{(1b_{3u})^2\}$ and is x polarized. (An excellent review of work on the ultraviolet spectrum of ethylene to 1968 is given by Merer and Mulliken.[12] For a discussion of the selection rules for electronic and vibronic transitions see Refs. 13 and 14.) The vibrational structure of this band appears as a series of

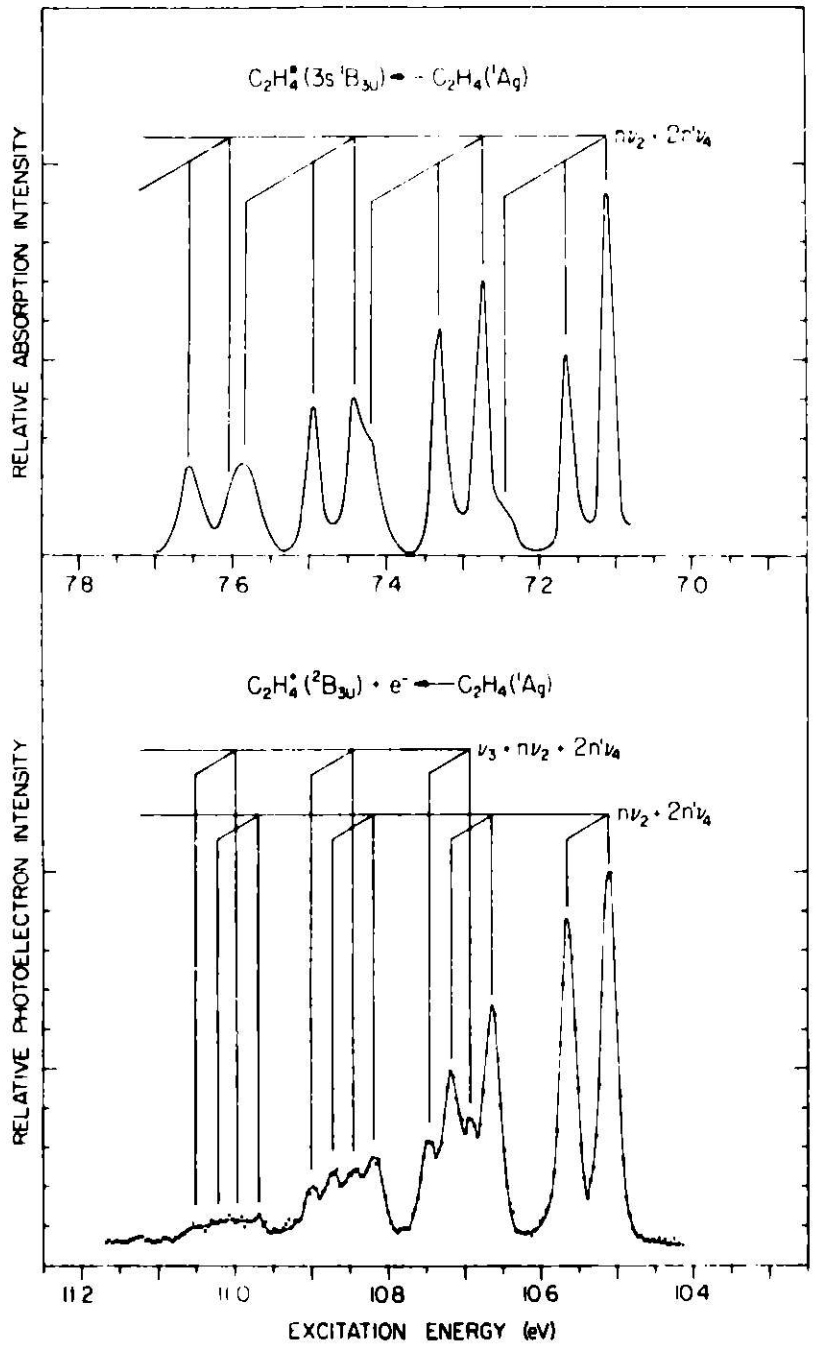

FIG. 1.--Comparison of the spectrum of the $C_2H_4^+\ ^2B_{3u} + e^- \leftarrow C_2H_4\ ^1A_g$ ionizing transition (lower trace) with the spectrum of the $C_2H_4^*3s\ ^1B_{3u} \leftarrow C_2H_4\ ^1A_g$ Rydberg transition at 1744 Å (upper trace). The intensities and positions of the vibrational components of the Rydberg band were taken from Ref. 17. The underlying $\pi^* \leftarrow \pi$ transition which produces a smoothly rising background which increases with increasing energy has been omitted from the figure. The actual shape of the Rydberg transition with the $\pi^* \leftarrow \pi$ transition included is shown in Fig. 1a of Ref. 17.

doublets, with the spacing between successive pairs of doublets commonly accepted as a progression in the totally symmetric (a_g) stretching frequency ν_2'. The smaller doublet spacing is interpreted as two quanta of the torsional frequency ν_4', which has a_u symmetry.[6,12] Vibronic selection rules for D_{2h} symmetry prohibit excitation of a single quantum of ν_4'. Although rotational structure has not been resolved in this transition, the assignment of the doublet spacing as $2\nu_4'$ has been substantiated by a number of theoretical investigations, among them the vibrational analysis of Merer and Schoonveld.[6]

Figure 1 shows the strong similarity between the 3s Rydberg transition and the present photoelectron spectrum. It was suggested by Baker et al.,[2] Branton et al.,[3] and Merer and Schoonveld[6] that the failure to resolve the second doublet in the photoelectron spectrum is due to an excitation in the totally symmetric HCH bending mode ν_3' which appears in transitions to the ion but not to the first Rydberg state, and results from a small difference in geometry between the two final states. The present high-resolution photoelectron spectrum supports this assignment, and shows that the spectrum most probably consists of a progression in $n\nu_2' + 2n'\nu_4'$ plus a similar progression shifted by the amount ν_3'. Table 1 summarizes our results and gives the observed vibrational frequencies for the ground state of the ethylene ion. For comparison, the vibrational frequencies for the ground state of the neutral and for the 3s Rydberg state are also given. The splitting between successive doublets (ν_2') is 1242 cm^{-1} in the ion and 1368 cm^{-1} in the Rydberg state; the splitting within the first doublet ($2\nu_4'$) is 432 cm^{-1} in the ion and 468 cm^{-1} in the Rydberg state. There is excellent agreement in both cases, and the trend toward decreasing values of ν_2' and ν_4' in going from the Rydberg state to the ion is as expected for the removal of a bonding π electron.

Recently, Watson and Nycum[7] presented an alternative analysis of the vibrational structure in the 3s Rydberg transition, based on the premise that this transition derives its intensity from the underlying $\pi^* \leftarrow \pi$ transition, which in D_{2h} symmetry is $^1B_{1u}\{(1b_{3u})(1b_{2g})\} \leftarrow {}^1A_g\{(1b_{3u})^2\}$ and is z polarized. In this mechanism, the 3s $^1B_{3u}$ Rydberg state couples with a vibration of b_{2g} symmetry to produce a final vibronic state of $^1B_{1u}$ symmetry,

Table 1. Vibrational Frequencies for C_2H_4 and $C_2H_4^+$

Vibrational mode	Frequency, cm^{-1}		
	$C_2H_4\ ^1A_g$ [a]	$C_2H_4^*$ 3s $^1B_{3u}$ [b]	$C_2H_4^+\ ^2B_{3u}$ [c]
ν_1	3026.4	—	—
ν_2	1622.9	1368	1242 ± 15
ν_3	1342.2	—	1468 ± 20
ν_4 [d]	1023	$2\nu_4 = 468$	$2\nu_4 = 432 \pm 15$

a. Reference 12, Table IV.

b. Reference 6. The reported frequencies are for the 0–1 band interval for ν_2 and for the 0–2 band interval for ν_4.

c. Present work. The reported frequencies are for the 0-1 band interval for ν_2 and ν_3 and for the 0–2 band interval for ν_4.

d. Note that the 0–2 band interval (i.e., $2\nu_4$) is reported for C_2H_4 3s $^1B_{3u}$ and $C_2H_4^+\ ^2B_{3u}$.

which can then interact with the $\pi^*\ ^1B_{1u}$ state. The result of their analysis was that the first member of each doublet gained intensity via the ν'_8 mode and the second member via the $\nu'_4 + \nu'_{10}$ mode, with the main spacing between the doublets still equal to ν'_2. (In the discussion of ethylene vibrations, Watson and Nycum use G. Herzberg's[15] notation to assign the normal modes, but use R. S. Mulliken's[16] suggested reference frame to determine the symmetries of the vibrations.) Thus, the peaks in the first doublet were assigned ($\nu'_2, \nu'_4, \nu'_8, \nu'_{10}$) = (0,0,1,0) and (0,1,0,1), the peaks in the second doublet were assigned (1,0,1,0) and (1,1,0,1), etc. A rather surprising result of this analysis is that all of the intensity of the 3s Rydberg transition comes from the dipole-forbidden processes, and the dipole-allowed transitions (i.e., (1,0,0,0), (2,0,0,0),...) are not observed. There are a number of possible objections to these assignments, several of which were discussed by the authors themselves; however, we would like to make one additional point here. This point

concerns the implication of the comparison of the profile of the 3s Rydberg transition with that of the photoelectron spectrum. The dipole-forbidden intensity stealing mechanism proposed for the 3s Rydberg transition cannot occur in transitions to the ground state of the ion, since there is no nearby ionic state analagous to the π^* state with which final state interactions may occur. Thus, the vibrational structure observed in the photoelectron spectrum corresponds to totally symmetric vibrational modes, and the strong similarity between the Rydberg spectrum and the photoelectron spectrum implies that the same totally symmetric vibrations are excited in transitions to the Rydberg state.

References

1. P. M. Dehmer and J. L. Dehmer, Argonne National Laboratory Radiological and Environmental Research Division Annual Report, October 1976–September 1977, ANL-77-65, Part I, pp. 49–53.
2. A. D. Baker, C. Baker, C. R. Brundle, and D. W. Turner, Int. J. Mass Spectry. Ion Phys. 1, 285 (1968).
3. G. R. Branton, D. C. Frost, T. Makita, C. A. McDowell, and I. A. Stenhouse, J. Chem. Phys. 52, 802 (1970).
4. C. R. Brundle and D. B. Brown, Spectrochim. Acta 27A, 2491 (1971).
5. R. Stockbauer and M. G. Inghram, J. Electron Spectrosc. 7, 492 (1975).
6. A. J. Merer and L. Schoonveld, Can. J. Phys. 47, 1731 (1969).
7. F. H. Watson, Jr. and M. W. Nycum, Spectrosc. Lett. 8, 223 (1975).
8. P. M. Dehmer and J. L. Dehmer, J. Chem. Phys. 68, 3462 (1978).
9. P. M. Dehmer and J. L. Dehmer, J. Chem. Phys. 69, 125 (1978).
10. J. L. Dehmer, Argonne National Laboratory Radiological and Environmental Research Division Annual Report, July 1974–June 1975, ANL-75-60, Part I, pp. 61–63.
11. J. L. Dehmer and D. Dill, Phys. Rev. A 18, 164 (1978).
12. A. J. Merer and R. S. Mulliken, Chem. Rev. 69, 639 (1969).
13. G. Herzberg, Electronic Spectra and Electronic Structure of Polyatomic Molecules, Van Nostrand, New York, Ch. II (1966).
14. H. Sponer and E. Teller, Rev. Mod. Phys. 13, 75 (1941).
15. G. Herzberg, Infrared and Raman Spectra, Van Nostrand Reinhold, New York, pp. 106–108 (1945).
16. R. S. Mulliken, J. Chem. Phys. 23, 1997 (1955).
17. P. G. Wilkinson and R. S. Mulliken, J. Chem. Phys. 23, 1895 (1955).

PHOTOELECTRON SPECTRUM OF N_2O

P. M. Dehmer and J. L. Dehmer

The He I 584 Å photoelectron spectrum of N_2O was determined at a spectrometer resolution of 16 meV using both effusive and supersonic molecular beam sources. New structure is observed in all of the electronic bands studied. A preliminary report is given here.

The He I 584 Å photoelectron spectrum of N_2O shows four electronic bands corresponding to the $X^2\Pi$, $A^2\Sigma$, $B^2\Pi$, and $C^2\Sigma$ electronic states of N_2O^+. The spectrum has been studied by Brundle and Turner[1] at a resolution of approximately 30 meV. Weiss[2] reinvestigated the fourth band and observed vibrational structure not seen by Brundle and Turner. We have remeasured this spectrum using high resolution, rotational cooling, and good counting statistics in order to observe very weak vibrational structure. We observe new structure in each

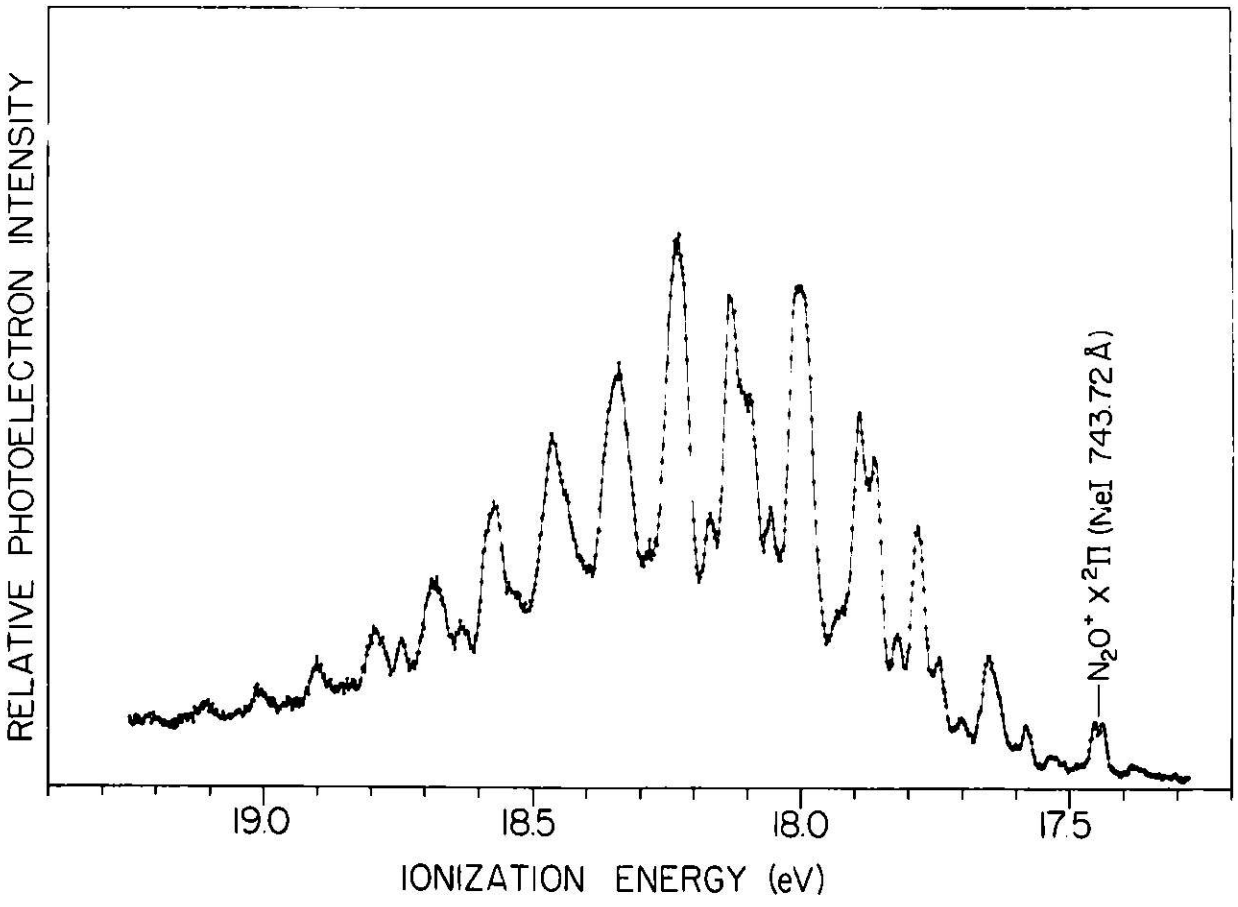

FIG. 1.--HeI photoelectron spectrum of N_2O^+ $B^2\Pi$ taken at 16 meV resolution.

of the four electronic bands. This structure has been analyzed for the X, A, and C states, and the results will be published soon. The structure in the B state is extremely complex and, as yet, has defied analysis. This band is shown in Fig. 1. The data were taken using the effusive molecular beam source with a spectrometer resolution of 16 meV. The energy scale of this spectrum is very accurately calibrated using the fortuitous appearance of the "impurity line" resulting from Ne I photoionizing the X band of N_2O. The main peaks in the B band are separated by 0.11 eV; however, the peaks show quite different profiles suggesting that the structure is not due simply to a single progression in the stretching frequency ν_1.

References

1. C. R. Brundle and D. W. Turner, Int. J. Mass Spectrom. Ion Phys. 2, 195 (1969).
2. M. J. Weiss, Chem. Phys. Lett. 39, 250 (1976).

OSCILLATOR-STRENGTH DISTRIBUTIONS FOR METHANOL AND ETHANOL FROM 7.5 TO 11.8 eV

J. C. Person and P. P. Nicole

A new absorption cell and split-beam detector system with photomultipliers and photon-counting equipment has been installed. We describe the data analysis and present new determinations of the oscillator strength for methanol from 7.66 to 11.76 eV and for ethanol from 7.52 to 11.76 eV.

As a part of a program to determine accurate oscillator-strength distributions we are measuring the absorption cross section σ over a wide range of photon energy E. We have recently improved our apparatus for measuring σ at low energies, and we report our new measurements for two simple alcohols.

The apparatus consists of a light source, monochromator, absorption cell, split-beam detection system, and microcomputer controller. A dc discharge in hydrogen produces light in a McPherson Model 630 lamp. The McPherson Model 225 monochromator has a 1200-lines/mm grating (Bausch and Lomb, 80-nm blaze, gold-coated), and it was used with a bandpass of 0.10 nm (FWHM). Data were recorded at 0.025 nm intervals. The new absorption cell is stainless steel with 3-mm thick LiF windows mounted on UHV flanges (Harshaw), and the optical path length is 8.486 cm. The gas pressure was measured with a capacitive manometer (MKS Instruments, Baratron Type 77H-1), and the cell temperature was measured with a platinum resistance sensor and a digital thermometer (Omega Engineering).

The detector system uses a split-beam technique to correct for fluctuations in the incident light intensity.[1] The light beam from the monochromator is split by a sodium salicylate-coated grid, with the portion passing through the grid going through the absorption cell and finally reaching a sodium salicylate-coated window in front of the photomultiplier that detects the transmitted-light intensity I_T. The splitter grid is at an angle of 45° with the light beam so that the sodium salicylate fluorescence is in view of a second photomultiplier, mounted perpendicularly. This photomultiplier detects the incident light intensity I_I, and the absorption cross section is given by

$$\sigma = \ln[(I_{T0}/I_{I0})/(I_{Tn}/I_{In})]/(nL) \quad ,$$

where L is the pathlength and the subscripts 0 and n refer to data taken with the cell empty and with the gas density equal to n, respectively. The differential oscillator strength in units of (1/eV) is then found by multiplying the σ values (in Mb units) by 0.0091116.

A new IMSAI 8080 microcomputer is used to control the experiment, compute preliminary corrections, provide real-time output of the processed data, and record the data on magnetic tape for later processing at the ANL Computer Center.

The photomultipliers in the detection system are RCA 4501-V3 tubes used at 1700 V. The amplifier-discriminators are Mech-Tronics Nuclear Model 511 (incident light) and Pacific Photometric Instruments Model AD-4 (transmitted light). The counters are fast enough to count every output pulse from the discriminators, but the photomultiplier-discriminator combination will fail to output additional pulses that arrive within a deadtime t_D. We determined that t_D is 26.6 ± 0.3 ns (incident light) and 16.9 ± 0.8 ns (transmitted light). The measured count rates C_m are corrected to C_c by an iterative solution to $C_c = C_m \exp(C_c t_D)$; the corrections are less than 5% for the present data.

The incident-light counts are corrected for dark counts, and two corrections are made to the transmitted-light counts. One is to correct for light generated at the splitter grid (or by fluorescence of the front window); this is estimated to be 0.025 of the counts detected by the incident-light detector. The other correction is for the combined effects of dark counts and scattered light, which is estimated by using the value of the count rate observed at 102 nm—below the transmission limit of the LiF windows. We plan to make more sophisticated corrections for scattered light,[2] and some small modulations of σ may result from improper correction for scattered light.

An additional correction is necessary when the light intensity is changing rapidly with wavelength, as the incident-light detector sees light at a wavelength 0.0003 nm longer than that of the transmitted-light detector. Apparently this is the result of a small misalignment of the monochromator,

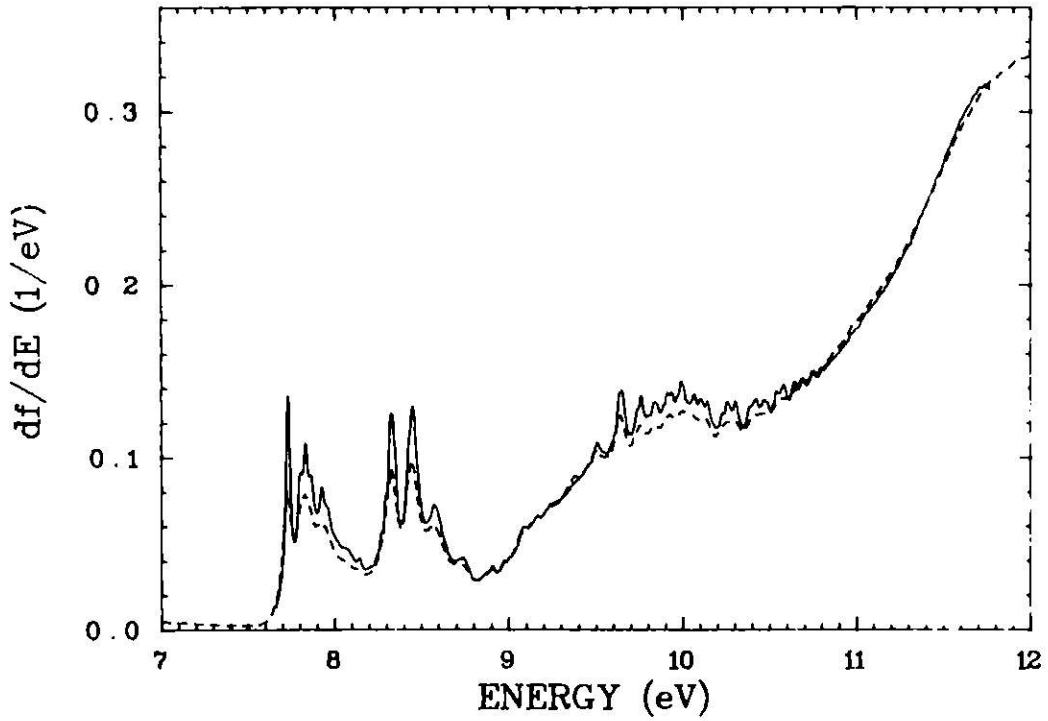

FIG. 1.--Oscillator-strength distribution for methanol. The broken line is data from Ref. 3 after renormalization.

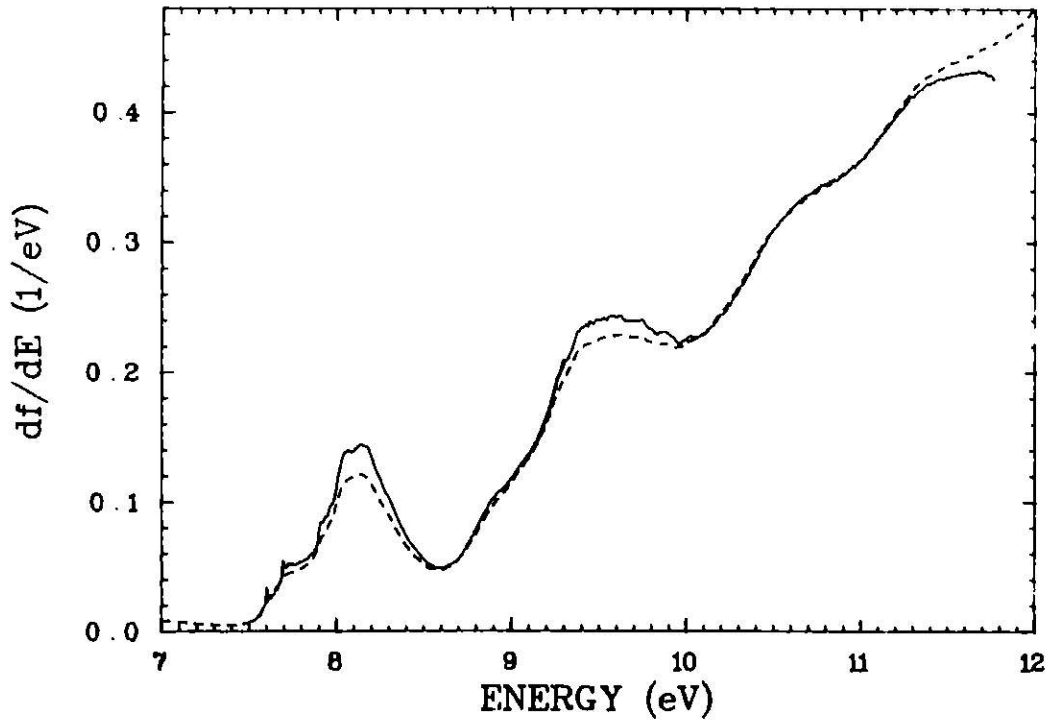

FIG. 2.--Oscillator-strength distribution for ethanol. The broken line is data from Ref. 3 after renormalization.

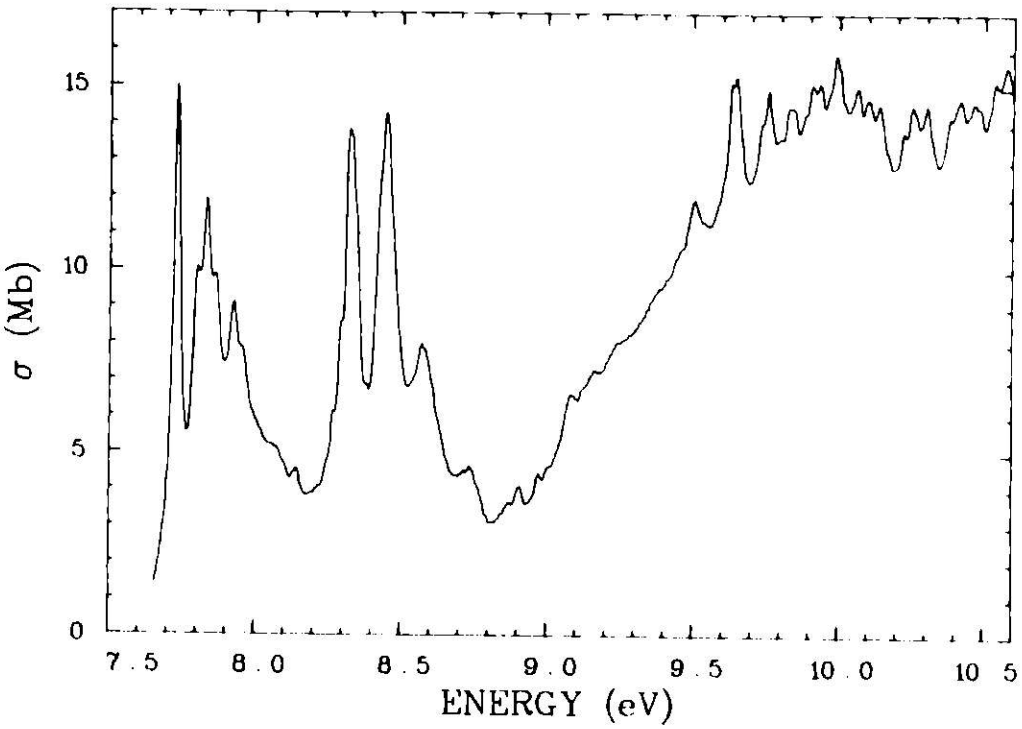

FIG. 3.--Absorption cross sections for methanol. (1 Mb = 10^{-18} cm^2)

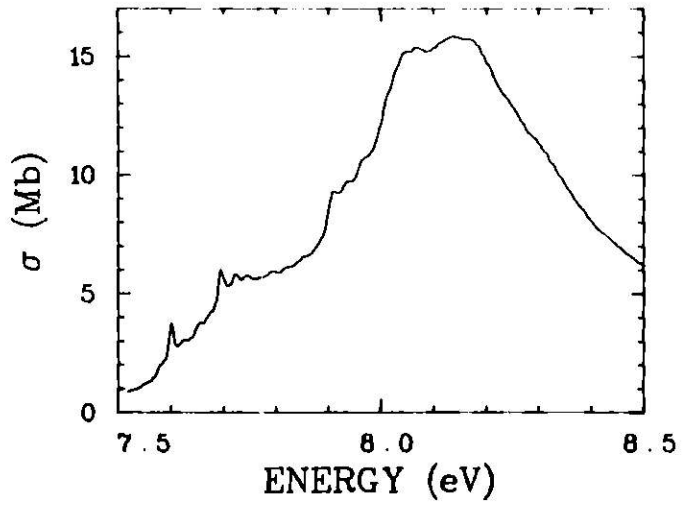

FIG. 4.--Absorption cross sections for ethanol.

causing the image of the emission line to move on the splitter grid as the wavelength is scanned.

There was a small change in the gas absorption during the time for a wavelength scan; repeated runs showed σ to be about 1% lower. The data were taken in two overlapping scans, each going towards decreasing E; the region of overlap is around 10.7 eV for methanol and 9.2 eV for ethanol.

The data presented are from a weighted-least-squares fitting routine, using data taken at 2 to 5 gas pressures and 2 to 11 empty cell runs. The data are preliminary in the sense that we need verification of the gas purity and the pressure and temperature calibrations, and we need a small correction for light that is reflected at the windows and makes three passes through the cell.

Figures 1 and 2 show the oscillator-strength distribution for methanol and ethanol, together with relative values of apparent df/dE, as measured by electron energy-loss (EEL) experiments at the National Bureau of Standards.[3] There is good agreement with the shape of the EEL spectra. The leveling-out or decrease of the optical values at $E > 11.7$ eV seems to be some artifact produced in this region of low window transmission, as it is not present in our data taken with windowless operation and a dual ion-chamber detector.[4] Some of the main areas of disagreement are regions with Rydberg transitions—areas where we have previously observed deviations,[4] probably resulting from a more rapid variation of the generalized oscillator strength with increasing momentum transfer for the Rydberg levels.[5] Figures 3 and 4 show enlarged views of the absorption spectra at lower energies. These reveal somewhat greater structure than previously reported.[6-8]

References

1. R. W. Ditchburn, J. Quant. Spectrosc. Radiat. Transfer 2, 361 (1962).
2. J. C. Person and P. P. Nicole, Argonne National Laboratory Radiological and Environmental Research Division Annual Report, October 1976–September 1977, ANL-77-65, Part I, p. 19.
3. R. H. Huebner and R. J. Celotta, Argonne National Laboratory Radiological and Environmental Research Division Annual Report, July 1971–June 1972, ANL-7960, Part I, p. 49.

4. J. C. Person and P. P. Nicole, Argonne National Laboratory Radiological and Environmental Research Division Annual Report, July 1973–June 1974, ANL-75-3, Part I, p. 53.
5. M. Krauss and S. R. Mielczarek, J. Chem. Phys. 51, 5241 (1969).
6. J. C. Person and P. P. Nicole, J. Chem. Phys. 55, 3390 (1971).
7. J. Hagège, P. C. Roberge, and C. Vermeil, Ber. Bunsenges. Phys. Chem. 72, 138 (1968).
8. D. R. Salahub and C. Sandorfy, Chem. Phys. Lett. 8, 71 (1971).

PHOTOIONIZATION OF THE OUTER SHELLS OF NEON, ARGON, KRYPTON, AND XENON, USING THE RELATIVISTIC RANDOM PHASE APPROXIMATION*

W. R. Johnson† and K. T. Cheng‡

Multichannel photoionization calculations using the relativistic random phase approximation for the outer shells in the rare gases, neon, argon, krypton, and xenon, are presented. Total cross sections and partial cross sections for ns subshells are determined and compared with experiment and with alternative calculations at low energies. Branching ratios of $^2P_{\frac{3}{2}}:^2P_{\frac{1}{2}}$ cross sections which are sensitive to relativistic and correlation effects are presented and compared with experiment. Angular distribution asymmetry parameters, β, determined for each subshell are found and compared with experiment; the differences between β values for $^2P_{\frac{1}{2}}$ and $^2P_{\frac{3}{2}}$ subshells in krypton and xenon emphasize the importance of relativistic effects in outer subshells of heavy elements. Values of β are given for outermost s electrons which show large relativistic effects near the "Cooper minima" of the corresponding partial cross sections. Eigenphases from the multichannel analysis are presented for argon to illustrate mathematical features of the present calculation.

*Abstract of a paper to be published.

†Physics Department, University of Notre Dame, Notre Dame, Indiana 46556.

‡Postdoctoral appointee from the University of Notre Dame.

RELATIVISTIC EFFECTS ON LOW-ENERGY $5s \rightarrow \epsilon p$ PHOTOIONIZATION FOR XENON*

W. R. Johnson† and K. T. Cheng‡

Under suitable conditions, relativistic corrections to the interaction of a photoelectron with its parent ion are enhanced, giving rise to large anisotropic final-state effects which can be observed in the photoelectron angular distribution. The particular example of $5s \rightarrow \epsilon p$ photoionization of Xe is considered in detail. It is shown that the angular asymmetry parameter β is reduced by a factor of 9 from its nonrelativistic value of 2 near the 5s "Cooper minimum," so that the energy dependence of β becomes a sensitive test of atomic correlation theories.

*Abstract of a paper published in Phys. Rev. Lett. 40, 1167 (1978).

†Physics Department, University of Notre Dame, Notre Dame, Indiana 46556.

‡Postdoctoral appointee from the University of Notre Dame.

ATOMIC PHOTOIONIZATION CALCULATIONS USING LOCAL CONTINUUM EXCHANGE APPROXIMATIONS

Jon Siegel, J. L. Dehmer, and Dan Dill*

The exchange interaction between a continuum electron and the bound electrons of an atom or molecule depends strongly on the kinetic energy of the electron. When our electron-molecule scattering calculations using the continuum multiple-scattering method[1,2] were modified to use energy-dependent approximations to the exchange interaction, immediate and substantial improvement was noted in the results.[3] No analogous improvement, however, was seen in corresponding photoionization calculations.[4] A study of atomic photoionization was therefore started to investigate this apparent discrepancy.

In a Hartree-Slater (HS)[5] photoionization calculation,[6] the continuum orbital is calculated in the same potential as all of the bound orbitals. This approximation has been widely used, and is fairly reliable compared to corresponding continuum Hartree-Fock calculations,[6] except in the region of a Cooper minimum. (Cooper minima do appear; however, their position and the height of the associated maxima are not accurate.) The inclusion of the energy-dependence of the exchange interaction, by the implementation of what we may term the Hartree-Hara (HH)[7] or Hartree-semiclassical (Hs)[8] model, restores this physical effect omitted from the HS model. These two models share with HS the restriction to independent electron interactions, and have the added deficiency that the continuum orbital is no longer automatically orthogonal to the bound orbitals.

HH and Hs results were calculated using all four forms of the dipole operator—length, velocity, acceleration based on the initial-state potential gradient, and acceleration based on the final-state potential gradient. In the HS model, of course, all four operators yield identical results (this was confirmed numerically). Calculations were performed on one or more subshells

*Consultant, Radiological and Environmental Research Division. Permanent address: Department of Chemistry, Boston University, Boston, Mass. 02215.

of six atoms, as shown in Table 1. In no case did a HH or Hs result agree better with the corresponding Hartree-Fock result[9,10] than did the HS calculation. To try to understand this, we compared the four operators' results within each subshell.

For some subshells, the results for all four operators coincided with each other and with the corresponding HS result (see Fig. 1 for an example) such results are denoted by the letter "a" in Table 1. For other subshells, the results using the four operators differed widely from each other and the HS result (Fig. 2); these are denoted by "c" in the table. Results showing moderate variation are denoted by "b."

In general, the best results are for cases where the open-shell nature of the final-state interaction would have little effect (e.g., core photoionization of Ne and Ar), while the worst are for valence orbitals where such interaction could be substantial (e.g., 2p of Ne and Ar, and 3p of Ar). This suggests to us that open-shell interactions must be taken into account in model

Table 1. Summary of atomic photoionization results. Energies are taken from Ref. 5.

Z	Atom	Subshell	E, Ry	HH	Hs
10	Neon	2p	- 1.47	c	c
		2s	- 3.17	c	b
		1s	- 62.99	a	a
18	Argon	3p	- 1.06	c	c
		3s	- 2.11	a	c
		2p	- 18.21	c	c
		2s	- 22.86	a	a
		1s	-232.5	a	a
54	Xenon	4d	- 5.26	c	a
3	Lithium	2s	- 0.40	b	b
		1s	- 4.40	c	c
11	Sodium	3s	- 0.38	a	c
80	Mercury	4f	- 9.39	a	a

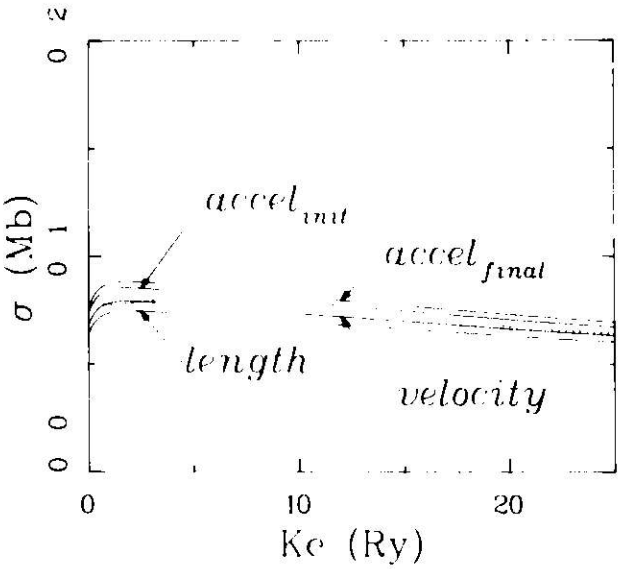

FIG. 1.--Sample calculation of Ar 12 → εp photoionization showing good agreement among all four forms of the dipole operator for the Hartree-Hara potential (solid lines), and the Hartree-Slater potential (dashed line).

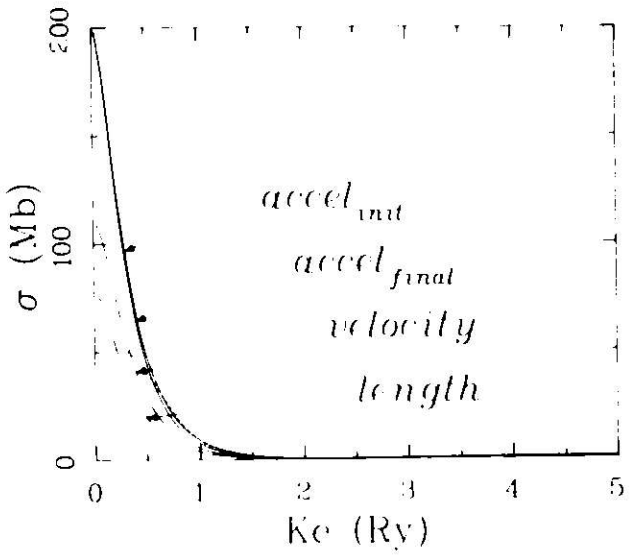

FIG. 2.--Sample calculation of Ar 3p → εp photoionization showing large discrepancies among the four forms of the dipole operator for the Hartree-semiclassical potential (solid lines) and the Hartree-Slater potential (dashed line). For comparison, the Hartree-Fock results (Ref. 9) yield peak values of 30 Mb (length) and 20 Mb (velocity).

exchange potentials for photoionization. Wendin[11] has investigated the nature of such potentials by inversion methods, and shows that for open shells there exists an "exchange barrier," much like (but in addition to) the well-known centrifugal barrier. A local exchange potential which reproduced this barrier could possibly yield results approaching Hartree-Fock, and we are currently investigating one possible such potential.[12]

An untested implication of this conclusion is that our success with electron-molecule scattering calculations has been due to the restriction to electron closed-shell cases. If this is so, then we could encounter increasing diffficulty with such open-shell targets as, e.g., NO or possibly even O_2. Thus, the importance of this problem may extend beyond photoionization applications.

References

1. D. Dill and J. L. Dehmer, J. Chem. Phys. 61, 692 (1974).
2. J. Siegel, D. Dill, and J. L. Dehmer, J. Chem. Phys. 64, 3204 (1976).
3. J. Siegel, Ph.D. Thesis, Boston University (1979).
4. S. Wallace, Ph.D. Thesis, Boston University (1979).
5. F. Hermann and S. Skillman, Atomic Structure Calculations, Prentice-Hall, Englewood Cliffs, N.J. (1963).
6. A. F. Starace, Theory of Atomic Photoionization, Handbuch der Physik, Vol. 31, W. Mehlhorn, Ed., Springer-Verlag, Berlin (to be published).
7. S. Hara, J. Phys. Soc. Japan 22, 710 (1967).
8. M. E. Riley and D. G. Truhlar, J. Chem. Phys. 63, 2182 (1975).
9. D. J. Kennedy and S. T. Manson, Phys. Rev. A 5, 227 (1972).
10. J. S. Shyn and S. T. Manson, Phys. Rev. A 11, 166 (1975).
11. G. Wendin, Many-electron effects in photoionization, Photoionization of Atoms and Molecules, Proc. Daresbury Mtg., 16 February 1978, B. D. Buckley, Ed., Science Research Council, Daresbury Laboratory, Daresbury, Warrington, WA4 4AD, U.K.
12. M. E. Riley and D. G. Truhlar, J. Chem. Phys. 65, 792 (1976).

GENERALIZED DIFFERENTIAL OSCILLATOR STRENGTHS FOR THE ELECTRON IMPACT IONIZATION OF HELIUM DETERMINED FOR LARGE AND INTERMEDIATE MOMENTUM TRANSFERS AT 300 AND 500 eV INCIDENT ENERGIES*

M. A. Dillon

Differential oscillator strengths for the electron impact ionization (ejected electron energy = 1 a.u.) of helium have been determined at ± 6% accuracy for incident electron energies of 300 to 500 eV and a scattering angular range of 7.5° to 30°. Relative measurements were made absolute by comparison with highly precise elastic differential cross sections. Small deviations from an accurate Born calculation are found throughout the range of experimental variables employed in the present work.

---

*Abstract of an article published in J. Chem. Phys. 68, 2037 (1978).

ELECTROSTATIC LENS CALCULATION

Michael A. Dillon

Introduction

Investigations employing beams of charged particles or studies which involve the detection of electrons and ions require the use of an apparatus with a number of strategically located electrostatic lenses. Until fairly recently, lens design has been largely the province ot specialists whose methods involve a judicious combination of model calculations, empirically derived lens data, and guesswork. However, beginning in 1967, Read and his co-workers calculated, in ab initio fashion, the properties of most important electrostatic lenses. Furthermore, they have determined and tabulated least squares coefficients which permit their calculations to be reproduced with high accuracy.[1]

The present article describes briefly a lens program in which the parameterizations of Read et al. appear as a block of subroutines. As an example, the code is used to optimize the performance of an electrostatic lens designed previously to implement electron scattering studies.

Formulation

A common application of an electrostatic lens system is illustrated in Fig. 1. Electrons, inelastically scattered from a target gas, exit the collision chamber through a pinhole, S_1, and ultimately reach an energy analyzer by way of an intervening lens. Typically, the system contains a second aperture S, which serves to limit the lens entrance angle. The purpose of the lens is to image the pinhole onto the focal plane of the analyzer and at the same time minimize α_2. This must be accomplished automatically over a considerable range of electron energies.

The ray depicted in the object space of the lens in the figure can be written

$$r_1 = \beta_1 + \alpha_1 z \quad . \tag{1}$$

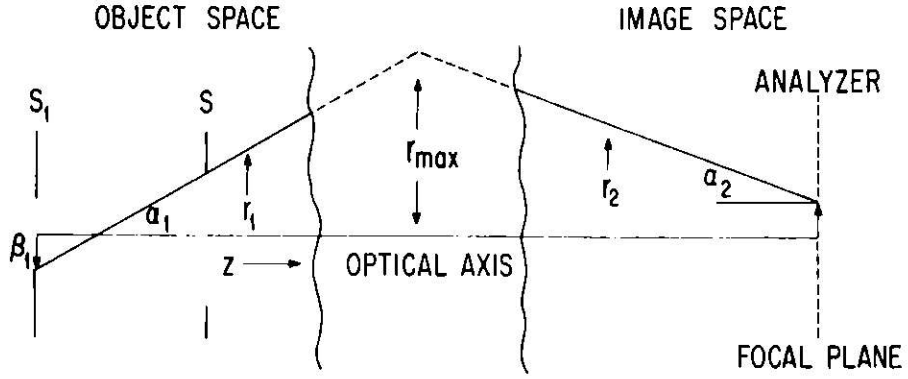

FIG. 1.--Diagram of an electron optical system depicting the ray of maximum angular aperture.

This is transformed by the action of the lens field to a linear representation in image space,

$$r_2 = \alpha_1 f_o + \frac{(\beta_1 + \alpha_i F_o)F_i}{f_i} - \frac{(\beta_1 + \alpha_1 F_o)z}{f_i} \quad . \tag{1b}$$

In Eq. 1b, F_o and F_i, the object and image focal distances, are measured from the point $z = 0$ rather than the conventional midplane. These two quantities, together with the object and image focal lengths f_o and f_i, constitute four cardinal elements from which all first order imaging properties can be derived. Let T_1 and T_2 be, respectively, the kinetic energies of electrons in the object and image space of a simple two-electrode or two-element lens. Its cardinal elements will be a function of a single lens ratio

$$\gamma = T_2/T_1 \quad . \tag{2a}$$

If an electrostatic lens consists, for example, of three electrodes, then in addition to γ the cardinal elements depend on a secondary lens ratio

$$G = T_1'/T_1 \quad , \tag{2b}$$

where T_1' is the electron kinetic energy at the surface of the intermediate electrode.

The most important properties of a lens can be written immediately in terms of its cardinal elements

$$I = \frac{f_o f_i}{F_o} + F_i \quad , \tag{3}$$

$$M = -\frac{f_o}{F_o} \quad , \tag{4}$$

$$A = -\frac{F_o}{f_i} \quad . \tag{5}$$

Here I, M, and A are, respectively, the image distance, lateral magnification, and angular magnification. The ray which possesses the largest possible initial angle α_1, is shown in Fig. 1. After traversing the lens, it enters the energy analyzer at an angle

$$\alpha_2 = -\frac{(\beta_1 + F_o\alpha_1)}{f_i} = -\frac{\beta_1}{f_i} + A\alpha_1 \quad , \tag{6}$$

relative to the optical (z) axis. The magnitude of α_2 can be used as an estimate of the angular spread of electrons accepted by the analyzer. In the same figure, the object and image space rays intersect a distance r_{max} above the optical axis. If δ is the maximum lens radius, then the filling factor, F is defined by

$$F = r_{max}/\delta = \left(\frac{\alpha_1\beta_2 - \beta_1\alpha_2}{\alpha_1 - \alpha_2}\right)/\delta \quad , \tag{7}$$

where α_1, α_2, and β_1 are defined in Fig. 1 and β_2 is the intercept of the image-space ray extrapolated to $z=0$ (cf. Eq. 1b).

When an electrostatic lens system consists of more than one independent lens, the cardinal elements of the composite system can be written in terms of parameters which describe the individual lenses. For example, in the case of two lenses, it can be readily shown that

$$f_o = \frac{f_{o1}f_{o2}}{F_{i1} - F_{o2}} \tag{8a}$$

$$f_i = \frac{f_{i1}f_{o1}}{F_{i1} - F_{o2}} \tag{8b}$$

$$F_o = \frac{f_{o1} f_{i1}}{F_{i1} - F_{o2}} + F_{o1} \tag{9a}$$

$$F_i = -\frac{f_{o2} f_{i2}}{F_{i1} - F_{o2}} + F_{i2} \tag{9b}$$

$$\gamma = \gamma_1 \gamma_2 \ , \tag{10}$$

where the subscripts 1 and 2 refer to the two lenses in the order of their displacement from $z = 0$. Then Eqs. 1–7 hold for the composite lens with its cardinal elements given by Eqs. 8a–9b. Moreover, Eqs. 8a–10 can be generalized to include the effects of more than two lenses. As an example, in Eq. 8a let $f_o = f_o^{(2)}$, $f_{o1} = f_o^{(1)}$, and $F_{o1} = F_o^{(1)}$. Then it is easily seen that for a chain of N lenses,

$$f_o^{(N)} = \frac{f_o^{(N-1)} f_{oN}}{F_1^{(N-1)} - F_{oN}} \ . \tag{11}$$

That is, a cardinal element of a composite of N lenses is obtained from a simple recursion relationship involving the elements of N^{th} lens and the $(N-1)^{th}$ composite lens.

Discussion

A computer code employing the approach outlined in the previous section was used to characterize the system displayed schematically in Fig. 2. The compound lens shown in the figure consists of two lenses separated by about 1.5". The first lens consists of three circular apertures with γ_1 and G_1 variable, while the second is a two-tube lens with γ_2 fixed in a retarding configuration. The lens is supposed to image S onto the object plane of a final (fixed) reduction lens. The design criteria call for $I = 2.713"$, $F < 0.5$ and $\alpha_2 \leq 5 \times 10^{-2}$.

For elastic scattering T_o, T_i, and T_f depicted in the figure, are the initial, intermediate, and final electron transit energies. If W is the energy lost in an inelastic collision, then the overall lens ratio varies according to

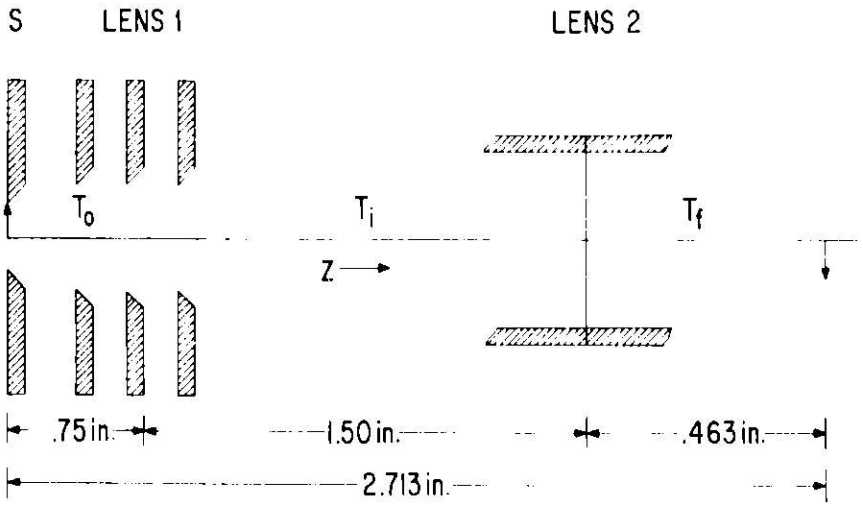

FIG. 2.--Outline of the practical lens system discussed in the text.

the relationship

$$\gamma = \gamma_1 \gamma_2 = \frac{T_i}{T_o - W} \cdot \frac{T_f}{T_i} \quad . \tag{12}$$

If T'_o is the voltage of the central electrode (measured with respect to the cathode) in lens 1, the secondary lens ratio G_1 varies in a similar manner;

$$G_1 = \frac{T'_o}{T_o - fW} \quad . \tag{13}$$

Normally f = 1. However, it is a simple matter to set up the electrical system so that f can vary between 0 and 1. Such an arrangement has been adopted in the present case.

In the application outlined above, the composite lens of Fig. 2 must image S onto a plane fixed with respect to z = 0. Hence, its major task is to maintain I = 2.713" while γ_1 and G_1 vary. Equation 3 can be rewritten with the aid of Eqs. 8a–9b to give

$$I = \frac{f_{o2} f_{i2}}{F_{o2} - I_1} + F_{i2} \quad , \tag{14}$$

where I_1 is the image distance of lens 1. Equation 14 reveals three distinct

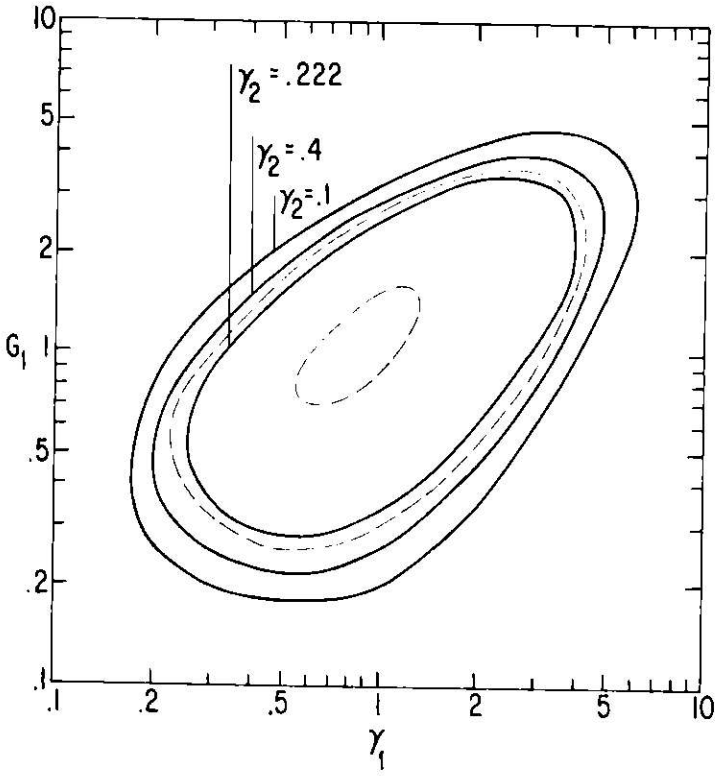

FIG. 3.--Zoom lens curves of the lens shown in Fig. 2. Pairs of γ_1 and G_1 for various values of γ_2 give rise to an image distance of 2.713".

Table 1. Spectrum simulation

W	G_1	γ_1	M	A, $\times 10$	α_2 $\times 10^2$	I_1 $\times 10^{-1}$	I	F
			A. Lens 2 = Two Tube ($\gamma_2 = 0.222$)					
0	2.750	1.251	-0.854	-2.22	-2.36	3.05	2.712	0.256
5	2.803	1.325	-0.831	-2.22	-2.35	-5.92	2.716	0.256
10	2.859	1.408	-0.809	-2.21	-2.35	-2.76	2.720	0.256
15	2.917	1.501	-0.788	-2.20	-2.35	-1.86	2.723	0.256
20	2.977	1.609	-0.771	-2.17	-2.35	-1.46	2.725	0.254
25	3.040	1.732	-0.756	-2.13	-2.36	-1.28	2.727	0.251
30	3.105	1.877	-0.745	-2.08	-2.37	-1.26	2.727	0.246
35	3.173	2.047	-0.739	-2.01	-2.38	-1.33	2.726	0.240
40	3.245	2.252	-0.739	-1.91	-2.41	-1.79	2.723	0.230
45	3.319	2.502	-0.750	-1.79	-2.45	-5.06	2.717	0.218
			B. Lens 2 = Three Tube $G_2 = 0.528$ ($\gamma_2 = 0.222$)					
0	2.750	1.251	-1.47	-1.25	-1.84	3.05	2.713	0.241
5	2.803	1.325	-1.45	-1.23	-1.84	-5.92	2.714	0.240
10	2.859	1.408	-1.43	-1.21	-1.85	-2.76	2.718	0.240
15	2.917	1.501	-1.39	-1.16	-1.85	-1.86	2.722	0.235
20	2.977	1.609	-1.37	-1.13	-1.86	-1.46	2.725	0.230
25	3.040	1.732	-1.36	-1.09	-1.86	-1.28	2.725	0.224
30	3.105	1.877	-1.34	-1.05	-1.86	-1.26	2.723	0.216
35	3.173	2.047	-1.37	-1.12	-1.86	-1.33	2.720	0.214
40	3.245	2.252	-1.34	-1.05	-1.87	-1.79	2.718	0.212
45	3.319	2.502	-1.33	-1.00	-1.89	-5.06	2.716	0.204

optical configurations which minimize variations in I.

Case A: $I_1 = \text{constant} < F_{o2}$.

In this arrangement lens 1 operates as a zoom lens projecting an image of S into the object space of lens 2. However, in order to focus electrons over a wide range of kinetic energies, it is sometimes necessary to program f in Eq. 13 so that

$$f = f(W) \quad .$$

Case B: $|I_1| >> F_{o2}, f_{o2}f_{12} < 1$.

Then $I \sim F_{i2}$. For the lens depicted in Fig. 2, this condition is achieved only when $\gamma_2 = 0.222$. In order that a system of this type function over a range of γ_2, it is necessary that lens 2 be more complicated than a two-element lens.

Case C: $I_1 \sim F_{i1} - f_{i1} \neq F_{o2}$.

In this mode, I_1 is a small negative constant. Such behavior is not apparent from Eq. 14. However, $F_{i1} - f_{i1}$ corresponds to the location of the image principle plane of lens 1. Object and image principle planes are practically invariant over a broad range of primary and secondary lens ratios. For geometrical reasons, Case C cannot be applied to the present system.

One option of the computer program generaltes zoom lens curves for an arbitrary chain of N lenses. Three curves for the lens of Fig. 2 are displayed in Fig. 3. The curves labeled $\gamma_2 = 0.1$ and $\gamma_2 = 0.4$ correspond to Case A. The thickness of each curve provides an estimate of the range of γ_1 and G_1 that yields $I = 2.713\ (1 \pm 0.02)$. The conditions used for the curves labeled $\gamma_2 = 0.222$ were those outlined in Case B. The roughly annular region between the dashed curves shows the range of γ_1 and G_1 which gives $I = 2.713\ (1 \pm 0.02)$. Hence it is evident that the Case B electron optical configuration provides the most stable lens performance.

Suppose, for example, that a gas is bombarded by 90-eV electrons and that an electron spectrometer with the lens of Fig. 2 is set to scan electron energies from the elastic peak to an energy loss of 45 eV. Using $\gamma_2 = 0.222$ and $f = 0.343$, a second option of the program produces the output shown in Table 1A. Note that I is nearly constant over the entire range of kinetic energies,

while M varies by only 13%. Also, the magnitudes of α_2 and F fall well within minimum performance standards. When desired, α_2 can be reduced somewhat by changing lens 2 to a three-tube lens. The results of a similar scan are displayed in Table 1B where the two-tube lens has been replaced by a three-tube lens with a thickness of one diameter. In addition to a modest reduction in α_2, the angular magnification, A, is nearly halved. The latter effect is very important for at once it reduces both beam and pencil angles. Note, for example, in Eq. 6, when $\beta_1 = 0$, $\alpha_2 = A\alpha_1$. Defined in this manner, α_2 is the pencil half angle in image space. Moreover, the curve in Fig. 3 labeled $\gamma_2 = 0.222$ can be used with a three-tube lens over a range of γ_2.

In addition to the examples given above, the first order properties of a number of popular compound lenses have been calculated. Owing to the above-mentioned parameterizations, each system was characterized completely at little expense.

Reference

1. E. Harting and F. H. Read, Electrostatic Lenses, Elsevier Scientific Publ. Co., Amsterdam, 1976.

GENERALIZED OSCILLATOR STRENGTH FOR IONIZATION OF THE K AND L INNER SHELLS OF ATOMS *

Steven T. Manson † and Mitio Inokuti

We have used the Herman-Skillman central-field potential to evaluate wavefunctions for the ejected electron and thence the density of the generalized oscillator strength per unit range of energy transfer. Our study includes all atoms with $3 \leqq Z \leqq 30$, and covers a large range of energy transfer and of momentum transfer. Comprehensive comparison with hydrogenic approximations with Slater and Clementi inner screening constants has been made. Our results should provide a trustworthy basis for many applications, including the analysis of electron energy-loss spectra, the normalization of analytical electron microscopy data in the energy-loss mode, and the evaluation of inner-shell corrections to the Bethe formula for stopping power of charged particles. The study has uncovered several notable systematics of the generalized oscillator strength for the K and L shell.

*Abstract of a paper presented at the Xth Annual Meeting of the Division of Electron and Atomic Physics, The American Physical Society, Madison, Wisconsin, 29 November–1 December 1978. See Bull. Am. Phys. Soc. 23, 1090 (1978).

†Consultant, Radiological and Environmental Research Division. Permanent address: Department of Physics, Georgia State University, Atlanta, Georgia 30303.

ELECTRON-SCATTERING CROSS SECTIONS PERTINENT TO ELECTRON MICROSCOPY*

Mitio Inokuti

Since the early work by Marton and Schiff, Lenz, and others, it has been recognized that analytical microscopy requires quantitative and trustworthy data on electron scattering cross sections. Much progress has been made in the physics of electronic collisions, both experimentally and theoretically. The purpose of the present article is to discuss some elements of the physics that determine cross sections and to indicate various sources of data that should be useful for analytical microscopy.

Cross sections for inelastic scattering at electron energies of interest to microscopy are largely governed by the generalized oscillator strength, i.e., the key notion in the Bethe theory. Current understanding of the generalized oscillator strength of atoms, molecules, and solids is rapidly growing with the electron energy-loss spectroscopy and attendant theoretical developments. Cross sections for elastic scattering require a different treatment because the validity of the first Born approximation is limited to lighter atoms, higher incident energies, and certain ranges of momentum transfer. However, it is now almost a routine matter to calculate phase shifts for a central potential, and thence, elastic-scattering cross sections for atoms. The choice of the suitable potential presents a nontrivial issue. A more substantial issue concerns scattering by nonspherical potentials, consideration of which is necessary for the elucidation of molecular-binding effects and solid-state effects. Recent progress in this area, e.g., due to Dehmer, Dill, and co-workers, is extremely encouraging.

Differences between a free atom or molecule and a solid in inelastic-scattering cross sections pose an important problem in microscopy. Again,

*An extended summary of an invited lecture at Workshop on Analytical Electron Microscopy, Ithaca, New York, July 1978. See article published in Ultramicroscopy 3, 423 (1978).

we are witnessing considerable progress, mostly in experiments on electron-energy losses. Sometimes, the interpretation of the differences is quite clear, for instance, when there are easily recognizable elementary excitations in solids, such as plasmons in metals and excitons in insulating crystals. The situation is not very clear when the spatial and spectral concentration of the monomer oscillator strength, as described by Fano's index, is only modest, as seems to be the case in organic substances, including biomolecules.

THE CONTINUUM MULTIPLE-SCATTERING APPROACH TO ELECTRON MOLECULE SCATTERING AND MOLECULAR PHOTOIONIZATION *

J. L. Dehmer and Dan Dill †

We review the formulation of the continuum multiple-scattering model (CMSM) and its application to electron-molecule scattering and molecular photoionization. The key elements of the theory are abstracted from earlier work and are presented together for the first time. Applications to electron scattering from N_2, CO_2, OCS, CS_2, and SF_6 are described, including integrated and differential cross sections for vibrationally elastic and inelastic collisions. Photoionization studies on N_2 and CO are also presented, including integrated photoionization cross sections, photoelectron angular distributions, EXAFS structure, the oriented-molecule case, electron-optical aspects of inner-shell photoionization, and the dynamic-symmetry-breaking effects of hole localization. Throughout all of these applications, special emphasis is given to the central role of shape resonances in the continuum dynamics of molecules.

* Abstract of an invited paper presented at the Electron and Photon Molecule Collisions Workshop, Asilomar Conference Grounds, Pacific Grove, California, 1–4 August 1978. The full article will be published in Electron and Photon Molecule Collisions, V. McKoy, T. Rescigno, and B. Schneider, Eds., Plenum Press, New York.

† Consultant, Radiological and Environmental Research Division. Permanent address: Department of Chemistry, Boston University, Boston, Massachusetts 02215.

SHAPE RESONANCES IN MOLECULAR PHOTOIONIZATION*

J. L. Dehmer and Dan Dill†

Shape resonances have begun to play a central role in the study of spectroscopy and dynamics of molecular photoionization. They manifest themselves as bands of enhanced absorption in the spectra of most (nonhydride) molecules and often stand out prominently against a nonresonant background. These resonances arise from centrifugal barriers in the molecular potential experienced by the escaping photoelectron, and their gross features can be described in terms of simple barrier-penetration concepts. Using both experimental data and recent theoretical calculations, we survey the properties (e.g., symmetry, spatial distribution, and dominant partial waves) of several molecular shape resonances and show how this information relates to the analysis of wavelength-dependent photoelectron spectra, photoelectron angular distributions, and photoabsorption spectra of molecules in different physical states. Special emphasis will be given to the correspondence between resonances in molecular photoionization and electron-molecule scattering.

*Abstract of an invited talk for the joint American Chemical Society-Chemical Society of Japan Chemical Congress, Honolulu, Hawaii, 1–6 April 1979.

†Consultant, Radiological and Environmental Research Division. Permanent address: Department of Chemistry, Boston University, Boston, Massachusetts 02215.

COMPREHENSIVE DIPOLE OSCILLATOR STRENGTH DISTRIBUTION FOR N_2

S. Wallace,* W. Kosman,† J. L. Dehmer, and Dan Dill‡

We present a preliminary account of our effort to compute the first comprehensive, ab initio dipole oscillator strength distribution for a molecule, using the continuum multiple-scattering method.

The continuum multiple scattering model[1,2] was developed to be a realistic tool to study molecular photoionization and electron-molecule scattering over wide spectral ranges. We are beginning to realize one of the specific objectives of this work—synthesis of purely theoretical, comprehensive dipole oscillator strength distributions of molecules. (Recent work on e-N_2 scattering[3,4] from 0 to 1000 eV illustrates the analogous scope in electron molecule scattering.) By computing all dipole transitions from the first excitation threshold to hundreds of volts above the K-shell ionization threshold, we hope to (a) test our theoretical method over the entire spectrum; (b) place in a broad perspective the novel molecular effects in photoabsorption spectra such as (shape) resonantly enhanced transitions to discrete and continuum states and EXAFS; (c) compute moments of the oscillator strength distribution to study molecular effects on macroscopic properties such as polarizability, stopping power, straggling, etc. Figure 1 shows four energy windows of the total dipole oscillator strength distribution for N_2 with a selection of scales to emphasize different parts of the spectrum. The most prominent features are (1) the intense $1\sigma_u \rightarrow 1\pi_g$ resonance transition just below the K-shell threshold at $\sim$29 Ry; (2) the well-known (see, e.g., Refs. 2,5,6) σ_u shape resonance

*Department of Chemistry, Boston University, Boston, Massachusetts 02215.

†Summer Faculty Research Participation Program Appointee, 1978. Permanent address: Department of Chemistry, Valparaiso University, Valparaiso, Indiana 46383.

‡Consultant, Radiological and Environmental Research Division. Permanent address: Department of Chemistry, Boston University, Boston, Massachusetts 02215.

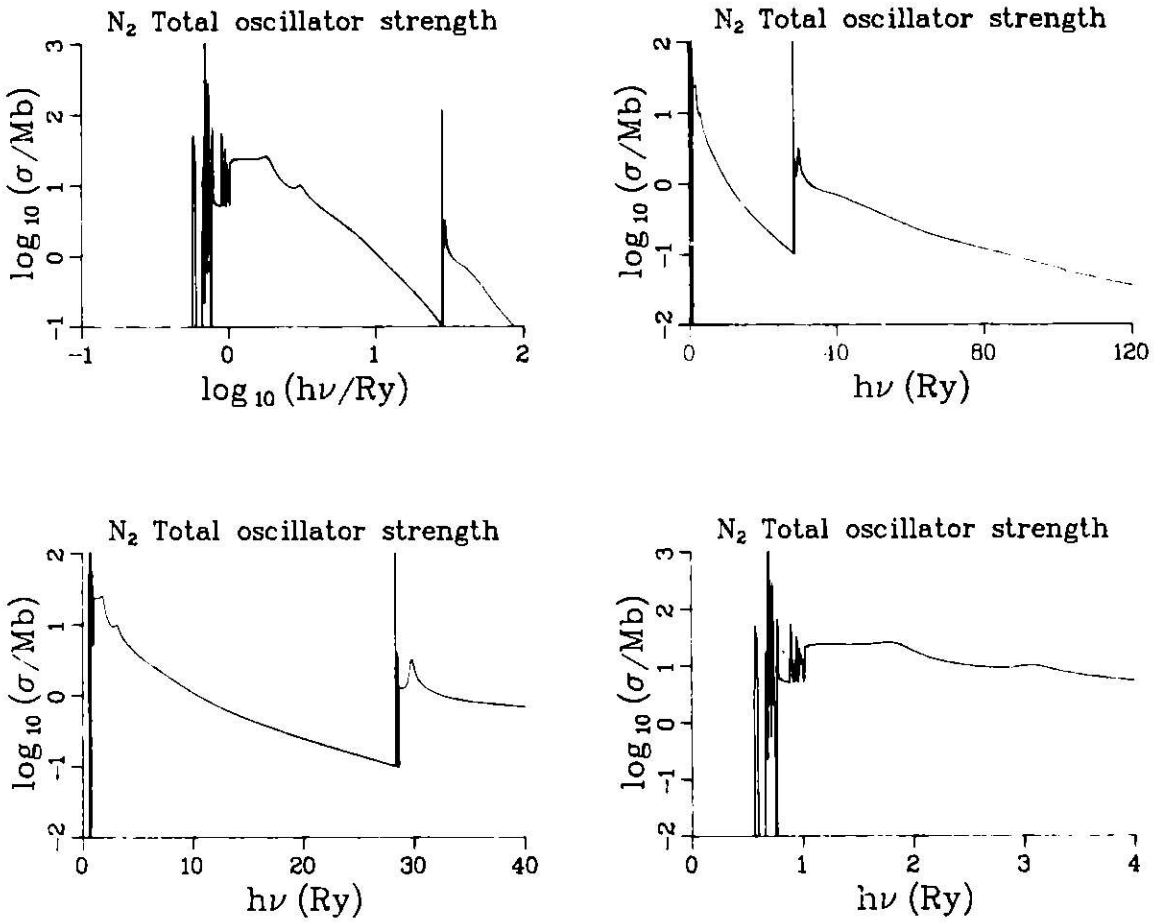

FIG. 1.--Total dipole oscillator strength distribution for N_2 computed with the continuum multiple scattering model. Four selections of energy window and energy scales are presented to emphasize different features in the spectrum.

in the continuum above the $1,2,3\sigma_g$ thresholds at $h\nu \sim 30$, 3, and 2 Ry, respectively; and (3) intense discrete structure below $h\nu \sim 1$ Ry. Barely perceptible in the upper right frame is the weak (~1%~ modulation due to EXAFS structure in the K-shell continuum. Extension to the high energy limit may be accurately made by filling to atomic cross sections at ~1000 eV above the K-shell threshold. Such supplementation (both in the high energy limit and higher portion of the Rydberg

series) is needed in addition to the calculation of moments of resulting distribution to meet the objectives (a–c) stated above. Work on these facets of the problem are proceeding.

References

1. D. Dill and J. L. Dehmer, J. Chem. Phys. 61, 692 (1974).
2. J. L. Dehmer and D. Dill, in Electron and Photon Molecule Collisions, V. McKoy, T. Rescigno, and B. Schneider, Eds., Plenum Press, New York, 1979.
3. D. Dill and J. L. Dehmer, Phys. Rev. A 16, 1423 (1977).
4. J. Siegel, J. L. Dehmer, and D. Dill, submitted to Phys. Rev. A.
5. J. L. Dehmer and D. Dill, J. Chem. Phys. 65, 5327 (1976).
6. R. B. Kay, Ph. E. Van der Leeuw, and M. J. van der Wiel, J. Phys. B 10, 2513 (1977).

PHOTOIONIZATION OF THE NITROGEN K-SHELL IN HCN

J. L. Dehmer, Jon Siegel, and Dan Dill*

Preliminary calculations of the photoionization cross section for the nitrogen K-shell in HCN are reported. The one-electron features resemble those of the isoelectronic molecule N_2.

Prompted by recent "pseudo-photon" measurements of the K-shell photoionization spectra of HCN by Brion and co-workers,[1] we have used the continuum multiple-scattering model[2,3] (CMSM) to investigate the purely one-electron aspects of this process. The nitrogen K spectrum starts flat at the I.P., has a prominent peak ~ 5 eV above threshold ($h\nu \sim 411$ eV), followed by a dip at $h\nu \sim 413$ eV and a broad maximum centered anywhere from $h\nu \sim 418$ to 422 eV. (A couple of minor features also occur, but we will focus only on the gross structure here.) In the absence of calculations to guide the interpretation of this spectrum, several alternative schemes were hypothesized; however, since these were rather tentative, we won't detail them here.

The calculations were performed in standard fashion (see, e.g., Ref. 4), using the CMSM, employing the Latter cutoff,[5] and the Slater exchange approximation[6] with the Schwarz values of α,[7] touching spheres, and an outer sphere centered on the center of mass. These calculations are somewhat more subject to error than earlier ones since the dipole field of HCN was neglected and the geometry of the CMSM field in this case led to a relatively large interstitial region. Nevertheless, we feel the qualitative aspects of this calculation should be reliable.

The results are given in Fig. 1. There we see that the cross section for π final continuum states steadily decreases, whereas that for σ states shows a broad shape resonance at ~ 422 eV. Hence, this calculation implies

*Consultant, Radiological and Environmental Research Division. Permanent address: Department of Chemistry, Boston University, Boston, Massachusetts 02215.

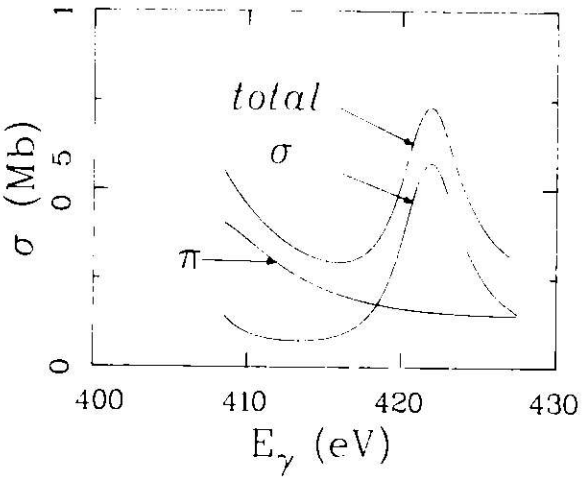

FIG. 1.--Cross sections for photoionization from the nitrogen K-shell in HCN.

an interpretation of the experimental spectrum which closely parallels that for the isoelectronic N_2 (see, e.g., Refs. 4, 8, 9, and references therein). Namely, an $\ell = 3$ type shape resonance produces the broad bump at $h\nu \sim 422$ eV (419 eV in N_2), and the narrow peak at $h\nu \sim 411$ eV (415 eV in N_2) represents one or more multiply-excited states formed by simultaneous excitation of a K-shell electron and an electron(s) from the valence shell. The dip is more pronounced in HCN since the many-electron and one-electron features are further apart. Actually, the narrow multiply-excited feature occurs at the same kinetic energy in both molecules, but the σ-type shape resonance lies higher in the kinetic energy spectrum in HCN. The degree to which the 411-eV feature interacts with and alters the shape of the one-electron continuum, i.e., produces an asymmetric Fano-Beutler profile,[10] cannot be assessed by us at this time; however, a simple superposition of a high-q profile at 411 eV on top of the one-electron continuum shape in Fig. 1 is the simplest and most plausible explanation of the experimental spectrum. Had the one-electron spectrum been nearly flat between threshold and 420 eV, one would then have had strong reason to believe that the dip was produced by an asymmetric Fano-Beutler profile resulting from a strong interaction between multiply-excited states and the underlying one-electron continuum.

References

1. C. E. Brion, private communication (1978).
2. D. Dill and J. L. Dehmer, J. Chem. Phys. 61, 692 (1974).
3. J. L. Dehmer and D. Dill, in Electron and Photon Molecule Collisions, V. McKoy, T. Rescigno, and B. Schneider, Eds., Plenum Press, New York, (1979).
4. J. L. Dehmer and D. Dill, J. Chem. Phys. 65, 5327 (1976).
5. R. Latter, Phys. Rev. 99, 510 (1955).
6. J. C. Slater, Quantum Theory of Molecules and Solids, Vol. IV, McGraw-Hill, Englewood Cliffs, N.J., (1974).
7. K. Schwarz, Phys. Rev. B 5, 2466 (1972).
8. R. B. Kay, Ph. E. van der Leeuw, and M. J. van der Wiel, J. Phys. B 10, 2513 (1977).
9. A. P. Hitchcock and C. E. Brion, to be published.
10. U. Fano, Phys. Rev. 124, 1866 (1961).

MOLECULAR PHOTOELECTRON ANGULAR DISTRIBUTIONS AS A PROBE OF DYNAMIC SYMMETRY BREAKING*

Dan Dill,[†‡] Scott Wallace,[†] Jon Siegel, and J. L. Dehmer

Molecular photoelectron angular distributions are shown to depend qualitatively on symmetry-breaking hole localization during inner-shell photoionization. This is illustrated by comparing localized and delocalized calculations of the asymmetry parameter $\beta(\epsilon)$ for K-shell photoionization of N_2 in the vicinity of the f-type shape resonance at approximately 10 eV above threshold. Comparison with the isoelectronic CO shows that the K-shell $\beta(\epsilon)$ for N_2, in the localized treatment, resembles that for the K shell of oxygen rather than carbon in CO, as shown in Fig. 1. This effect is traced to additional couplings in the

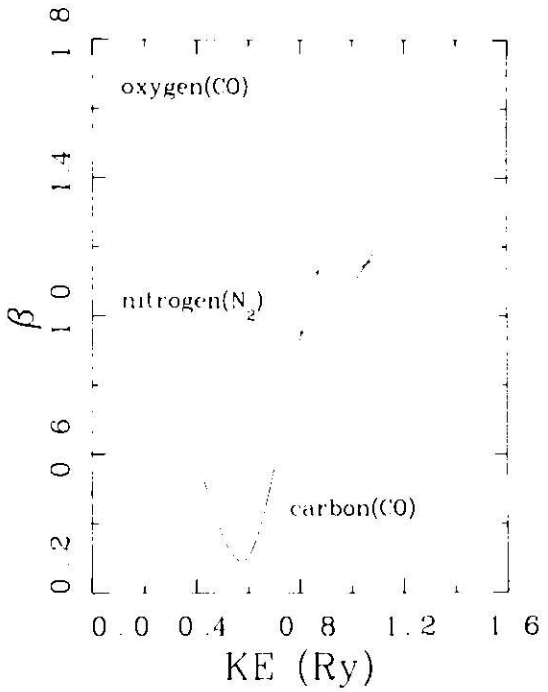

FIG. 1.--Photoelectron asymmetry parameters from a hole-localized treatment of K-shell photoionization of CO and N_2.

final state, induced by the lowered symmetry of the molecular core. Hence, photoelectron angular distributions probe the effects of hole localization on

---

*Summary of an article which appeared in Phys. Rev. Lett. 41, 1230 (1978); Erratum 42, 411 (1979).

†Department of Chemistry, Boston University, Boston, Massachusetts 02215.
‡Consultant, Radiological and Environmental Research Division.

the ejected electron's wavefunction, and thus complement the evidence based on the total energy of the ionic hole state first described by Bagus and Schaefer.[1]

Reference

1. P. Bagus and H. Schaeffer, J. Chem. Phys. 56, 224 (1972).

PHOTOELECTRON BRANCHING RATIOS AND ANGULAR DISTRIBUTIONS FOR ALL SHELLS OF SELECTED MOLECULES

Scott Wallace,* Dan Dill,*† and J. L. Dehmer

Extensive theoretical calculations of photoelectron branching ratios and angular distributions have been performed for all shells of several molecules. An illustrative example from this work is given.

We have recently completed survey calculations of photoionization processes involving all of the molecular levels of N_2, CO, NO, O_2, and SF_6, using the continuum multiple scattering model (CMSM)[1,2] in the framework of the independent electron approximation. Topics treated include (a) partial photoionization cross sections and (b) photoelectron angular distributions from threshold to at least 100 eV kinetic energy, (c) transitions to discrete states below each ionization threshold, (d) nuclear motion effects on branching ratios and angular distributions for individual vibrational levels and unresolved vibrational bands, (e) electron-optical effects in inner-shell photoionization, (f) hole-localization effects, (g) EXAFS structure, (h) effects of alternative exchange approximations and relaxation effects, and (i) a constant focus on effects of shape resonances and their manifestations in these various quantities as they differ from shell to shell.

As a small illustrative example of the results, we present in Figs. 1 and 2, the cross sections and photoelectron asymmetry parameters for the six molecular orbitals of CO. The presence of the well-known σ-type ($\ell = 3$ dominated) shape resonance (see, e.g., Refs. 2, 6, 7 and references therein) is anticipated in all shells and stands out clearly in the spectra of all σ-type initial states. It is present in the cross section for the 1π level but is swamped by the $1\pi \rightarrow \epsilon\delta$ component. Agreement between experiment and calculations is fairly good overall, although the presence of extensive autoionization structure

*Department of Chemistry, Boston University, Boston, Massachusetts 02215.
†Consultant, Radiological and Environmental Research Division.

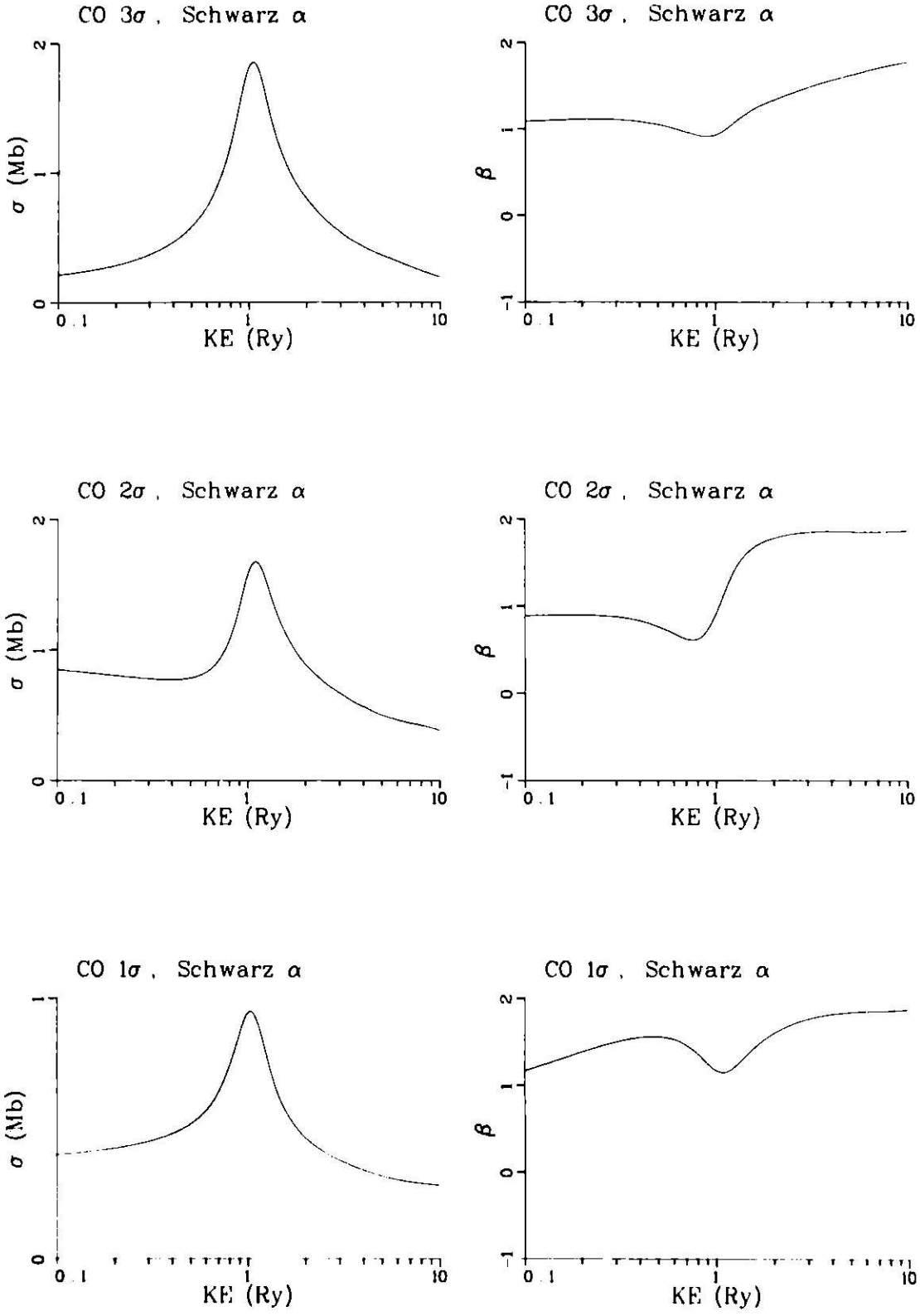

FIG. 1.--Partial photoionization cross sections and photoelectron asymmetry parameters for the 1, 2, and 3σ levels of CO.

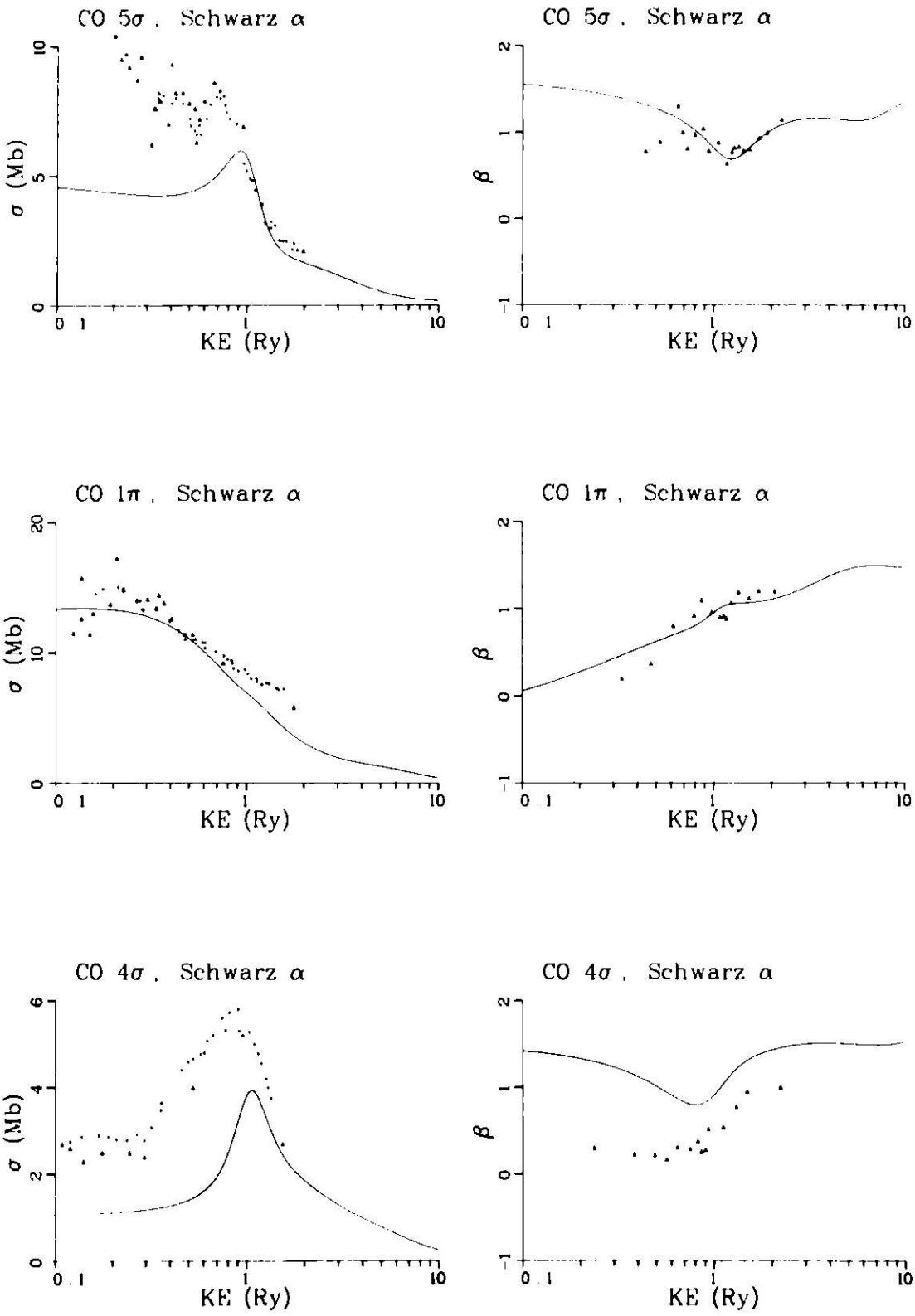

FIG. 2.--Partial photoionization cross sections and photoelectron asymmetry parameters for the 4 and 5σ and 1π levels of CO. Experimental cross section data from Plummer et al.[3] (+) and Samson et al.[4](Δ). Angular distribution data from Marr et al.[5]

in the valence shell data makes the comparison difficult. Good agreement between extensive angular distribution measurements and CMSM calculations is shown here for the first time. Previous comparisons[7] of the K-shell cross sections have indicated good qualitative agreement but a general tendency for the theoretical resonance profiles to be too narrow and intense. We have shown in our work on N_2 that this is, in large part, attributable to the neglect of nuclear motion, as an adiabatic-nuclei treatment of nuclear motion smears out the resonance structure, lowering and broadening it. Note similar valence shell calculations on CO over part of the present energy range were described earlier by Davenport.[8]

References

1. D. Dill and J. L. Dehmer, J. Chem. Phys. 61, 692 (1974).
2. J. L. Dehmer and D. Dill, Electron and Photon Molecule Collisions, V. McKoy, T. Rescigno, and B. Schneider, Eds., Plenum Press, New York, (1979).
3. E. W. Plummer, T. Gustafsson, W. Gudat, and D. E. Eastman, Phys. Rev. A 15, 1339 (1977).
4. J.A.R. Samson, G. N. Haddad, and J. L. Gardner, J. Phys. B 10, 1749 (1977).
5. G. V. Marr, J. M. Morton, R. M. Holmes, and D. G. McCoy, J. Phys. B 12, 43 (1979).
6. J. L. Dehmer and D. Dill, J. Chem. Phys. 65, 5327 (1976).
7. R. B. Kay, Ph. E. Van der Leeuw, and M. J. van der Wiel, J. Phys. B 10, 2513 (1977).
8. J. W. Davenport, Ph.D. Thesis, Department of Physics, University of Pennsylvania (1976).

FIXED-MOLECULE PHOTOELECTRON ANGULAR DISTRIBUTIONS: FIXED-ATOM (ISOTROPIC) LIMIT

Dan Dill,[*†] Scott Wallace,[†] and J. L. Dehmer

Ejection of photoelectrons along the electric vector of the light from an orbital $n_0\ell_0m_0$ in an atomic (isotropic) environment yields the angular distribution $|Y_{\ell_0 m_0}|^2$. This result, pointed out to us by Fadley, is obtained here in the general formalism of fixed-molecule angular distribution (FMAD) developed in recent papers. The dynamical requirements for the result and its generalization to photoelectron detection at arbitrary (fixed) angle relative to the electric vector are given. The intensity of the angular distribution reflects interference between the alternative orbital momenta of the ejected electron and should be, therefore, a sensitive function of light frequency near threshold, where effects of the Coulomb field are strong, and across photoionization resonances. The analysis may be relevant to, e.g., photoionization of orbitals protruding from transition-metal surfaces.

In a recent series of papers[1-4] a general formalism has been developed for the analysis of angular information in photoemission experiments on targets with fixed (but not necessarily known) orientation. Applications by us and others have probed successfully such diverse questions as chemisorption-site geometry[2,3,5] and photofragment angular distributions.[6] A key feature of the formalism is its geometrical basis. The dynamics of a particular (electric-dipole) process determine transition amplitudes $D^{-\Gamma_0}_{\ell m m_\gamma}$, which can either be the goal of a theoretical model or can be taken as parameters to be extracted from experiment. The former view has been taken in recent chemisorption studies,[2,3,5] whereas the latter view has been taken in the photofragmentation work.[6]

*Consultant, Radiological and Environmental Research Division.

†Department of Chemistry, Boston University, Boston, Massachusetts 02215.

Against this conceptual background we have recently learned from C. S. Fadley[7] that if the fixed target is approximated as a particular atomic orbital $n_0\ell_0m_0$ and if the photoelectron is detected along the electric vector of the light, then the angular distribution will map out the angular variation $|Y_{\ell_0 m_0}|^2$ of the initial atomic orbital. This intuitively correct result can be illustrated most simply by considering an ns atomic orbital. Then the photoelectron will have a p-type distribution peaked along the electric vector of the light (see, for example, Ref. 8). As the atom is rotated the photoelectron distribution will remain aligned along the electric vector; there will be no intensity variation along the electric vector, reflecting the spherical distribution of the ns atomic orbital. We show here that Fadley's result emerges from the general FMAD formalism when the transition amplitudes are specialized to an atomic target in an isotropic environment. The analysis makes clear when the result cannot hold and also provides its generalization to arbitrary experimental geometry.

The general formula for the FMAD $d\sigma(\vec{k}_e^{\gamma})/d\hat{R}_{\gamma}|_{m_p}$ measured from a position fixed with respect to the light source is Eq. 1 of Ref. 3, with the coordinates illustrated in Fig. 1 there: $\hat{k}_e^{\gamma}$ is the fixed detection direction, $\hat{R}_{\gamma}$ is the orientation of the target with respect to the electric vector ($m_p = 0$, linear polarization) or the propagation direction ($m_p = \pm 1$, left-, right-circular polarization) of the light. The dynamical transition amplitudes for atomic targets have the general form (see Eqs. 61–63, Ref. 9)

$$D^{-\Gamma_0}_{\ell m n_\gamma}(k_e^{\gamma}) = -\sum_{\ell' m'} (\ell_0 m_0, 1 m_\gamma | \ell' m')(10, \ell' 0 | \ell_0 0) A^{-}_{\ell m, \ell' m'} \bar{R}_{\epsilon\ell' \leftarrow n_0 \ell_0}, \tag{1}$$

where the photoelectron kinetic energy is $\epsilon = (k_e^{\gamma})^2$. The reduced transition moment

$$\bar{R}_{\epsilon\ell' \leftarrow n_0\ell_0} = \int_0^{\infty} r^2\, dr\, \bar{f}_{\epsilon\ell'}(r)\, r f_{n_0\ell_0}(r) \tag{2}$$

connects the $n_0\ell_0$ bound orbital (normalized to unity) to the $\epsilon\ell'$ continuum

orbital (normalized to be energy independent at r = 0). The complex transmission amplitudes $A^{-}_{\ell m,\, \ell' m'}$ characterize the rescattering of the $\epsilon \ell' m'$ continuum wave into asymptotic channels $\epsilon \ell m$ as the photoelectron escapes the atom to infinity.

The key approximation of our analysis is to assume the electron experiences an isotropic environment during its escape and therefore undergoes no rescattering. Then the transition amplitudes, Eq. 1, become

$$D^{-\Gamma 0}_{\ell m n_\gamma}(k_e^\gamma) = -(\ell_0 m_0, 1 m_\gamma | \ell m)(10, \ell 0 | \ell_0 0) A^{-}_{\ell}\, \bar{R}_\ell \quad , \tag{3}$$

where we have simplified the notation for the transition moment, Eq. 2, and the amplitudes A^{-}_{ℓ} now depend only on $\ell = \ell_0 \pm 1$. In this limit $A^{-}_{\ell} = e^{i\,\delta_\ell} \cos \delta_\ell A_\ell$, in terms of the phase shift δ_ℓ of the continuum electron wavefunction component with orbital momentum ℓ relative to Coulomb waves, and the real coefficient A_ℓ of the continuum wavefunction component at the nucleus, when the complete wavefunction is normalized in a standing-wave basis per unit energy range (Eqs. 61–63, Ref. 9).

By the approximation of Eq. 3 the dependence of the FMAD expression, Eq. 1 of Ref 3, on all orbital momentum projections is made explicit in terms of sums over m, m', and m'_ℓ of the product of five Wigner coefficients. As is shown in the Appendix, the sums can be carried out analytically to yield

$$\sum_{\substack{mm' \\ m_\gamma m'_\gamma}} (-1)^{m+m'} \gamma (\ell_0 m_0, 1m)_\gamma | \ell m)(\ell_0 m_0, 1 m'_\gamma | \ell' m')$$

$$\times (\ell m, \ell' - m' | K_e M_e)(1 m_\gamma, 1 - m'_\gamma | K_\gamma M_\gamma)(K_e - M_e, K_\gamma M_\gamma | KM)$$

$$= (-1)^{m_0} \hat{\ell}\, \hat{\ell}'\, \hat{\ell}_0^{-2} \sum_{\substack{mm' \\ m_\gamma m'_\gamma}} (1 - m_\gamma, \ell m | \ell_0 m_0)(1 m'_\gamma, \ell' - m' | \ell_0 - m_0)$$

$$\times (\ell - m, \ell' m' | K_e - M_e)(1 m_\gamma, 1 - m_\gamma | K_\gamma M_\gamma)(K_e - M_e, K_\gamma M_\gamma | K0)$$

$$= (-1)^{m_0} \hat{\ell}\,\hat{\ell}'\,\hat{\ell}_0^{-2} (\ell_0 m_0, \ell_0 - m_0 | K0)((\ell 1)\ell_0(\ell' 1)\ell_0 | (\ell\ell')K_e(11)K_\gamma)^{(K)} \quad , \qquad (4)$$

where we use the notation $\hat{x} = (2x+1)^{1/2}$ and the facts that $m_0 = m - m_\gamma = m' - m'_\gamma$ and that $\ell + \ell' - K_e$ and K_γ are restricted by Wigner coefficients in the general FMAD expression to be even. For computation the recoupling coefficient[10] in Eq. 4 is given in terms of the 9j symbol $X(j_1 j_2 j_{12}/j_3 j_4 j_{34}/j_{13} j_{24} j)$ by (see e.g., Ref. 10, Eq. 12.11 and related discussion)

$$((\ell 1)\ell_0(\ell' 1)\ell_0 | (\ell\ell')K_e(11)K_\gamma)^{(K)} = \hat{\ell}_0^2 \hat{K}_e \hat{K}_\gamma X(\ell 1 \ell_0/\ell' 1 \ell_0/K_e K_\gamma K) \quad . \qquad (5)$$

The last equality in Eq. 4 follows from the definition of the recoupling coefficient[10] and is verified in the Appendix. (See also Ref. 11.)

The essence of the important result in Eq. 4 is that it restricts the maximum harmonic K_{max} to $2\ell_0$, rather than the usual[1,3] restriction to $2\ell_{max}+2$, where ℓ_{max} is the maximum orbital momentum of the continuum electron. That is, in the atomic (isotropic) limit, the maximum harmonic of the FMAD is determined by the initial state rather than the final state and the dipole character of the interaction.

Substituting Eqs. 3–5 in the general FMAD expression, Eq. 1 of Ref. 3, we obtain for the atomic (isotropic) limit

$$d\sigma(\vec{k}_e^{\gamma})/d\hat{R}_\gamma\big|_{m_p} = 4\pi^2 \alpha h\nu (4\pi)^{-\frac{1}{2}} \sum_{\ell\ell'} i^{(\ell'-\ell)} e^{i(\sigma_\ell - \sigma_{\ell'})} \hat{\ell}^2 \hat{\ell}'^2 A_\ell^- A_{\ell'}^{-*} \bar{R}_\ell \bar{R}_{\ell'} (-1)^{m_p}$$

$$\times (10, \ell 0 | \ell_0 0)(10, \ell' 0 | \ell_0 0) \sum_{K_e M} (-1)^M (\ell 0, \ell' 0 | K_e 0) Y_{K_e - M}(\hat{k}_e^{\gamma})$$

$$\times \sum_{K_\gamma} \hat{K}_\gamma (1 m_p, 1 - m_p | K_\gamma 0) \sum_K (K_e M, K_\gamma 0 | KM)(-1)^{m_0} (\ell_0 m_0, \ell_0 - m_0 | K0)$$

$$\times X(\ell 1 \ell_0/\ell' 1 \ell_0/K_e K_\gamma K) D^K_{0M}(\hat{R}_\gamma) \quad , \qquad (6)$$

where $\sigma_\ell = \arg \Gamma(\ell + 1 - i/k_e^{\gamma})$ is the Coulomb phase. This result, then, pertains to arbitrary detection direction $\hat{k}_e^{\gamma}$. If, however, we further restrict ourselves to detection along the electric vector of the light, i.e., if we set $m_p = 0$ and

$\hat{k}_e^\gamma = (\theta_e^\gamma, \phi_e^\gamma) = (0, \phi_e^\gamma)$, then the summation over M reduces to a single term by[12]

$$Y_{K_e - M}(0, \phi_e^\gamma) = \delta_{M0} \hat{K}_e (4\pi)^{-\frac{1}{2}} \quad , \tag{7}$$

and we can use the contraction[11]

$$\sum_{K_e \overline{K}_\gamma} \hat{K}_e \hat{K}_\gamma (\ell 0, \ell' 0 | K_e 0)(10, 10 | K_\gamma 0)(K_e M, K_\gamma 0 | KM) X(\ell 1 \ell_0 / \ell' 1 \ell_0 / K_e K_\gamma K)$$

$$= \hat{\ell}_0^{-2} (\ell 0, 10 | \ell_0 0)(\ell_0 0, \ell_0 0 | K0) \quad , \tag{8}$$

and the spherical harmonic addition theorem[12]

$$(-1)^{m_0} \hat{\ell}_0^2 \sum_{\overline{K}} (\ell_0 m_0, \ell_0 - m_0 | K0)(\ell_0 0, \ell_0 0 | K0) D^K_{00}(\hat{R}_\gamma) = 4\pi |Y_{\ell_0 m_0}(\theta_\gamma, \phi_\gamma)|^2 \tag{9}$$

to obtain

$$d\sigma(\vec{k}_e^\gamma, \theta_e^\gamma = 0)/d\hat{R}_\gamma |_{m_p = 0} = |Y_{\ell_0 m_0}|^2 4\pi^2 \alpha h\nu$$

$$\times \sum_{\ell\ell'} (\ell_0 0, 10 | \ell 0)^2 (\ell_0 0, 10 | \ell' 0)^2 i^{(\ell' - \ell)} e^{i(\sigma_\ell - \sigma_{\ell'})} A_\ell^{-*} A_\ell^- \overline{R}_{\ell'} \overline{R}_\ell$$

$$= |Y_{\ell_0 m_0}|^2 4\pi^2 \alpha h\nu \, (2\ell_0 + 1)^{-2} [(\ell_0 + 1)^2 \cos^2 \delta_+ A_+^2 \overline{R}_+^2 + \ell_0^2 \cos^2 \delta_- A_-^2 \overline{R}_-^2$$

$$- 2\ell_0 (\ell_0 + 1) \cos \delta_+ \cos \delta_- A_+ A_- \overline{R}_+ \overline{R}_- \cos(\phi_+ - \phi_-)] \quad , \tag{10}$$

where the second equality follows from explicit expressions for the Wigner coefficients.[13] The subscripts ± denote $\ell = \ell_0 \pm 1$ and similarly for ℓ', the phase $\phi = \sigma - \delta$ has been introduced, and we have expressed A^- in terms of δ and A. Equation 10 corresponds to the Fadley result.[7]

We see from Eq. 10 that the intensity is modulated by the interference between the alternative orbital-momentum components $\ell_\pm$ of the ejected electron wavefunction. This modulation is expected to be quite pronounced (i) near threshold, where the Coulomb phaseshift difference $\sigma_+ - \sigma_-$ varies rapidly with energy,[14] and (ii) across photoionization resonances where often one

orbital-momentum component phaseshift δ_ℓ is rapidly varying.[14,15] In particular, the interference terms mean the spectral variation of the fixed-atom photocurrent should be more pronounced than the corresponding random-atom (integrated) photoionization cross section, for which no interference terms occur.[1-4]

Summarizing, if photoemission is assumed to be from a single orbital $n_0\ell_0m_0$ in an isotropic environment, then the dynamical relation, Eq. 3, leads immediately to the restriction that the maximum harmonic of the FMAD be no greater than $2\ell_0$, by the sum rule, Eq. 4, and the cross section in Eq. 6 results. Furthermore, if the photoelectron is detected along the axis of linear polarization, then Eq. 6 simplifies to Eq. 10, which determines the FMAD simply as the angular distribution $|Y_{\ell_0 m_0}|^2$ of the initial-state orbital $n_0\ell_0m_0$. Deviations of measured "fixed-atom" angular distributions from Eqs. 6 or 10 will reflect the breakdown of the approximation in Eq. 3.

Acknowledgement

We are grateful to C. S. Fadley for his remarks which prompted this study.

Appendix

The relations 4 and 8 in the text are examples of a general class of relations between Wigner coefficients and recoupling coefficients for four angular momenta. The definition of the four-momenta recoupling coefficient is [see Eq. 12.8 of Ref. 10]

$$(j_{12}j_{34}|j_{13}j_{24})^{(j)} \quad ((j_1j_2)j_{12}(j_3j_4)j_{34}|(j_1j_3)j_{13}(j_2j_4)j_{24})^{(j)}$$

$$= \sum_{\substack{m_1m_2m_3m_4 \\ m_{12}m_{34}m_{13}m_{24}}} (jm|j_{12}m_{12},j_{34}m_{34})(j_{12}m_{12}|j_1m_1,j_2m_2)(j_{34}m_{34}|j_3m_3,j_4m_4)$$

$$\times (j_1m_1,j_3m_3|j_{13}m_{13})(j_2m_2,j_4m_4|j_{24}m_{24})(j_{13}m_{13},j_{24}m_{24}|jm) \quad . \qquad (A1)$$

This is equivalent to the alternative definition[11] in terms of 3j symbols. By use of the orthonormality relation

$$\sum_{m_{12}m_{34}} (jm|j_{12}m_{12},j_{34}m_{34})(j_{12}m_{12},j_{34}m_{34}|j'm') = \delta_{jj'}\delta_{mm'} \qquad (A2)$$

we can obtain from the relation A1 the result

$$(j_{12}m_{12},j_{34}m_{34}|jm)(j_{12}j_{34}|j_{13}j_{24})^{(j)}$$

$$= \sum_{\substack{m_1m_2m_3m_4 \\ m_{13}m_{24}}} (j_{12}m_{12}|j_1m_1,j_2m_2)(j_{34}m_{34}|j_3m_3,j_4m_4)$$

$$\times (j_1m_1,j_3m_3|j_{13}m_{13})(j_2m_2,j_4m_4|j_{24}m_{24})(j_{13}m_{13},j_{24}m_{24}|jm) \quad . \qquad (A3)$$

The relation 4 in the text is an example of this result. By use of

$$\sum_{j_{12}m_{12}} (j_1m_1',j_2m_2'|j_{12}m_{12})(j_1m_1,j_1m_1|j_{12}m_{12}) = \delta_{m_1m_1'}\delta_{m_2m_2'} \quad , \qquad (A4)$$

the inverse relation to Eq. A2, we can obtain from the relation A3 the result

$$\sum_{j_{12}m_{12}} (j_1 m_1, j_2 m_2 | j_{12} m_{12})(j_{12} m_{12}, j_{34} m_{34} | jm)(j_{12} j_{34} | j_{13} j_{24})^{(j)}$$

$$= \sum_{m_3 m_4} (j_{34} m_{34} | j_3 m_3, j_4 m_4)$$

$$\times (j_1 m_1, j_3 m_3 | j_{13} m_{13})(j_2 m_2, j_4 m_4 | j_{24} m_{24})(j_{13} m_{13}, j_{24} m_{24} | jm) , \qquad (A5)$$

where the moot sums over m_{13} and m_{24} have been omitted. Finally, by use of

$$\sum_{j_{34}m_{34}} (j_3 m_3', j_4 m_4' | j_{34} m_{34})(j_{34} m_{34} | j_3 m_3, j_4 m_4) = \delta_{m_3 m_3'} \delta_{m_4 m_4'} \qquad (A6)$$

we can obtain from the relation A6 the result

$$\sum_{\substack{j_{12}m_{12} \\ j_{34}m_{34}}} (j_1 m_1, j_2 m_2 | j_{12} m_{12})(j_3 m_3, j_4 m_4 | j_{34} m_{34})$$

$$\times (j_{12} m_{12}, j_{34} m_{34} | jm)(j_{12} j_{34} | j_{13} j_{23})^{(j)}$$

$$= (j_1 m_1, j_2 m_2 | j_{12} m_{12})(j_3 m_3, j_4 m_4 | j_{34} m_{34})(j_{12} m_{12}, j_{34} m_{34} | jm) . \qquad (A7)$$

The relation 8 in the text is an example of this result.

Expressions equivalent to the relations A3, A5, and A7 are available in terms of 3j symbols,[11] but we find the expressions in terms of transformation (Wigner) coefficients more transparent, by their emphasis on the inherent recoupling process.

References

1. D. Dill, J. Chem. Phys. 65, 1130 (1976).
2. D. Dill, J. Siegel, and J. L. Dehmer, J. Chem. Phys. 65, 3158 (1976).
3. S. Wallace, D. Dill, and J. L. Dehmer, Phys. Rev. A 17, 2004 (1978).
4. S. Wallace and D. Dill, Phys. Rev. B 17, 1692 (1978).
5. J. W. Davenport, Phys. Rev. Lett. 36, 945 (1976).
6. J. L. Dehmer and D. Dill, Phys. Rev. A 17, 164 (1978).
7. C. S. Fadley, private communication (1978); to be published.
8. J. L. Dehmer and D. Dill, Phys. Rev. Lett. 37, 1049 (1976).
9. D. Dill and J. L. Dehmer, J. Chem. Phys. 61, 692 (1974).

10. U. Fano and G. Racah, Irreducible Tensorial Sets, Academic Press, New York (1959).
11. D. M. Brink and G. R. Satchler, Angular Momentum, Sec. Ed., Oxford University Press, London, p. 144 (1968).
12. M. E. Rose, Elementary Theory of Angular Momentum, Wiley and Sons, New York (1957).
13. A. R. Edmonds, Angular Momentum in Quantum Mechanics, Princeton University, Princeton, N.J. (1957).
14. D. Dill, Phys. Rev. A 7, 1976 (1973).
15. J. L. Dehmer and D. Dill, J. Chem. Phys. 65, 5327 (1977); also paper to be published.

ELASTIC ELECTRON SCATTERING CROSS SECTIONS FOR N_2 FROM 0 TO 1000 eV. ENERGY-DEPENDENT EXCHANGE POTENTIALS*

Jon Siegel, J. L. Dehmer, and Dan Dill†

Initial calculations of elastic e^--N_2 scattering[1,2] using the continuum multiple-scattering method (CMSM)[3,4] were reasonably successful in reproducing experimental integrated cross sections[1] over the wide energy range from threshold to 1000 eV, and differential cross sections[2] (DCS) to 30 eV (DCS calculations were not carried beyond 30 eV). Further, they provided a simple physical interpretation of the dominant spectral features in terms of molecular shape resonances and the l-composition of the continuum molecular wavefunctions. These calculations also displayed inherent limitations which stemmed not from the CMSM itself, but from the model potential employed with it,[5] which was based on the Slater Xα exchange approximation.[6] The Slater Xα exchange approximation is specialized for bound-state calculations,[6] and its use in continuum calculations is problematic.[1,5] Specifically, it is energy-independent and thus cannot reflect the decreasing exchange interactions with increasing electron kinetic energy, and it includes a self-interaction component[6] which distorts the electrostatic portion of the potential. We have, therefore, repeated the calculations of Refs. 1 and 2 using the Hara[7] and semiclassical[8] continuum exchange approximations, which avoid these two deficiencies.

Figure 1 contrasts the previous integrated cross section results using Xα potentials[1] A (long dashes) and B (short dashes) with the corresponding Hara (solid) and semiclassical (dash-dot) exchange potential calculations. All three calculations have had the polarization potential cutoff parameter adjusted to position the π_g resonance at the proper experimental energy of 2.39 eV.[9] Both Hara and semiclassical exchange show a clear improvement

---

*Summary of a paper submitted for publication.

† Consultant, Radiological and Environmental Research Division. Permanent address: Department of Chemistry, Boston University, Boston, Massachusetts 02215.

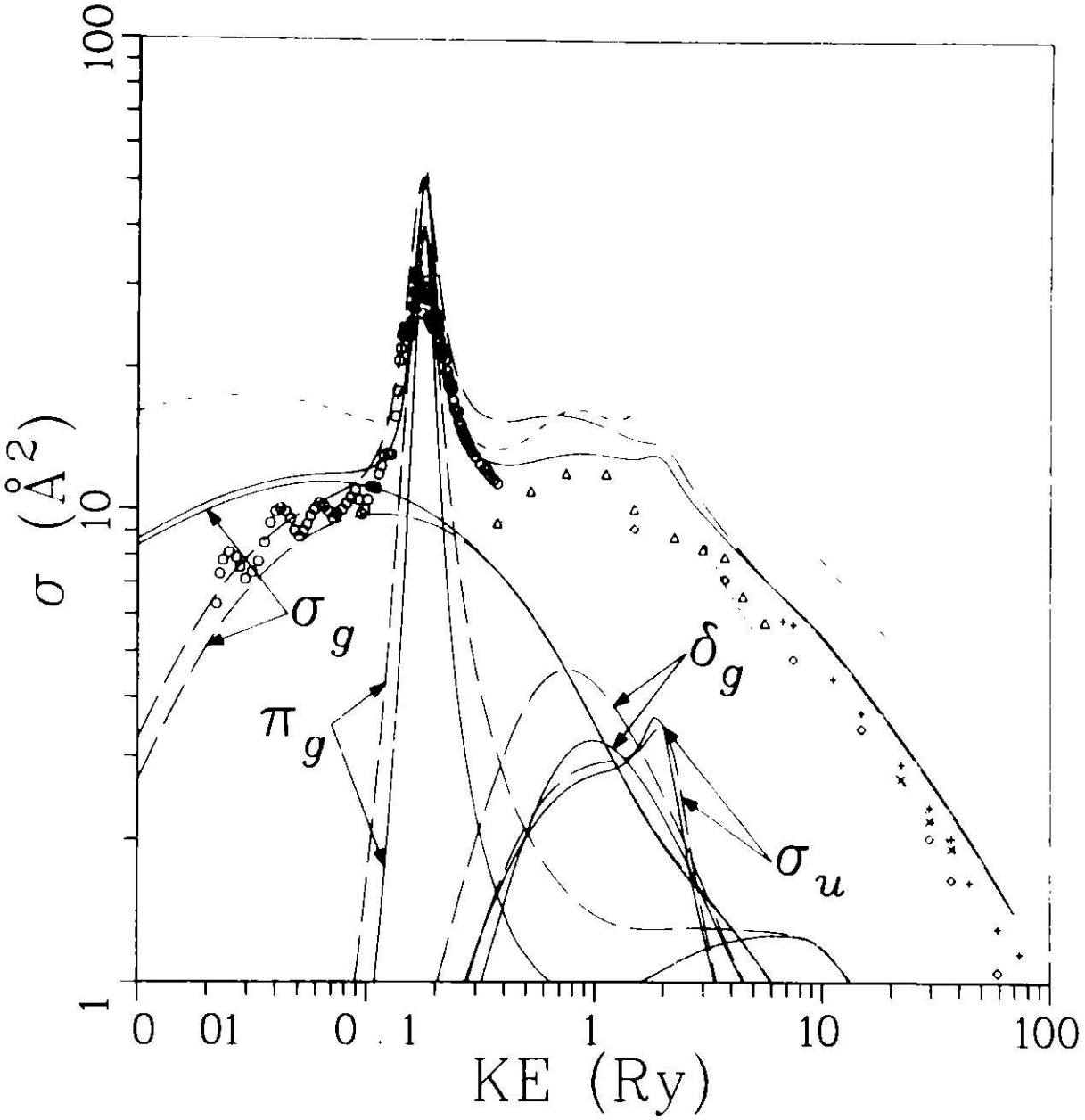

FIG. 1.--Integrated cross sections for elastic e^--N_2 scattering comparing various exchange approximations. Theoretical results include Hara exchange, —; Semiclassical exchange, -·-·-; Slater Xα potential A, — — —; and B, ---- (the latter two are reproduced from Ref. 1). Comparison is made to the following experimental data: Golden,[9] O; Bromberg,[10] ×; Dubois and Rudd,[11] ◇ ; Srivastava et al.,[12] △; and Hermann et al.,[13] +.

over Xα potential A, with the semiclassical result being better below the π_g resonance and the Hara result better above it. Note that the σ_u shape resonance which occurs at 26 eV in the Hara exchange calculation has recently been observed (at 22 eV) in the total cross section measurements of Kenergly.[14]

In the static-exchange-polarization (SEP) framework[15] employed here, the total potential V is constructed as the sum,

$$V(\vec{r}) = V_S(\vec{r}) + V_E(\vec{r}) + V_P(\vec{r}) \quad , \tag{1}$$

of electrostatic, exchange, and polarization components, so that the effects of each of these components may be investigated individually. Figure 2 contrasts the results using the full SEP potential with Hara exchange (solid line,

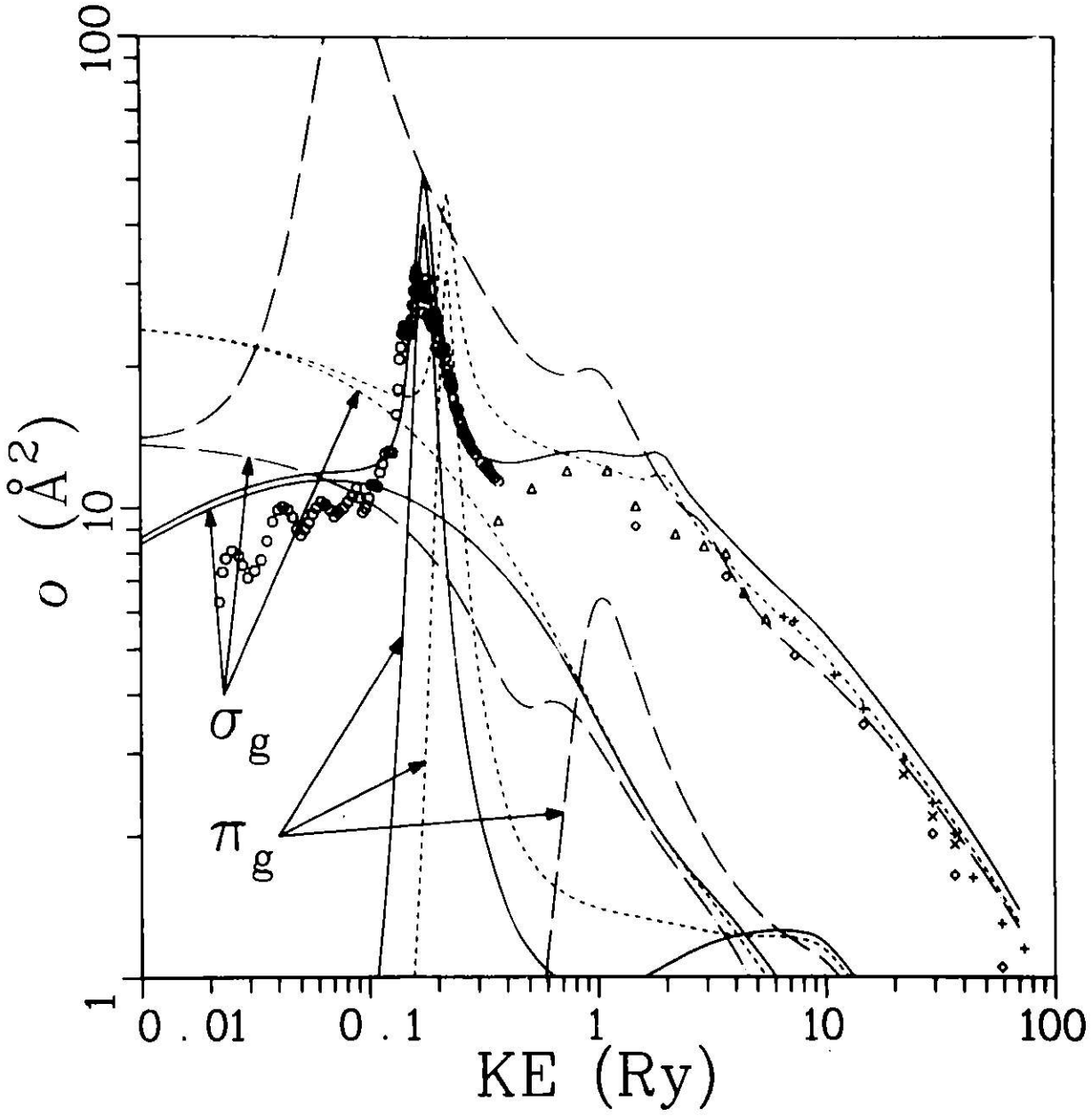

FIG. 2.--Integrated elastic e^--N_2 scattering cross sections in the SEP (—), SE (— —), and S (-·-·) approximations using Hara exchange. Experimental data are represented by symbols according to the convention in Fig. 1.

identical to Fig. 1) with the SE (dashed line) and static-only (dash-dot) calculations. Comparing the SE and SEP results, one sees that addition of the polarization potential brings the π_g resonance position into agreement with experiment, lowers the cross section below the resonance to better agree with experiment, and raises the cross section above 0.5 Ry, somewhat worsening agreement. The physical basis for this interesting observation is discussed further in the full paper. The close agreement between the static result and experiment at very high energy confirms that the present SEP model goes properly to vanishing exchange in this limit.

Figure 3 shows differential cross sections (DCS's) below 30 eV calculated using the Hara (solid line), semiclassical (dash-dotted line), and Xα exchange[2] approximations. The 1.4, 5, and 10 eV results indicate Hara, rather than semiclassical, exchange is to be preferred. Note in the bottom row the clear minima at 90° present in the Hara (and some semiclassical) exchange results, which the Xα potential A was unable to provide.

The DCSs at 300, 400, and 500 eV are shown in Fig. 4., along with the absolute experimental data of Bromberg.[10] These were calculated using the Hara exchange approximation only; based on the results shown in Fig. 3, it is unlikely that semiclassical exchange would show any difference. They were, however, done with (—) and without (---) polarization. In the upper row of Fig. 4, the agreement with experiment is very close in slope and magnitude at all three energies; however, the calculated spectra show a bump around 90° which is not seen in the experimental data. Even here the deviation is only 3 to 5 hundredths of an $Å^2$/sr. Polarization has a negligible effect except for small-angle scattering; however, in the forward direction polarization significantly increases the cross section, as shown in the bottom row of Fig. 4.

Conclusions

The central message of this work is that continuum exchange approximations (and in particular the Hara exchange approximation), rather than the Slater Xα exchange approximation, are necessary to construct potentials which yield realistic representations of electron-molecule scattering over

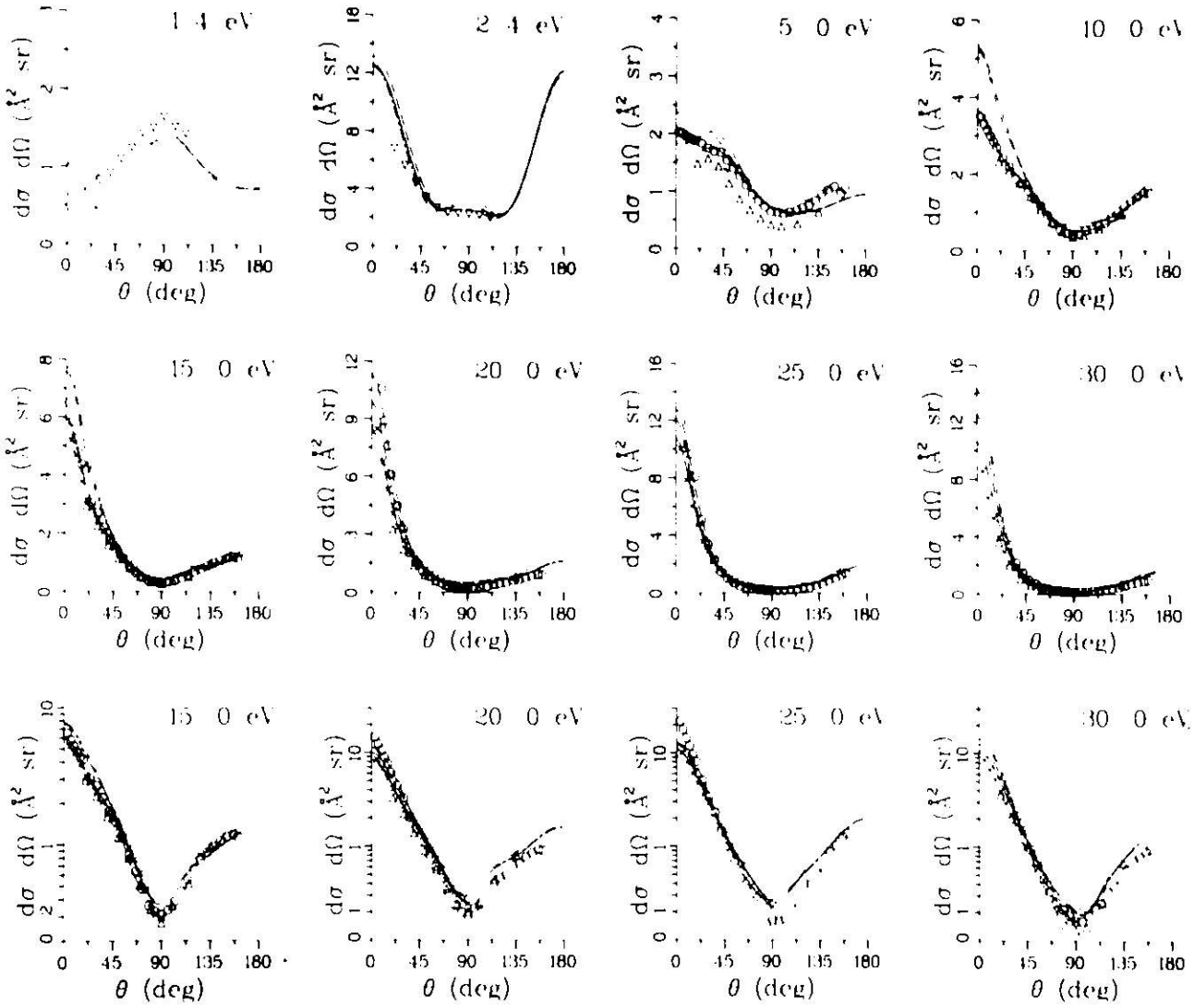

FIG. 3.--Differential cross sections for elastic e^--N_2 scattering at selected energies below 30 eV. Note that the middle and bottom rows display identical data on linear and logarithmic abscissae, respectively. Theoretical curves include Hara exchange (—), semiclassical exchange (-·-·), and Slater Xα potential A data of Ref. 2 (— —). Relative experimental results are normalized to the Hara exchange calculation at the energy and angle noted; Ehrhardt and Willmann,[16] ▽, normalized at 2.4 eV, 50°; Shyn et al.[17] O, normalized at 5 eV, 30°; Srivastava et al.,[12] △, in absolute units as given by the authors, and Finn and Doering,[18] ×, normalized at 15 eV, 30°.

large energy ranges. While our results pertain specifically to the CMSM, other workers[7,15,19] have shown the importance of continuum exchange approximations in the context of other molecular models. Our experience here, with N_2 (see Ref. 1), and in exploratory calculations on CO_2, COS, CS_2, and SF_6,

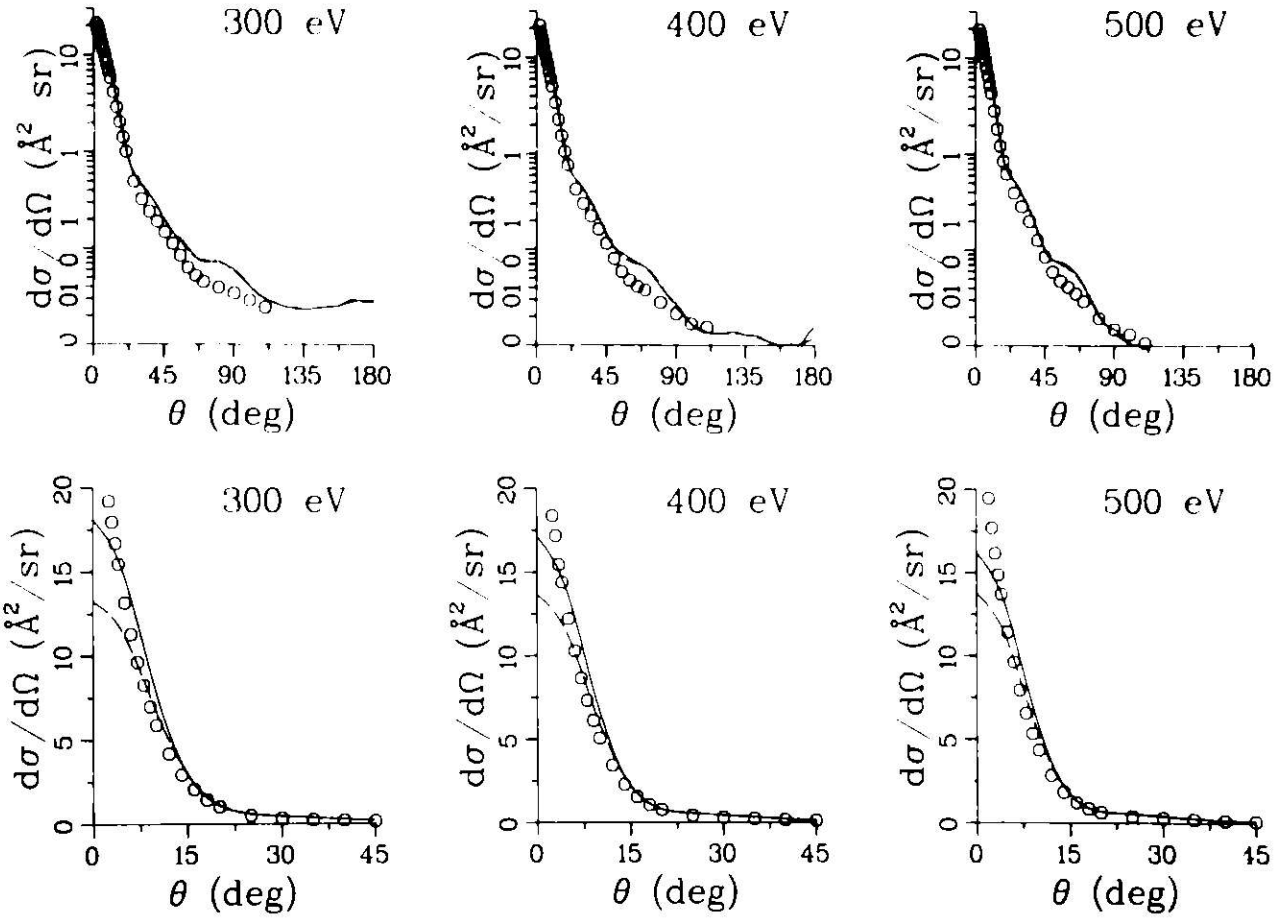

FIG. 4.--Differential cross sections for elastic e^--N_2 scattering at 300, 400, and 500 eV. Theoretical curves represent SEP (—) and SE (— —) calculations using the Hara exchange approximation. Symbols denote the absolute experimental data of Bromberg.[10]

indicates that excessive tuning of potentials based on the Slater Xα exchange approximation is required to reproduce experiment; and even then for some molecules, agreement is only qualitative. Using the Hara exchange approximation, on the other hand, we have immediately obtained semiquantitative results in each case, without any adjustment of the molecular potential. As such, we feel that continuum exchange approximations provide a reliable basis with which to conduct predictive studies of electron-molecule scattering using the continuum multiple-scattering method.

References

1. D. Dill and J. L. Dehmer, Phys. Rev. A 16, 1423 (1977).
2. J. Siegel, D. Dill, and J. L. Dehmer, Phys. Rev. A 17, 2106 (1978).
3. D. Dill and J. L. Dehmer, J. Chem. Phys. 61, 692 (1974).
4. J. Siegel, D. Dill, and J. L. Dehmer, J. Chem. Phys. 64, 3204 (1976).
5. J. Siegel, Ph.D. Thesis, Boston University (1979).
6. J. C. Slater, Quantum Theory of Molecules and Solids, Vol. IV, McGraw-Hill, New York (1974).
7. S. Hara, J. Phys. Soc. Japan 22, 710 (1967).
8. M. E. Riley and D. G. Truhlar, J. Chem. Phys. 63, 2182 (1975).
9. D. E. Golden, Phys. Rev. Lett. 17, 847 (1966).
10. J. P. Bromberg, J. Chem. Phys. 52, 1243 (1970).
11. R. D. Dubois and M. E. Rudd, J. Phys. B 9, 3657 (1976).
12. S. K. Srivastava, A. Chutjian, and S. Trajmar, J. Chem. Phys. 64, 1340 (1976).
13. D. Hermann, K. Jost, and J. Kessler, J. Chem. Phys. 64, 1 (1976).
14. R. E. Kennerly, Phys. Rev. A (in press).
15. M. A. Morrison and L. A. Collins, Phys. Rev. A 17, 918 (1978).
16. W. Ehrhardt and K. Willmann, Z. Physik 204, 462 (1967).
17. T. W. Shyn, R. S. Stolarski, and G. R. Carignan, Phys. Rev. A 6, 1002 (1972).
18. T. G. Finn and G. P. Doering, J. Chem. Phys. 63, 4399 (1975).
19. M. A. Morrison, N. F. Lane, and L. A. Collins, Phys. Rev. A 15, 2186 (1977).

ELASTIC ELECTRON SCATTERING BY CO_2, OCS, AND CS_2 FROM 0 TO 100 eV *

M. G. Lynch,† Dan Dill,†‡ Jon Siegel, and J. L. Dehmer

The continuum multiple-scattering model (CMSM)[1] was originally formulated as a survey tool for processes involving the electronic continua of molecules. Through prototype calculations of photoionization[2-5] and elastic electron scattering[6-9] from simple diatomic molecules, important refinements (e.g., use of the Hara rather than the Slater Xα exchange approximation in electron scattering problems[8,10]) have been made which set the stage for more or less routine survey calculations in families of polyatomic molecules. In this spirit, we present here elastic scattering cross sections for the related triatomic molecules CO_2, OCS, and CS_2 and attempt to identify the systematic variation of resonant features as a function of atomic substitution. Indeed, we reproduce the π_u shape resonance in e^--CO_2 scattering (Fig. 1) at ~3.8 eV and follow its shift to lower impact energy in OCS (Fig. 2) and CS_2 (Fig. 3). In addition, we observe weakly resonant scattering in other scattering channels at higher energy and follow its evolution through this molecular series. The e^--CO_2 results are in good agreement with earlier calculations by Morrison et al.,[11] and the computed resonance positions for all three molecules agree well with experimental results.[12-17] The computed cross sections are not in complete quantitative agreement with experiment, however, for two main reasons. First, we have fixed the nuclei at their equilibrium separations, thus neglecting the effects of nuclear motion. For CO_2, we show evidence that nuclear motion affects the cross section significantly only at the resonance positions, smearing out the peaks and improving their agreement with experiment (Fig. 4). A complete consideration of the effects of nuclear motion, e.g., R-averaging and vibrational excitation, is given elsewhere in the context of the adiabatic nuclei approximation.[18] Second, we neglect the effect of

---

*Summary of a paper to be submitted for publication.

†Department of Chemistry, Boston University, Boston, Massachusetts 02215.
‡Consultant, Radiological and Environmental Research Division.

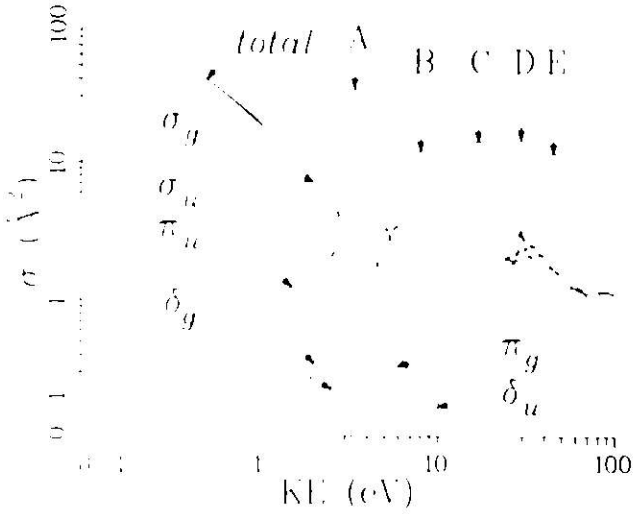

FIG. 1.--Total and partial elastic cross sections for e^--CO_2 scattering for $\lambda = 0$ to $\lambda = 2$ from 0 to 100 eV.

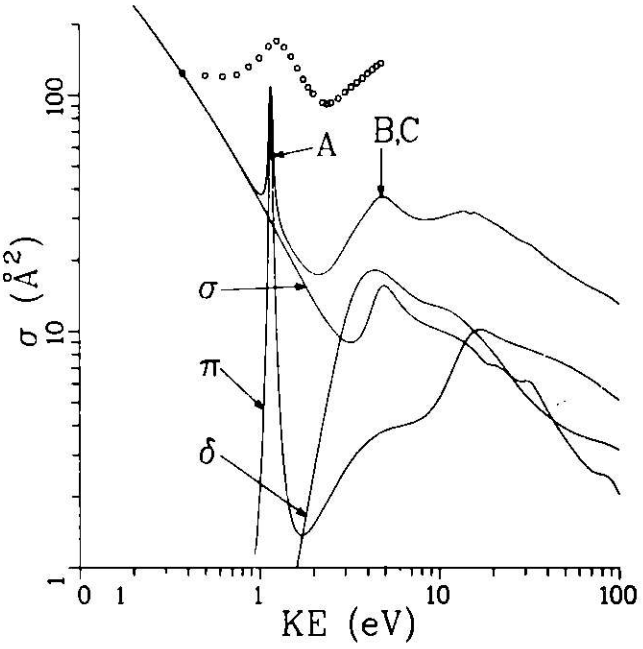

FIG. 2.--Total and partial elastic cross sections for e^--OCS scattering for $\lambda = 0$ to $\lambda = 2$ from 0 to 100 eV. Figure includes experimental work of Szymtkowski and Zubek[16] (+).

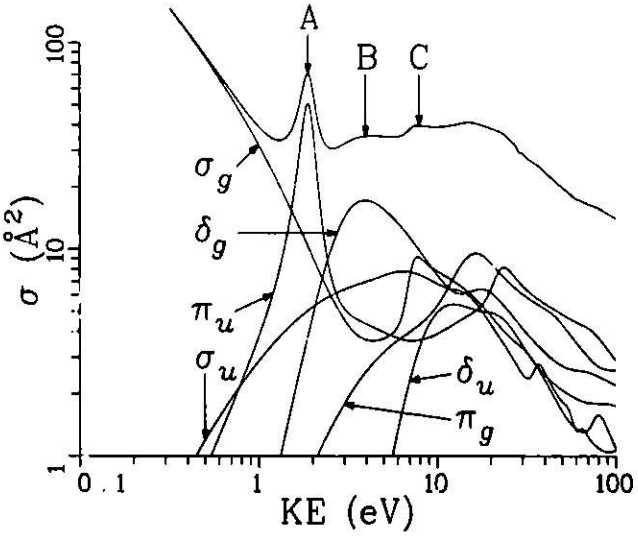

FIG. 3.--Total and partial cross sections for e^--CS_2 scattering for $\lambda = 0$ to $\lambda = 2$ from 0 to 100 eV.

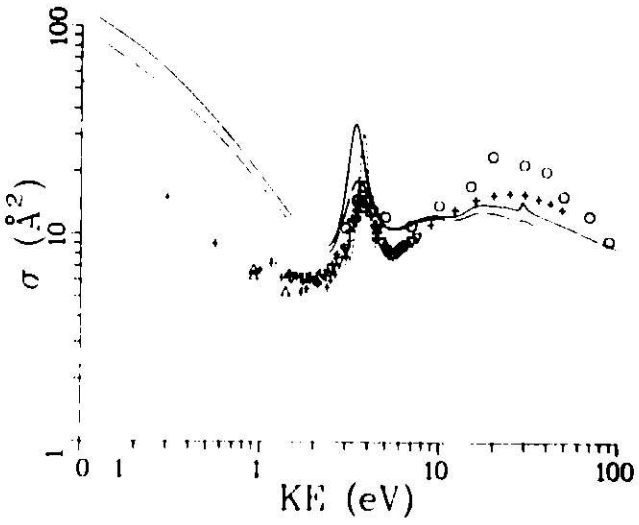

FIG. 4.--Total e^--CO_2 scattering from 0 to 100 eV. Figure includes theoretical work of Morrison, Lane, and Collins[11] (----), J. Welch et al.[18] for the fixed nuclei (——) and adiabatic nuclei (— — —) cases, and the experimental work of Ramsauer[14] (Δ), Brüche[12,13] (+), Shyn et al.[15] (o), and Szymtkowski and Zubek[16] (∇).

scattering by the permanent dipole in OCS. This causes a gross underestimation of the background (nonresonant) cross section for this molecule, but appears to have little effect on the π-shape resonance. Full treatment of the dipole scattering in the context of CMSM will be given later.

References

1. D. Dill and J. L. Dehmer, J. Chem. Phys. 61, 692 (1974).
2. J. L. Dehmer and D. Dill, Phys. Rev. Lett. 35, 213 (1975).
3. J. L. Dehmer and D. Dill, J. Chem. Phys. 65, 5327 (1976).
4. J. W. Davenport, Phys. Rev. Lett. 36, 945 (1976).
5. J. W. Davenport, Ph.D. Thesis, University of Pennsylvania (1976).
6. D. Dill and J. L. Dehmer, Phys. Rev. A 16, 1423 (1977).
7. J. Siegel, D. Dill, and J. L. Dehmer, Phys. Rev. A 17, 2106 (1978).
8. J. Siegel, Ph.D. Thesis, Boston University (1978).
9. J. Siegel, D. Dill, and J. L. Dehmer, submitted for publication.
10. S. Hara, J. Phys. Soc. Japan 22, 710 (1967).
11. M. Morrison, N. Lane, and L. Collins, Phys. Rev. A 15, 2186 (1977).
12. E. Brüche, Ann. Phys. (Leipz.) 83, 1065 (1927).
13. R. B. Brode, Rev. Mod. Phys. 5, 257 (1933).
14. C. Ramsauer, Ann. Phys. (Leipz.) 83, 1129 (1927).
15. T. W. Shyn, W. E. Sharp, and G. R. Carignan, Phys. Rev. A 17, 1855 (1978).
16. C. Szymtkowski and M. Zubek, Chem. Phys. Lett. 57, 105 (1978).
17. P. D. Burrow, private communication.
18. J. Welch, et al., to be published.

SHAPE RESONANCES IN e-SF_6 SCATTERING*

J. L. Dehmer, Jon Siegel, and Dan Dill†

Shape resonances play a central role in studies of electron-molecule scattering. They often stand out against a nonresonant background in the total scattering cross section, impose the angular character of their dominant partial wave(s) on the differential cross section, and enhance vibrational excitation. Nevertheless, the theoretical study of resonance structure in electron-molecule scattering has been limited mainly to diatomic systems, most notable e-N_2 (see, e.g., Refs. 1–10), and has only recently been extended to the linear triatomic molecules CO_2,[11–13] CS_2,[13] and OCS.[13] In this letter, we report calculations of e-SF_6 elastic scattering cross sections, constituting a major jump in the complexity of the target molecule. The resulting spectrum is rich in resonance structure, exhibiting resonances of the a_{1g}, t_{1u}, t_{2g}, and e_g symmetries between 0 and 40 eV, plus nonresonant but enhanced scattering at thermal energies.

In Fig. 1 we show the eigenphase sums for nine of the ten symmetries for e-SF_6 scattering (the a_{1u} contribution is negligible). The eigenphase sum is a fingerprint in multichannel scattering processes, and its rapid rise indicates the presence of a shape resonance in the scattering process. In Fig. 1, four channels, a_{1g}, t_{1u}, t_{2g}, and e_g, exhibit distinct resonance behavior. As expected, the integrated elastic cross section in Fig. 2 shows resonant enhancement at the energy locations of each step in the eigenphase sums—at 2.1 eV (a_{1g}), 7.2 eV (t_{1u}), 12.7 eV (t_{2g}), and 27.0 eV (e_g). In addition, the a_{1g} cross section increases sharply near zero energy owing to the departure of its eigenphase sum from zero phase shift near zero energy.

Although e-SF_6 scattering has been measured by several authors,[14–16]

---

*Summary of paper published in J. Chem. Phys. 69, 5205 (1978).

†Consultant, Radiological and Environmental Research Division. Permanent address: Department of Chemistry, Boston University, Boston, Massachusetts 02215.

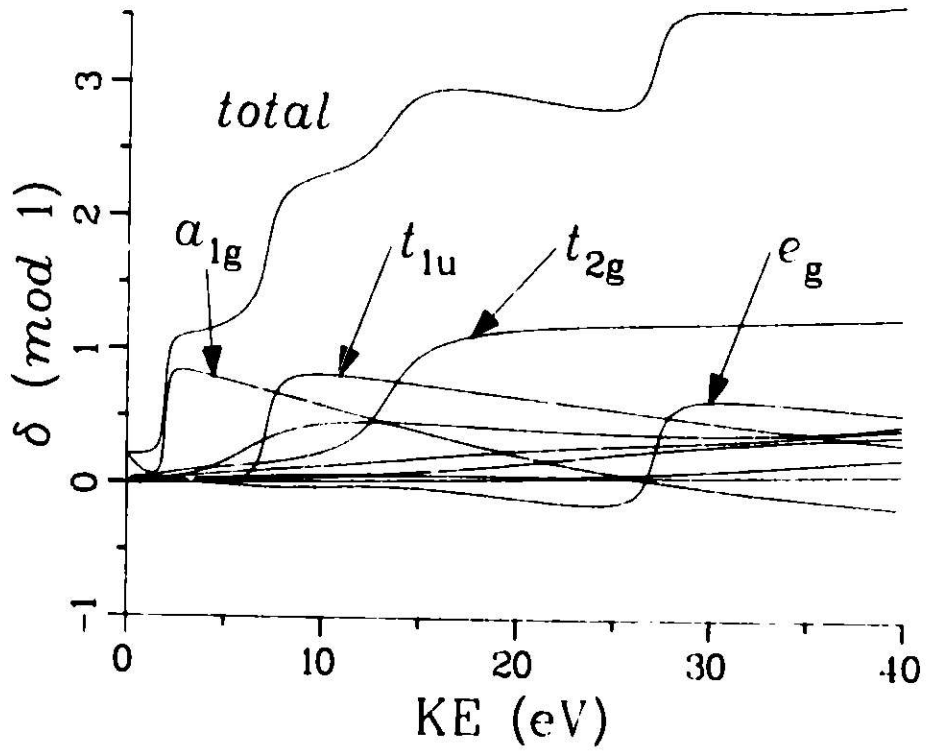

FIG. 1.--Eigenphase sums for elastic e-SF_6 scattering. Resonant a_{1g}, t_{1u}, t_{2g}, and e_g channels are labeled. To permit identification of other channels we note that, in order of increasing eigenphase sum at 40 eV, the channel symmetries are a_{1g}, t_{1g}, a_{2g}, t_{1u}, e_u, a_{2u}, t_{2u}, e_g, and t_{2g}, respectively.

we will focus on recent measurements of total e-SF_6 scattering by Kennerly et al.,[14] since they are absolute, on a fine mesh, and are dominated by elastic scattering. In Fig. 2 the (dashed) experimental spectrum exhibits three distinct peaks at 2.6 eV, 7.2 eV, and 11.8 eV in good agreement with the calculated resonance positions. Moreover, the average magnitude of the cross section is in good agreement above ~5 eV, and the sharp rise at thermal energies is tentatively accounted for by the rise in the a_{1g} cross section. The agreement is not exact, however, as the a_{1g} and t_{1u} resonances are narrower and stronger than experiment, the e_g resonance is not clearly observed, and the deep minimum in the nonresonant cross section near 2.5 eV is not present in the measurement. A final comparison must await consideration of effects of nuclear motion as this is likely to alter quantitative features of the cross section, especially at low energy, and is definitely known, in some cases,[3,10,12,13] to significantly lower and broaden resonance structures calculated at R_e.

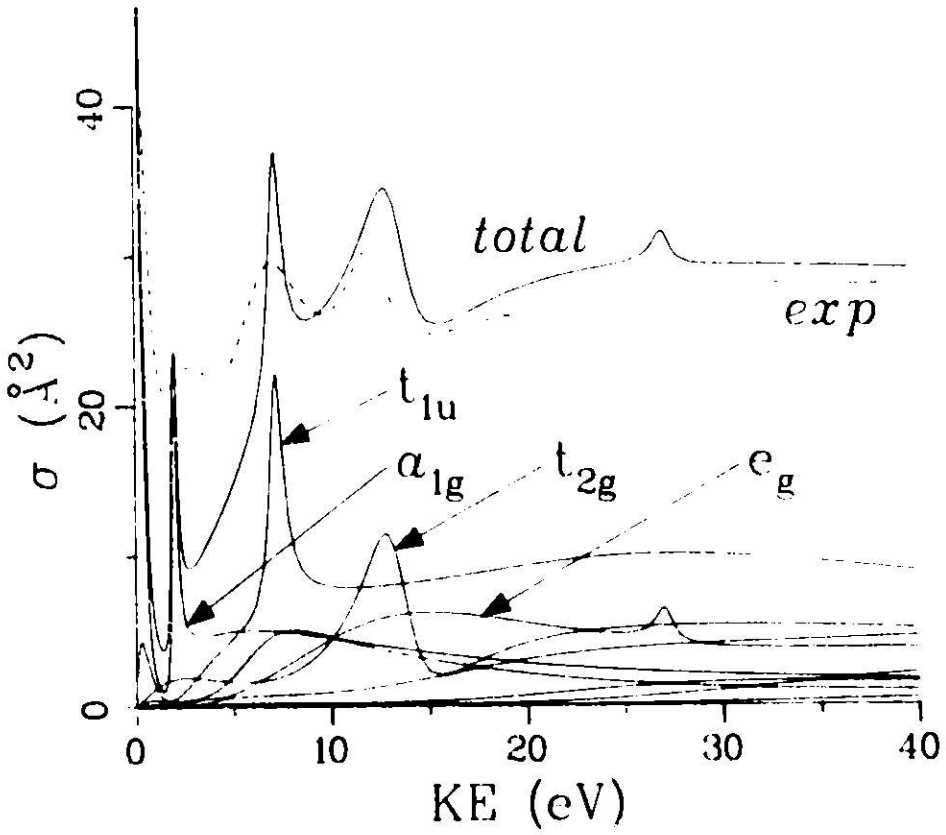

FIG. 2.--Comparison of e-SF_6 scattering cross sections. Solid curves are theoretical elastic cross sections. The dashed curve is the absolute total cross section measured by Kennerly et al.[14] Partial cross sections for resonant channels are labeled. To permit identification of other channels, we note that, in order of increasing cross section at 40 eV, the channel symmetries are a_{2g}, a_{2u}, e_u, a_{1g}, t_{1g}, e_g, t_{2u}, t_{2g}, and t_{1u}, respectively.

References

1. M. Krauss and F. H. Mies, Phys. Rev. A 1, 1592 (1970).
2. P. G. Burke and N. Chandra, J. Phys. B 5, 1696 (1972).
3. N. Chandra and A. Temkin, Phys. Rev. A 13, 188 (1976).
4. B. D. Buckley and P. G. Burke, J. Phys. B 10, 725 (1977).
5. D. Dill and J. L. Dehmer, Phys. Rev. A 16, 1423 (1977).
6. M. A. Morrison and B. I. Schneider, Phys. Rev. A 16, 1003 (1977).
7. J. Siegel, D. Dill, and J. L. Dehmer, Phys. Rev. A 17, 2106 (1978).
8. M. A. Morrison and L. A. Collins, Phys. Rev. A 17, 918 (1978).
9. A. W. Fliflet, D. A. Levin, M. Ma, and V. McKoy, to be published.
10. J. Siegel, J. L. Dehmer, and D. Dill, to be published.
11. M. A. Morrison, N. F. Lane, and L. A. Collins, Phys. Rev. A 15, 2186 (1977).
12. J. Welch, D. Dill, and J. L. Dehmer, to be published.
13. M. G. Lynch, D. Dill, J. Siegel, and J. L. Dehmer, to be published.

14. R. E. Kennerly, R. A. Bonham, and M. McMillan, J. Chem. Phys., to be published.
15. S. K. Srivastava, A. Chutijan, and S. Trajmar, J. Chem. Phys. 64, 2767 (1967).
16. S. Trajmar and A. Chutijan, J. Phys. B 10, 2943 (1977).

SHAPE RESONANCES IN ELECTRON SCATTERING FROM SMALL HYDROCARBONS: C_2H_4

Jon Siegel, J. L. Dehmer, and Dan Dill*

The ability of low-energy (0 to 50 eV, but especially 1 to 10 eV) electron-scattering experiments to probe low-lying negative ion states makes them important to chemists, especially organic chemists whose use of molecular-orbital arguments is extensive. Such scattering experiments have already been performed on a variety of small, "building-block" organic molecules (see Refs. 1–4 for a few of the many papers in this area) and their results interpreted as either shape or Feshbach resonances on the basis of either molecular-orbital calculations or group-theoretical arguments. To date, no theoretical scattering calculations on such molecules have appeared in the literature, probably because of the inability of the single-center expansion technique in common use to handle molecules beyond triatomics.[5] The continuum multiple-scattering method, however, is ideally suited for such molecular calculations, as was shown by our recent successful treatment of e^--SF_6 scattering.[6] We have therefore begun to examine, specifically, shape resonances in low-energy electron scattering by small hydrocarbons. Here we report preliminary results on the first molecule, ethylene (C_2H_4).

We started with ethylene for several reasons: (1) It is a small molecule but its two carbon atoms make it "pseudo-diatomic" (e.g., compared to O_2) rather than "pseudo-atomic" (e.g., like CH_4 compared to Ne); (2) it has a high degree of symmetry (e.g., higher than ethane, C_2H_6); and finally (3) experimental data, showing a prominent resonance,[1,4] are available in the energy range of interest.

*Consultant, Radiological and Environmental Research Division. Permanent address: Department of Chemistry, Boston University, Boston, Massachusetts 02215.

Calculations

Multiple-scattering calculations of bound-state ethylene had already been published by Rösch et al.;[7] these authors used four different sets of parameters differing in (a) the value of α used in the hydrogen spheres, and (b) whether or not the carbon spheres were allowed to overlap. From their results it was clear that one should employ the "spin-unrestricted" value of α_H. Not so clear was the possible benefit to us of overlapping the spheres; we therefore performed our calculations using both non-overlapped [Rösch case (c)] and overlapped [Rösch case (d)] carbon spheres. The only difference, then, between our bound-state calculation and theirs was that we applied the Latter cutoff[8] during the SCF process, while they did not.

Scattering calculations were performed from threshold to 40 eV, using partial waves up to $\ell = 11$ on the outer sphere, 5 on the carbons, and 3 on the hydrogens. Polarization was applied in the outer sphere as the asymptotic form, $-\alpha_0/r^4$, using the value[9] $\alpha_0 = 28.62$. To determine whether or not the polarization potential should be extended into region II, calculations were performed under the four alternative sets of conditions described in Table 1.

Table 1. Comparison of the four trial scattering calculations for ethylene

	Overlapped carbon spheres	Polarization potential in region II	Resonance potential, eV
1	no	no	1.2
2	no	yes	0.2
3	yes	no	2.6
4	yes	yes	1.5

Results were evaluated on the basis of a potential's ability to reproduce the observed resonance peak at 1.8 eV. The two best runs on this basis, numbers 1 and 4, display resonance peaks which were almost identical in shape and character except for the slight shift in energy. The better of these two, number 4, employed overlapping spheres. These are the conditions that produced the best agreement with experimental ionization potentials in the work of Rösch

et al., suggesting that sphere radii might be determined during the bound-state portion of the calculation on this basis.

Results

According to Mulliken,[10] the approximate order of the lowest-lying unoccupied orbitals of ethylene is b_{2g}, a_g, b_{1u}, and b_{2u}. Our calculated phase shifts (Fig. 1) show a sharp rise in the b_{2g} channel followed by a somewhat shallower rise in a_g, consistent with this ordering. At a somewhat higher energy one sees a very shallow rise in the b_{1g}. The corresponding cross sections (Fig. 2) are consistent with this. Note that the b_{2g} and a_g resonances combine into a single peak. Then the b_{1g} channel shows an extremely broad, low structure centered at 4.6 eV.

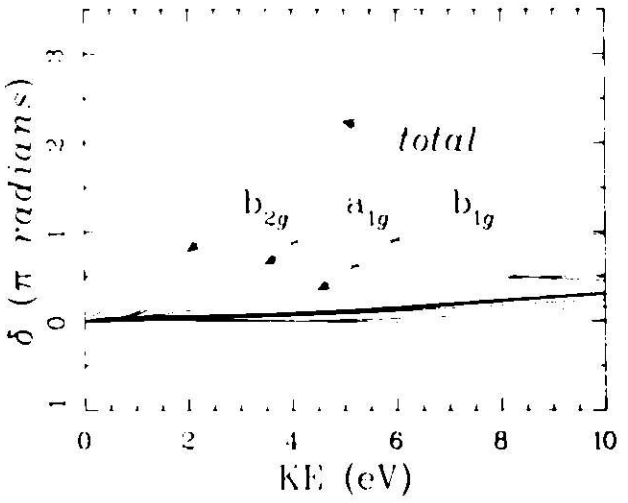

FIG. 1.--Eigenphase sums for electron-ethylene scattering.

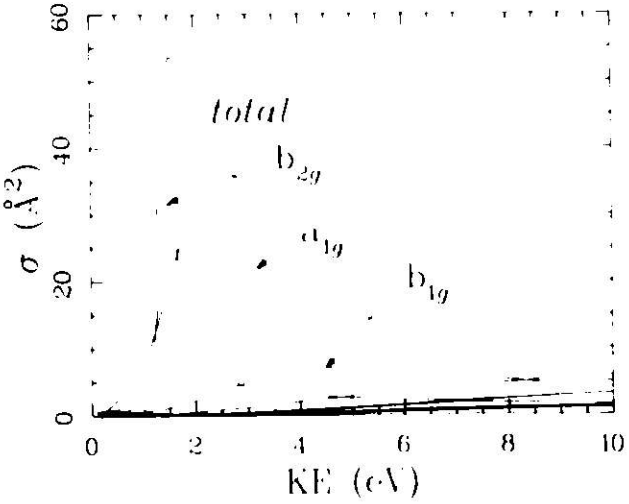

FIG. 2.--Cross sections for electron-ethylene scattering

One expects that experimental studies of either the differential cross section spectrum, or of vibrationally-inelastic scattering, might be able to probe the double nature of the first peak. A detailed study of electron-impact vibrational excitation of ethylene has just been published by Walker, Stamatovic, and Wong, and they, in fact, pay particular attention to this structure.[4] They conclude, in contradiction to our results, that the resonance is solely b_{1g} in character, although when they examine different vibrational modes associated

with it (their Fig. 3 and comments) they find two differential cross sections of one character, and a third substantially different. They also observe a resonant structure centered at 7.5 eV, which they ascribe to an a_g shape resonance. Mulliken[10] tentatively ascribes this to an electronic quadrupole transition to a Rydberg state. In order to resolve these conflicts, we plan to calculate the inelastic differential cross sections measured by Walker et al. Also in this regard, we would like to have an experimentally determined elastic cross section spectrum, to compare with our Fig. 2. We expect that these assignments will be resolved shortly, and that we will then be able to study the other small hydrocarbons.

References

1. L. Sanche and G. J. Schulz, J. Chem. Phys. 58, 479 (1973).
2. S. F. Wong and G. J. Schulz, Phys. Rev. Lett. 35, 1429 (1975).
3. K. D. Jordan and P. Burrow, Acc. Chem. Res. 11, 341 (1978).
4. I. C. Walker, A. Stamatovic, and S. F. Wong. J. Chem. Phys. 69, 5532 (1978).
5. M. A. Morrison, N. F. Lane, and L. A. Collins, Phys. Rev. A 15, 2186 (1977).
6. J. L. Dehmer, J. Siegel, and D. Dill, J. Chem. Phys. 69, 5205 (1978).
7. N. Rösch, W. G. Klemperer, and K. H. Johnson, Chem. Phys. Lett. 23, 149 (1973).
8. R. Latter, Phys. Rev. 99, 510 (1955).
9. Landolt-Börnstein, Zahlentwerte und Funktionen, Vol. 1, Part 3, Springer-Verlag, Berlin, pp. 509 ff. (1951).
10. R. S. Mulliken, J. Chem. Phys. 66, 2448 (1977).

ORIGIN OF ENHANCED VIBRATIONAL EXCITATION IN N_2 BY ELECTRON IMPACT IN THE 15 TO 35 eV REGION

J. L. Dehmer, Jon Siegel, J. Welch,[†] and Dan Dill[‡]

Several years ago, Pavlovic, Boness, Herzenberg, and Schulz reported[1] that "the vibrational cross section by electron impact on N_2 exhibits a broad maximum near 22 eV." Prompted by the great width (FWHM > 5 eV) and the complex energy dependence of the differential cross section, those authors interpreted this enhanced vibrational excitation in terms of a large manifold of "overlapping compound states above 20 eV," including possible shape resonances and singly and multiply core-excited Feshbach resonances. In this paper, we document our earlier proposal[2] of a very simple, one-electron mechanism—a σ_u shape resonance—as a likely candidate to explain the observations of the above authors. At the very least, this resonance is shown to be responsible for enhanced vibrational excitation in the 15 to 35 eV range. Its ability to account for the energy dependence of the differential cross section is currently under investigation and will be reported separately. The possible role of the σ_u resonance was anticipated by Pavlovic et al.,[1] but they had insufficient theoretical information to identify its primary role. This interpretation suggested itself to us during an earlier study[3] of $e\text{-}N_2$ scattering using the continuum multiple-scattering model[4,5] (CMSM) with Slater exchange. That work identified weak, intermediate resonances in the σ_u and δ_g channels in addition to the well-known π_g resonance (see, e.g., Ref. 6) at 2.4 eV. More recent work[7] employing the CMSM with the Hara exchange approximation[8] has proved to be considerably superior but indicates the same three resonances, only the σ_u and δ_g features were weaker, especially the δ_g. This is consistent with recent total electron scattering measurements[9] on N_2 which indicate a

---

*Summary of an article submitted for publication.

†Work performed at the Department of Chemistry, Boston University, Boston, Mass., 02215. Present address: Dept. of Chemistry, Harvard University, Cambridge, Mass. 02138.

‡Consultant, Radiological and Environmental Research Division. Permanent address: Dept. of Chemistry, Boston University, Boston, Mass. 02215.

very weak, broad feature at 22 eV, corresponding to the σ_u resonance, and no sign of the δ_g resonance at ~13 eV. Notwithstanding the extreme weakness of these intermediate-energy features in the elastic scattering cross section, we felt they may be important in alternative scattering channels such as vibrational excitation. We show that the σ_u is, indeed, important in this role, whereas the δ_g is not, owing to its weakness and off-axis orientation. Results for vibrational excitation due to the strong π_g resonance are also presented.

Our results are shown in Fig. 1. The vibrationally elastic results ($0 \rightarrow 0$) have been discussed elsewhere.[7] Here we only note that although the

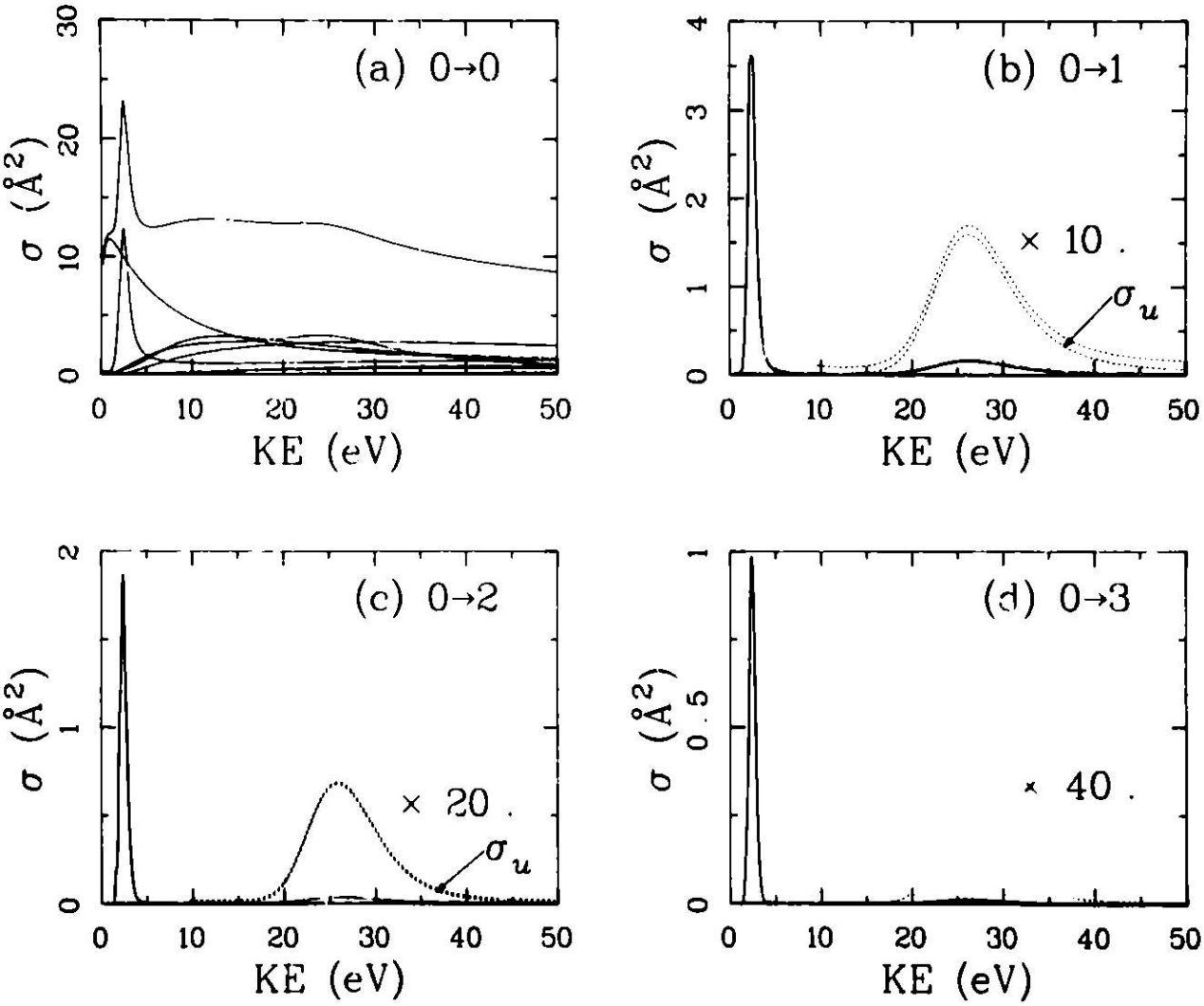

FIG. 1.--Vibrationally elastic and inelastic cross sections for e-N_2 scattering between 0 and 50 eV. Figures 1a, b, c, d contain results for $v=0 \rightarrow v'=0,1,3$, respectively.

π_g resonance is prominent, the bulk of the cross section is made up of nonresonant contributions. By contrast, vibrational excitation is overwhelmingly dominated by resonant processes. In Fig. 1 the total cross section is indistinguishable from the resonant π_g (2.4 eV) and σ_u (26 eV) partial cross sections, indicating that nonresonant processes are negligible. Similarly, the weak δ_g shape resonance, located at ~13 eV, is ineffective in enhancing vibrational excitation since it is not a strong, localized resonance (like the π_g), nor an axially oriented resonance (like the σ_u) and, therefore, couples only weakly with the nuclear motion.

References

1. Z. Pavlovic, M. J. W. Boness, A. Herzenberg, and G. J. Schulz, Phys. Rev. A 6, 676 (1972).
2. J. Siegel, J. L. Dehmer, D. Dill, and J. Welch, Bull. Am. Phys. Soc. 23, 1082 (1978).
3. D. Dill and J. L. Dehmer, Phys. Rev. A 16, 1423 (1977).
4. D. Dill and J. L. Dehmer, J. Chem. Phys. 61, 692 (1974).
5. J. L. Dehmer and D. Dill, Electron and Photon Molecule Collisions, V. McKoy, T. Rescigno, and B. Schneider, Eds., Plenum Press, New York (1979).
6. G. J. Schulz, Rev. Mod. Phys. 45, 378 (1973).
7. J. Siegel, J. L. Dehmer, and D. Dill, submitted for publication.
8. S. Hara, J. Phys. Soc. Japan 22, 710 (1967).
9. R. E. Kennerly, Phys. Rev. A, to be published.

ELECTRON SCATTERING FROM N_2 BELOW 30 eV. ROTATIONALLY-INELASTIC AND MOMENTUM-TRANSFER CROSS SECTIONS

Jon Siegel, J. L. Dehmer, and Dan Dill*

When an electron collides with a molecule, one or more fundamental processes may occur. In order of increasing $|\Delta E|$ (where E is the kinetic energy of the electron), these scattering processes are elastic, rotationally inelastic, vibrationally inelastic, and electronically inelastic. (In addition, various ionization, attachment, and dissociation phenomena may result from the collision, but these are not discussed here.) Another specific cross section, relating especially to electron transport in gases, is the momentum-transfer cross section. Previously we have examined elastic[1-3] and collisions of electrons with N_2. Here we shall examine rotationally-inelastic collisions and momentum-transfer cross sections. Remaining for future work, then, will be (1) vibrationally-inelastic differential cross sections (DCS's) and (2) electronically-inelastic cross sections.

Rotationally-Inelastic Scattering

Rotational close coupling, first formulated by Arthurs and Dalgarno,[5] furnishes a means of calculating rotationally-inelastic scattering including dynamical interaction between the electron and the rotational motion of the molecule. However, if the collision time is sufficiently short compared to a rotational period so that the adiabatic approximation is justified, then essentially the same results may be obtained by performing the calculations in the body frame and transforming geometrically[6] to the laboratory frame. This latter method allows use of the continuum multiple-scattering formalism[7,8] and machinery which we have developed to deal with complex molecular systems. The adiabatic approximation for e^--N_2 scattering has already been used successfully to study the vibrational interaction;[4] in the rotational problem the

*Consultant, Radiological and Environmental Research Division. Permanent address: Department of Chemistry, Boston University, Boston, Massachusetts 02215.

period is much longer and the adiabatic approximation even better justified.

The T matrix, defined by

$$\underline{T} = \underline{I} - \underline{S} \quad , \tag{1}$$

where $\underline{S}$ is the scattering matrix, defines the corresponding cross sections.[2,9] In the body frame the T matrix is indexed by, e.g., ℓ, m, ℓ', m', where (ℓ, m) defines a basis function in terms of the spherical harmonics (an alternative basis is that of the symmetry point group of the molecule). Total angular momentum is not conserved in the body frame, but integrated and differential cross sections based on random molecular orientation may be calculated from these T matrices using formulae given in, e.g., Refs. 2 and 7.

In the laboratory frame, on the other hand, the T matrix is indexed by total angular momentum J, electronic orbital momentum ℓ, ℓ', and rotational angular momentum j, j'. Total angular momentum is conserved so that only certain combinations of the indices J, j, j', ℓ, ℓ' can have non-zero T-matrix elements. The formula for the DCS from such T matrices has general application (many scattering processes involve two component angular momenta and their sum); thus for these calculations we are able to employ the formalism of Blatt and Biedenham[9] as implemented by Brandt et al.[10] In the adiabatic approximation the two forms of the T matrix are related by[6]

$$\begin{aligned} {}^{J}T_{j\ell, j\ell'} = (-)^{\ell+\ell'} \sum_{m}{}' \, & (J-m, \ell' m \,|\, j' 0) \\ & \times (J-m, \ell m \,|\, j_0) T_{\ell m, \ell' m} \end{aligned} \tag{2}$$

for linear molecules. Note that parity conservation restricts $(-)^{j} = (-)^{j'}$ for homonuclear diatomic molecules.

The rotational constant for N_2 is only $\sim 2\ cm^{-1}$,[11] and it is unlikely that the rotational spectra to be presented here will be resolved experimentally in the near future. However, these calculated rotational spectra are useful in several other ways: (1) they provide insight into the dynamics of the electron-molecule interaction; (2) they complement the j_t-basis analysis of Ref. 2; (3) they find application in calculation of electron thermalization in gases;[12] and (4) they form a prototype for the study of similar processes in electron-

dipolar molecule scattering, where consideration of rotational effects is an essential part of the problem.[13]

Figure 1 shows our rotationally inelastic DCS's calculated at six of the energies of Ref. 3, Fig. 4. (Note that the total DCS's were compared to experiment in that reference.) In general, the cross sections go to higher final j and become more complex as energy increases: at 2.4 eV only final j = 0, 2 contributes, while at 30 eV non-negligible contribution is made by final j = 6. Also, note the general trend for higher final j to peak more toward large θ (backscattering); this will yield proportionately larger momentum-transfer cross sections for these transitions. The integrated cross sections corresponding to these data are presented in the first part of Table 1.

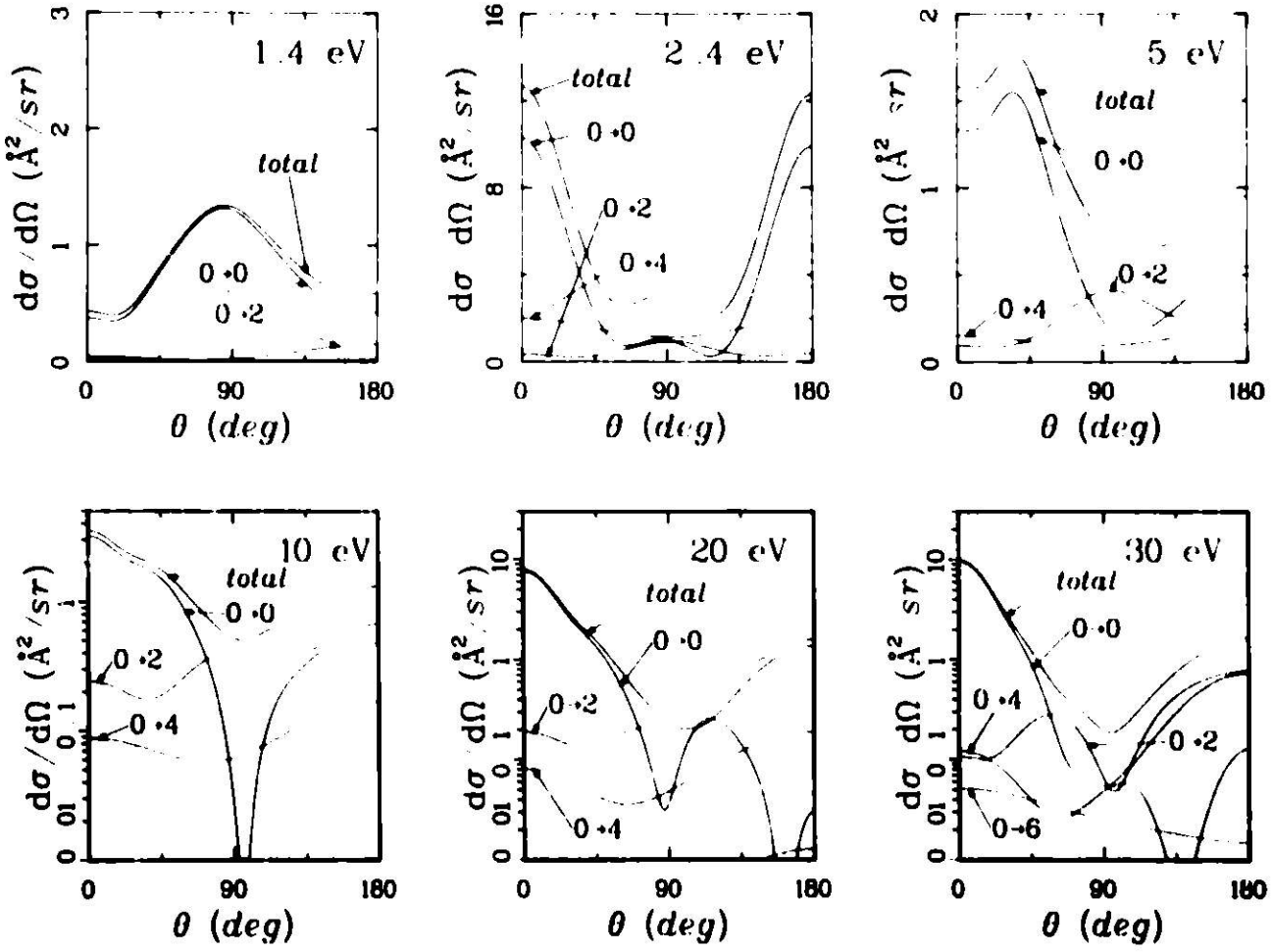

FIG. 1.--Rotationally-inelastic differential cross sections for electron-N_2 scattering.

In Table 2 we compare our integrated cross sections with those of three other theoretical calculations. Burke and Chandra[14] treated rotation adiabatically; Chandra and Temkin[15] included dynamic vibrational effects in a "hybrid" theory, and Truhlar et al.[16] included both vibration and rotation dynamics in a close-coupling expansion which was, however, truncated at an unrealistically small number of states. In general, agreement with the two adiabatic rotational treatments is acceptable, with the 5 eV, $0 \rightarrow 0$ cross sections showing the

Table 1. Rotationally inelastic integrated and momentum-transfer cross sections ($\AA^2$) for N_2 through $j' = 6$. Values less than 0.01 are represented by a dash.

E (eV)	1.1	2.4	5.0	10.0	15.0	20.0	25.0	30.0
$\sigma_{j \rightarrow j'}$								
$0 \rightarrow 0$	11.6	26.31	7.57	7.59		8.01		6.81
$0 \rightarrow 2$	0.55	6.99	3.49	4.54		3.90		2.99
$0 \rightarrow 4$	0.13	17.49	1.47	1.03		0.90		1.72
$0 \rightarrow 6$	—	—	—	0.01		0.06		0.34
Total	12.28	50.79	12.53	14.17		12.88		11.97
$\sigma_{m,j \rightarrow j'}$								
$0 \rightarrow 0$	11.42	24.79	4.81	4.05		2.65		1.26
$0 \rightarrow 2$	0.77	7.17	3.83	5.24		5.28		3.69
$0 \rightarrow 4$	0.13	17.49	1.54	1.18		1.13		2.59
$0 \rightarrow 6$	—	—	—	—		0.07		0.28
Total	12.32	49.45	10.18	10.47	9.77	9.13	8.94	7.82

Table 2. Integrated rotationally inelastic ($\sigma_{jj'}$) and momentum-transfer ($\sigma_{m,jj'}$ and $\sigma_{m,tot}$) cross sections ($\AA^2$) for N_2.

	5 eV					10 eV				
	σ_{00}	σ_{02}	$\sigma_{m,00}$	$\sigma_{m,02}$	$\sigma_{m,tot}$	σ_{00}	σ_{02}	$\sigma_{m,00}$	$\sigma_{m,02}$	$\sigma_{m,tot}$
This work	7.57	3.49	4.81	3.83	10.15	7.59	4.54	4.05	5.24	10.47
Burke and Chandra[14]	10.19	2.69	6.41	2.97	10.36	8.65	3.98	4.76	4.87	10.53
Chandra and Temkin[15]	10.16	2.72	6.33	2.97	10.44	8.68	4.00	4.73	4.84	10.53
Truhlar et al.[16]	9.13	10.50	3.98	15.71	19.77	5.63	6.66	3.00	9.88	12.91

greatest deviation. Truhlar's cross sections for $j = 0 \rightarrow 2$ are greater than for $0 \rightarrow 0$; he ascribes this to the premature truncation of the rotational basis at final $j = 2$. His $0 \rightarrow 0$ cross sections, which appear more accurate, presumably do not suffer as much from these truncation effects.

Momentum-Transfer Cross Sections

The momentum-transfer cross section is defined as

$$\sigma_m \int (1 - \cos\theta) \frac{d\sigma}{d\Omega} d\Omega \quad , \tag{3}$$

where σ is either a total or a partial cross section (thus, e.g., each rotationally or vibrationally inelastic transition has an associated momentum-transfer cross section). This relation was used to extract momentum-transfer cross sections from the DCS's of Fig. 1, as well as those in Refs. 2 and 3.

Figure 2a shows our total momentum-transfer cross sections from data of Ref. 2 (solid line) and Ref. 3 (circles). Corresponding experimental results[17] are shown in Fig. 2b. The more realistic treatment of exchange in Ref. 3 leads to marked improvement in σ_m, and we are extending this treatment to the energy range of 0 to 50 eV.

In Tables 1 and 2 we tabulate and compare rotationally inelastic and total σ_m. Note, comparing Fig. 1 and Table 1, that where backscattering predominates, $\sigma_{m,jj'}$ exceeds $\sigma_{jj'}$. In Table 2 agreement with the adiabatic theories is acceptable, with the total σ_m's exhibiting the most striking agreement.

Conclusion

Electron-N_2 interactions are well represented in the rotationally inelastic and momentum-transfer cross sections presented here, as well as in the integrated[1-3] and vibrationally inelastic[4] results presented previously. Only a few more calculations (low-energy σ_m using Hara exchange,[18] and vibrationally-resolved DCS's and σ_m's) are necessary to complete our survey of electronically-elastic e^--N_2 scattering using the continuum multiple-scattering model in the adiabatic approximation.

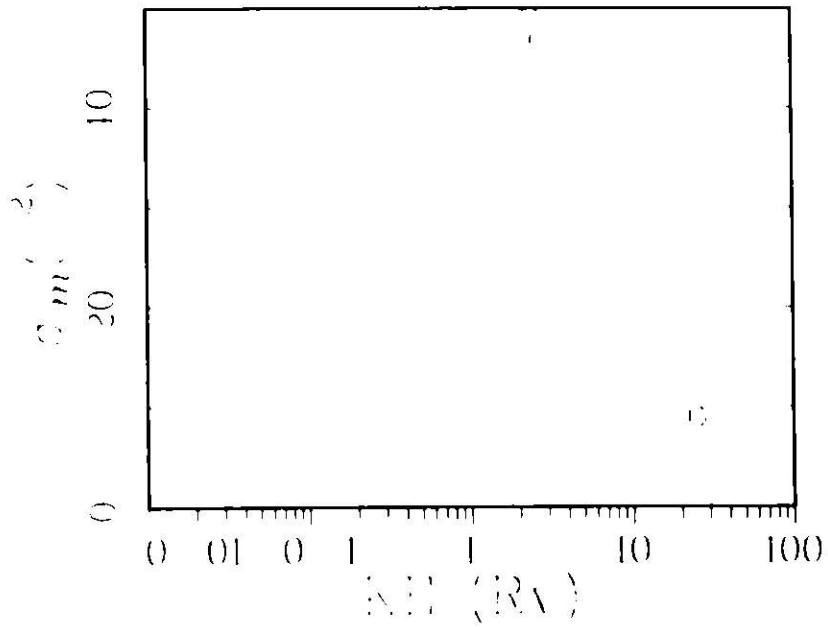

FIG. 2a.--Calculated momentum-transfer cross sections for electron-N_2 scattering. Solid line, from Ref. 2 data, circles from Ref. 3 data.

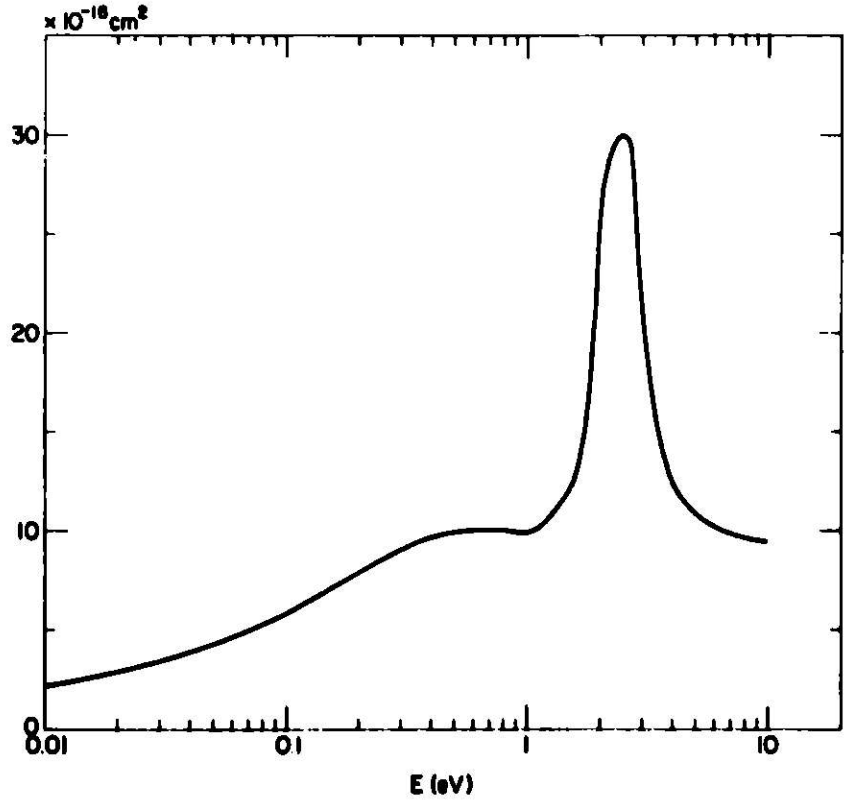

FIG. 2b.--Experimental electron N_2 momentum transfer cross sections, reprinted from Ref. 17.

References

1. D. Dill and J. L. Dehmer, Phys. Rev. A 16, 1423 (1977).
2. J. Siegel, D. Dill, and J. L. Dehmer, Phys. Rev. A 17, 2206 (1978).
3. J. Siegel, J. L. Dehmer, and D. Dill, submitted for publication.
4. J. L. Dehmer, J. Siegel, J. Welch, and D. Dill, submitted for publication.
5. A. M. Arthurs and A. Dalgarno, Proc. Roy. Soc. (London) A 256, 540 (1969).
6. E. S. Chang and U. Fano, Phys. Rev. A 6, 173 (1970).
7. D. Dill and J. L. Dehmer, J. Chem. Phys. 61, 692 (1974).
8. J. Siegel, D. Dill, and J. L. Dehmer, J. Chem. Phys. 64, 3204 (1976).
9. J. M. Blatt and L. C. Biedenharn, Rev. Mod. Phys. 24, 258 (1952).
10. M. A. Brandt, D. G. Truhlar, and R. L. Smith, Comput. Phys. Commun. 5, 456 (1973).
11. G. Herzberg, Spectra of Diatomic Molecules, Van Nostrand, New York (1950).
12. A. Gilardini, Low Energy Electron Collisions in Gases, Wiley and Sons, New York (1972).
13. W. R. Garrett, Mol. Phys. 24, 465 (1972).
14. P. G. Burke and N. Chandra, J. Phys. B 5, 1696 (1972).
15. N. Chandra and A. Temkin, Phys. Rev. A 13, 188 (1976).
16. D. G. Truhlar, M. A. Brandt, A. Chutjian, S. K. Srivastava, and S. Trajmar, J. Chem. Phys. 65, 2962 (1976).
17. Y. Itikawa, Argonne National Laboratory Report ANL-7939 (April 1972).
18. S. Hara, J. Phys. Soc. Japan 22, 710 (1967).

ELECTRON-DIPOLAR MOLECULE SCATTERING: LiF

Jon Siegel, J. L. Dehmer, and Dan Dill*

When an electron collides with a dipolar molecule such as LiF, the radial dipole potential

$$V_D(\vec{r}) = -D/r^2 \quad , \tag{1}$$

where D is the dipole moment of the molecule in a.u., dominates the interaction at all $\vec{r}$ except in the molecular core region. The r^{-2} character of this potential is so long ranged that its attenuation by molecular rotation must be taken into account if the resulting cross sections are to be finite.[1] This would require complex rotational close-coupling[2] or frame-gransformation[3] calculations, but recently Collins and Norcross[4] proposed a series of simplifications which make it possible for us to base such calculations on the continuum multiple-scattering treatment[5,6] of the core region which, it turns out, retains a strong influence on the scattering even in the presence of the long-ranged dipole potential.

The three key simplifications of Collins and Norcross are: (1) the rotation of the molecule is treated adiabatically; (2) T-matrix elements for intermediate ℓ are obtained from point-dipole model calculations; and (3) a completion formula is used to converge the cross-section expansion to infinite partial waves. Briefly, these three simplifications are justified as follows:

(1) At the energies to be considered here, the transit time of the electron across the molecular core region is sufficiently short compared to a rotational period that the adiabatic approximation may be invoked. This allows one to perform the scattering calculations in the body frame and transform using the relation[3]

*Consultant, Radiological and Environmental Research Division. Permanent address: Department of Chemistry, Boston University, Boston, Massachusetts 02215.

$$^{J}T_{j\ell,j'\ell'} = (-)^{\ell+\ell'} \sum_{m} (J-m, \ell' m \,|\, j' 0)$$

$$\times (J-m, \ell m \,|\, j0) T_{\ell m, \ell' m} \quad , \tag{2}$$

(for linear molecules) to obtain the desired T-matrix elements in the basis of total J. Collins and Norcross have confirmed the accuracy of this procedure calculationally by comparing such adiabatically-transformed T-matrix elements with those obtained from close-coupling calculations. This approximation does not apply at higher ℓ, where the interaction is longer-ranged and the transit time proportionately longer (see next paragraph).

(2) Because of the barrier associated with its potential, a partial wave of sufficiently high ℓ will be excluded from the molecular core region and experience only pure dipole scattering. Therefore, T-matrix elements representing a point-dipole potential may be used for $\ell, \ell' > \ell_{PD}$, where ℓ_{PD} is the partial wave whose barrier is just sufficient to exclude it from the core region. Such approximate T-matrix elements may be calculated in several approximations and used to extend the T matrix to arbitrary J. Collins and Norcross extended their T matrix in two stages for LiF, using point-dipole close-coupling elements for $4 \le J \le 20$, and the Born approximation for $20 < J \le 48$. We chose to extend using instead the semiclassical method of Mukherjee and Smith;[7] this is considerably more accurate than the Born approximation and is, in fact, a good replacement for the close-coupling model at the intermediate ℓ values where we switched over from the adiabatic calculation.[7]

(3) Convergence in J of integrated and differential cross sections is quite slow; even at $J_{max} = 75$ our $j = 0 \rightarrow 1$ differential cross section (DCS) for LiF was far from converged, as will be described below. Crawford and Delgarno[8] have given a completion formula which extends the summation to $J = \infty$ based on the analytic Born DCS and a rapidly converging sum of differences; use of this completion formula is the third step of the Collins and Norcross procedure.

We have implemented the first two of these simplifications to calculate e^--LiF scattering at 5.44 eV. Body-frame calculations were performed using

the continuum multiple-scattering method with $\ell_{max} = 10$ in the asymptotic region and $\lambda_{max} = 6$, and transformed to the laboratory frame using Eq. 2. The corresponding semiclassical T-matrix elements were also generated; by $\ell, \ell' \approx 8$ these two T matrices agreed to better than 1% so the final "hybrid" matrices contained semiclassical values above this point. DCS's from initial $j = 0$ to final $j' = 0$ through 6 were calculated using the formalism of Blatt and Biedenharn[9] as implemented by Brandt et al.[10] Three different bases were used, having $J_{max} = 25, 50$, and 75. Even at $J_{max} = 75$, the DCS for $j \rightarrow j' = 0 \rightarrow 1$ was (a) not converged at small θ and (b) extremely jagged owing to incomplete cancellation of the many component partial waves. Implementation of the completion formula is expected to remedy these deficiencies.

The jaggedness was smoothed by computer[11] to produce the results shown in Fig. 1, along with the absolute experimental determination of Vušković et al.[12] Even on the logarithmic abscissa which mangifies discrepancy at small cross sections the agreement is satisfactory, certainly as good as that of Collins and Norcross.[4] A trial calculation at 20 eV yielded results almost as good, in spite of possible lack of convergence in the body-frame calculations.

We are in the process of implementing the completion formula. Once this is done, we will complete our survey calculations on LiF and commence

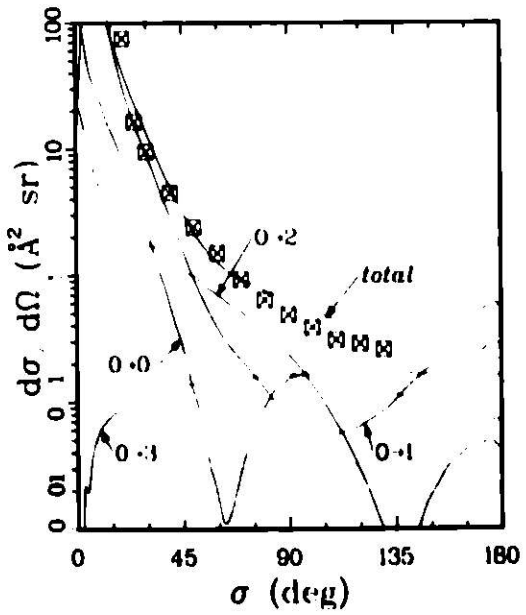

FIG. 1.--Electron-LiF scattering differential cross sections for indicated rotational transitions at 5.44 eV. —, calculated result; ⊠, experimental determination of Vušković et al. (Ref. 12).

work on such triatomic molecules as HCN, OCS, KOH, H_2O, and larger dipole molecules, where the continuum multiple-scattering method is more practical than the single-center expansion procedure used by Collins and Norcross.[4]

References

1. W. R. Garrett, Mol. Phys. 24, 465 (1972).
2. A. M. Arthurs and A. Dalgarno, Proc. Roy. Soc. (London) A256, 540 (1960).
3. E. S. Chang and U. Fano, Phys. Rev. A 6, 173 (1970).
4. L. A. Collins and D. W. Norcross, Phys. Rev. A 18, 467 (1978).
5. D. Dill and J. L. Dehmer, J. Chem. Phys. 61, 692 (1974).
6. J. Siegel, D. Dill, and J. L. Dehmer, J. Chem. Phys. 64, 3204 (1976).
7. D. Mukherjee and F. T. Smith, Phys. Rev. A 17, 954 (1978).
8. O. H. Crawford and A. Dalgarno, J. Phys. B 4, 494 (1971).
9. J. M. Blatt and L. C. Biedenham, Rev. Mod. Phys. 24, 258 (1952).
10. M. A. Brandt, D. G. Truhlar, and R. L. Smith, Comput. Phys. Commun. 5, 456 (1973).
11. DISSPLA (Display Integrated Software System and Plotting LAnguage, Integrated Software Systems Corp., California) Intermediate Manual, Sections 11.7 and 11.8 (1971).
12. L. Vuškovic, S. K. Srivastava, and S. Trajmar, J. Phys. B 11, 1643 (1978).

ELEMENTARY EXPRESSION OF THE BORN PARTIAL-WAVE CROSS SECTIONS FOR SCATTERING OF ELECTRONS BY ANY PURE MULTIPOLE ELECTROSTATIC-POTENTIAL FIELD*

Mitio Inokuti

In the calculation of the cross section for rotational excitation or de-excitation of a molecule by electron impact, one often needs to evaluate certain kinds of hypergeometric functions.[1-3] More specifically, these hypergeometric functions $F(\alpha, \beta, \gamma,$ and $x^2)$ are subject to the following conditions: (1) α is a positive integer; (2) β is a positive or negative half integer; (3) $\gamma = \alpha + \beta +$ integer; and finally, (4) x is a real number, often close to unity. (The symbol x^2 represents the ratio of the kinetic energies of the electron before and after scattering.) It has been shown that this class of hypergeometric function is expressed in the form

$$p(x^{-2})(2x)^{-1} \ln [(1+x)/(1-x)] + q(x^{-2}) + r(x^2), \qquad |x| < 1 ,$$

where p, q, and r are finite polynomials, and are readily determined by simple algorithms. This finding should be useful for a number of workers, including J. Siegel and C. W. Clark, whose stimulus has led to this work.

References

1. K. Takayanagi, J. Phys. Soc. Japan 21, 507 (1966).
2. Y. Itikawa and K. Takayanagi, J. Phys. Soc. Japan 26, 1254 (1969).
3. C. W. Clark, Phys. Rev. A 16, 1419 (1977).

---

*Summary of a paper now being prepared for publication.

RESONANT DISSOCIATION OF N_2 BY ELECTRON IMPACT*

David Spence and P. D. Burrow†

In an earlier brief publication[1] and report,[2] we noted a new process leading to the dissociation of N_2 by electron impact at energies just above the dissociation limit. The key features of our observation were the detection of a narrow band of slow electrons produced over a 1.5 to 2 eV range of impact energies with an abrupt onset for production near the dissociation energy. Neither of these features is characteristic of excitation to a bound or repulsive excited state of N_2. This was the basis for our interpretation that a resonance process forming a temporary negative ion, N_2^-, was involved in the dissociation. Furthermore, we reported[2] that the N_2^- state dissociates to the products $N(^4S) + N^-(^3P)$, followed by autoionization of the atomic negative ion yielding a slow electron whose energy is equal to the magnitude of the atomic electron affinity.

The dissociative attachment process leading to the formation of negative ion and neutral fragments by electron impact on small molecules is well known. Such processes in diatomic molecules, for example, are initiated by the attachment of an incident electron to form a temporary negative molecular ion, or resonance.[3] If attachment occurs above the ionic dissociation limit, the molecule may dissociate, yielding a neutral atom and a stable negative ion.

Strictly speaking, a proper dissociative attachment process cannot take place in molecules whose component atoms possess only unstable negative ions, since the electron must ultimately detach in the separated atom limit. Nevertheless, the analogous process may be envisioned in which the unstable atomic negative ion survives to large internuclear separation, then decays by ejection of an electron having a kinetic energy equal to the magnitude of the atomic electron affinity. The process provides a mechanism for dissociation

---

*Summary of a paper published in J. Phys. B: Atom. Molec. Phys. 12, L179 (1979).

†Consultant, Radiological and Environmental Research Division. Permanent address: Behlen Laboratory, University of Nebraska, Lincoln.

through the intermediate formation of a temporary negative ion, and hence could be classified as "resonant dissociation by electron impact." In an electron scattering experiment, the existence of the resonant dissociative process would be signaled by the production of slow electrons having kinetic energies equal to the magnitude of the electron affinity of atomic nitrogen. Furthermore, such electrons would be produced over a continuous range of energies reflecting favorable Franck-Condon overlap between the N_2 ground state and the repulsive portion of the relevant N_2^- potential curve. In addition, the lowest energy at which the slow electrons appear should lie above the dissociation energy for N_2, $D_0 = 9.76$ eV, by an amount equal to the magnitude of the electron affinity of atomic nitrogen.

We have examined the production of slow electrons in the region of the dissociation energy, using a trapped electron apparatus incorporating the modification devised by Knoop et al.[4] With this technique, we are able to adjust the potential trap so that only those scattered or ejected electrons which possess a selected final energy are detected.

Within the resolution limitations of our appratus, the distribution of slow electron energies may be obtained by plotting the trapped electron current as a function of residual electron energy at fixed impact energy. In Fig. 1 we illustrate two such curves taken at impact energies of 10.28 and 10.72 eV. These distributions, with widths 65 meV, are considerably narrower than the overall energy resolution of the apparatus (about 115 meV), and reflect the resolution of the "analyzer" section of the apparatus, which suggests that the emerging slow electrons possess an even narrower range of final energies. Indeed, Mazeau et al.,[5] with the superior resolution afforded by their electrostatic analyzer, determined that the energy distribution had width at half-maximum of 16 ± 5 meV. Our data suggest an electron affinity of -65 to -90 meV for N, in agreement with the more reliable value of -0.07 ± 0.02 eV of Mazeau et al.[5] These values are in good agreement with theoretical predictions.[6]

The total cross section for production of electrons with residual energy ~ 0.09 eV is shown in Fig. 2. We obtain the magnitude of the cross section for production of nitrogen atoms by reference to the $B^3\Pi_g$ ($v = 5$) peak, which we

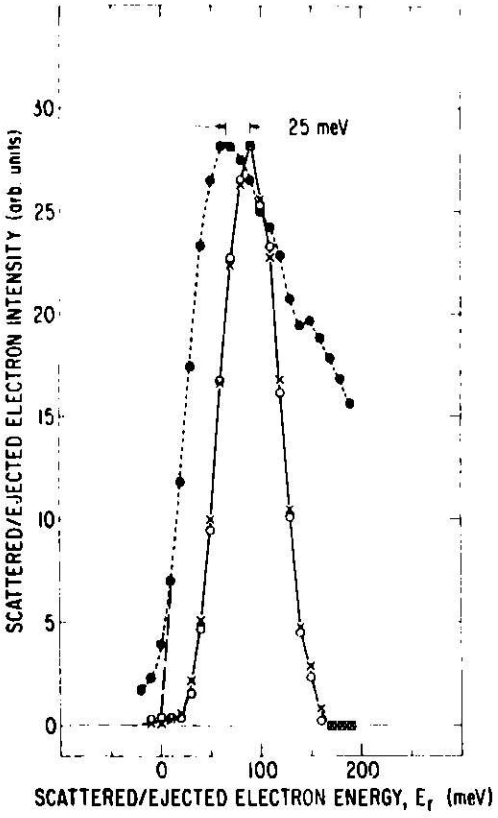

FIG. 1.--Ejected electron energy distribution taken at 10.72 eV (—o—) and 10.28 eV (—x—) incident energy in molecular nitrogen within the continuum, with observed onset at about 9.76 eV. The two distributions have been normalized to equal magnitude. The total excitation function for excitation of $E^3\Sigma_g^+$ state (--•--) obtained from the same experimental data is included as an aid in locating the zero energy of the scattered/ejected electrons. (ANL Neg. 149-79-102)

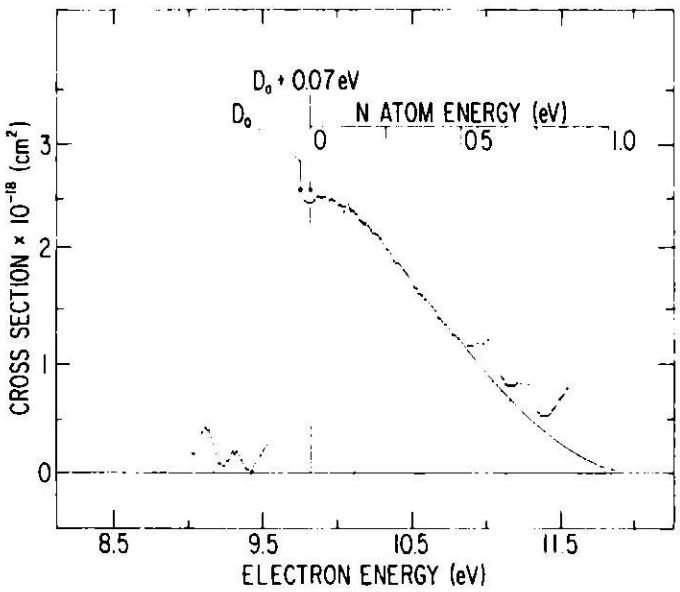

FIG. 2.--Total cross section for production of N atoms (shaded area) from the reaction $e + N_2 \rightarrow (N_2^{-*}) \rightarrow N + N + e(0.07\ eV)$ as a function of incident electron energy. The estimated error in the cross section is ±50%. The additional scale along the abscissa indicates the kinetic energies of the superthermal N provided by this process. (ANL Neg. 149-79-104)

normalize to the absolute integral cross sections for this state.

The resonant dissociation mechanism discussed here provides a source of superthermal N atoms from N_2 at the lowest possible impact energy; thus, it is likely to play a role of some importance in nitrogen plasmas (e.g., N_2 lasers and MHD plasmas) and in upper atmospheric phenomena such as auroras.

Finally, the reverse reaction, three-body recombination of N^4S atoms with an electron acting as the third body, should be greatly enhanced because of the resonance mechanism. This process may explain an observation by Brandt,[8] who reported that electrons were 10^7 or 10^8 times more efficient than ground state N_2 molecules in promoting recombination of N^4S atoms.

References

1. D. Spence, R. Huebner, and P. D. Burrow, Bull. Am. Phys. Soc. 23, 143 (1978).
2. D. Spence and P. D. Burrow, Radiological and Environmental Research Division Annual Report, October 1976–September 1977, ANL-7765, Part I, pp. 87–89.
3. G. J. Schulz, Rev. Mod. Phys. 45, 423–486 (1973).
4. F. W. E. Knoop, H. H. Brongersma, and A. J. H. Boerboom, Chem. Phys. Lett. 5, 450–452 (1970).
5. J. Mazeau, F. Gresteau, R. I. Hall, and A. Huetz, J. Phys. B: Atom. Molec. Phys. 11, L577–L560 (1978).
6. P. G. Burke, K. A. Berrington, M. LeDourneuf, and Vo Ky Lan, J. Phys. B: Atom. Molec. Phys. 7, L531–L535 (1974).
7. D. C. Cartwright, S. Trajmar, A. Chutjian, and W. Williams, Phys. Rev. A 16, 1041–1051 (1977).
8. B. Brandt, Proc. 6th Int. Conf on Ionization Phenomena in Gases, Vol. 1, North Holland Publ. Co., Amsterdam, p. 43 (1963).

ON THE POSSIBLE ROLE OF RESONANT DISSOCIATION PROCESSES AS A SOURCE OF ATMOSPHERIC HEATING IN THE THERMOSPHERE

David Spence and P. D. Burrow*

In considering physical and chemical processes in the atmosphere, it is usual to regard the atmosphere as being divided into layers (more properly called regions). However, one must remember that these regions do not co-exist independently, in that in a vertical plane mass, momentum and energy transfer must be considered under the equilibrium conditions that exist. Thus, to a large extent, conditions in the lower atmosphere are dependent upon conditions existent at the highest reaches of the atmosphere, i.e., the thermosphere, which is defined as the region from an altitude of about 100 km to the far reaches of space. The thermosphere derives its name because of the large increase in kinetic temperature with altitude, about 200°K at 100 km, increasing to 1000°K at 300 km.[1] A long-standing problem concerning mathematical modeling of the thermosphere has concerned the energy balance necessary to maintain the large temperature gradient. In order to calculate the energy input, two requirements are necessary: (1) a detailed knowledge of the flux of solar radiation onto the atmosphere as a function of photon energy, and (2) the fraction of this total energy converted into kinetic energy by known physical and chemical processes.

The constitution of the atmosphere at high altitudes is very simple, being approximately 20% molecular nitrogen and 80% atomic oxygen at 300 km.[1] All other species constitute only about 1% by composition. Whereas at lower altitudes (80–100 km) most of the energy input comes from O_2 absorption in the Schumann-Runge continuum,[2] at higher altitudes there is practically no O_2 for this mechanism to occur. The primary mechanism for energy deposition in the thermosphere is the photoionization of the constituents,[2] which then undergo

*Consultant, Radiological and Environmental Research Division. Permanent address: Behlen Laboratory, University of Nebraska, Lincoln, Nebraska 68588.

various physical processes, such as dissociative recombination, converting photon energy to kinetic energy. A second conversion mechanism is dissociative ionization by the free electrons.

The energy-loss mechanisms of the thermosphere can be accurately calculated and are predominantly:[2] (a) conduction to lower layers, and (b) infrared emissions from the 0 ground state at a wavelength of 63 μm. These mechanisms are of comparable magnitude. However, mass spectrometric rocket measurements (see Ref. 3 and references therein) give rise to a problem, since the concentration of atomic nitrogen in the thermosphere is too high to be explained by known electron-impact dissociation cross sections.[4,5] In fact, it has been determined[3] that electron dissociation cross sections would have to be increased by a factor of 3 at 15 eV and scaled accordingly to account for the measured concentration of N.

Early attempts to balance the energy flow in the thermosphere were made by Bates,[2,6] who, partially because of the relatively poor knowledge of the solar flux at wavelengths shorter than uv, found the heat input to the thermosphere to be too low by a factor of 20 to 60 to maintain the known temperature gradient when balanced against the well-characterized energy losses. To explain this imbalance, Bates[2] proposed modifying factor (2) on the preceding page by postulating a mechanism of energy conversion by "hidden" dissociative recombination—hidden in the sense that the reaction rate would be too fast for radar detection of the true electron concentration.

More recent measurements of solar flux at a wavelength shorter than the uv, and x-ray regions, have yielded a fairly well characterized solar photon flux distribution, thus improving factor (1) on the preceding page. However, recent model calculations[7] still yield a factor of 2 difference between the known energy input and that required to produce the large temperature gradient. Alternative sources of input such as joule heating of the atmosphere have been considered to balance the energy equation.[8]

However, an additional source of heating would be an increase in the conversion rate, i.e., factor (2) on the preceding page. A possible mechanism for this process could be that of resonant dissociation by electron impact

recently proposed by Spence and Burrow.[9] This process will produce superthermal atoms, which would probably be equilibrated with the surrounding species. Mazeau et al.[10] have found the same mechanism to occur in NO, although the concentration of NO in the thermosphere is too low for this mechanism to provide much energy conversion.

The electron concentration at 300 km is about 10^{-3} of the total composition[1] during the daytime, and furthermore the energy distribution is known from the measurements of Doering et al.[11] to peak at about 10 eV (at $\approx$ 100 km), exactly the right energy for resonant dissociation of N_2. The electron flux falls off very rapidly with increasing energy, decreasing by 3 orders of magnitude from 10 eV to 60 eV.

It is instructive to examine the product of known cross sections for N atom production and the measured electron flux. Such a plot is shown in Fig. 1, which may be conveniently divided into 3 regions: (a) The sharp spike at 10 eV results from the resonant dissociation process producing superthermal atoms (discussed in Ref. 9). Although the cross section for this process is low, the electron flux is at a maximum at the energy. (b) This large area results from straightforward electron-impact dissociation of N_2 calculated from the measurements of Winters.[4,5] Although the area of b is very large, probably a large fraction results in thermal atoms which will not cause significant energy conversion. (c) This region results from dissociative ionization of N_2 which is

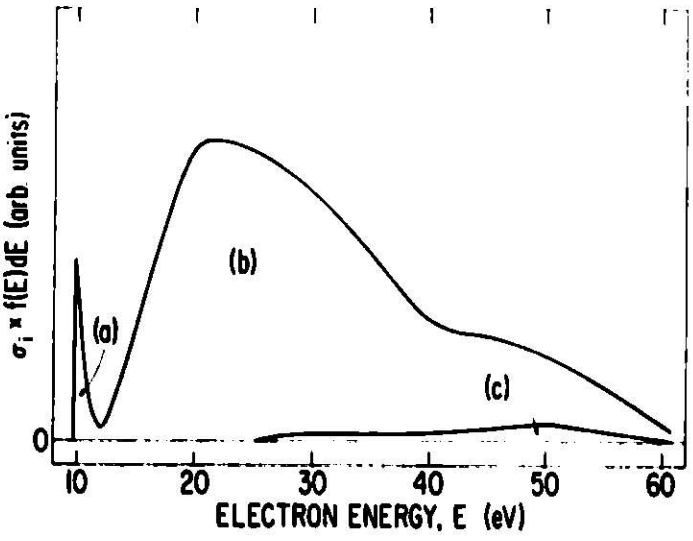

FIG. 1.--Plot of the product of cross section x electron flux (arbitrary units) as a function of electron energy typical of conditions in the thermosphere. Three regions are indicated, corresponding to a) resonant dissociation $e + N_2 \rightarrow (N_2^-)^* \xrightarrow{\sigma_1} N + N + e$; b) electron dissociation $e + N \xrightarrow{\sigma_2} N + N + e$; and c) dissociation ionization $e + N_2 \xrightarrow{\sigma_3} N^+ + N + e$. (ANL Neg. 149-79-101)

based on the measurements of Rapp et al.[12] for production of ions (and atoms) of energies ≥0.25 eV. The area of region c is seen to be comparable to that of region a. Although it is not possible to say that reaction a will result in a significant energy conversion, (and Fig. 1 would seem to indicate that reaction a provides little additional N to explain the anomalous N atom concentrations), we must point out that the cross-section data used to calculate region a were obtained for nitrogen in its ground vibrational level.

The significance of this is that the resonant dissociation process is the direct analog of dissociative electron attachment. Dissociative attachment cross sections are known to be often extremely dependent on the vibrational state of the target gas,[13-18] and in some cases they can increase by several orders of magnitude[16-18] for vibrationally and rotationally excited target states. Note that dissociative ionization cross sections also increase,[19,20] but at a much slower rate.

We stress that at the present time the discussion above is highly speculative, but in view of the important nature of the problem, we feel that further study is justified. We note that in auroras there is also evidence of an unknown process pumping energy into the system, and that superthermal N atoms of unknown origin have been observed.[21]

References

1. DNA Reaction Rate Handbook, 2nd Ed., DASIAC DoD Nuclear Information and Analysis Center, General Electric, TEMPO, Santa Barbara, California.
2. D. R. Bates, Proc. Phys. Soc. 64B, 805 (1951).
3. E. S. Oram, D. F. Strobell, and K. Maversberger, J. Geophys. Res. 83, 4877 (1978).
4. H. F. Winters, D. E. Horne, and E. E. Donaldson, J. Chem. Phys. 41, 2766 (1964).
5. H. F. Winters, J. Chem. Phys. 44, 1472 (1966).
6. D. R. Bates, Proc. Roy. Soc. 253A, 451 (1959).
7. R. G. Robb and R. E. Dickenson, J. Geophys. Res. 78, 249 (1973).
8. B. B. Hinton, J. Geophys. Res. 83, 707 (1978).
9. D. Spence and P. D. Burrow, to appear in J. Phys. B: Atom. Molec. Phys.
10. J. Mazeau, F. Gresteau, R. I. Hall, and A. Huetz, J. Phys. B: Atom. Molec. Phys. 11, L557 (1978).

11. J. P. Doering, W. K. Peterson, C. O. Bostrom, and T. A. Potemra, Geophys. Res. Lett. 3, 129 (1976).
12. D. Rapp, P. Englander-Golden, and D. A. Briglia, J. Chem. Phys. 42, 4081 (1965).
13. W. R. Henderson, W. L. Fite, and R. T. Brockmann, Phys. Rev. 183, 157 (1969).
14. D. Spence and G. J. Schulz, Phys. Rev. 188, 280 (1969).
15. T. F. O'Malley, Phys. Rev. 150, 14 (1969).
16. D. Spence and G. J. Schulz, J. Chem. Phys. 58, 1800 (1973).
17. P. J. Chantry, J. Chem. Phys. 51, 3369 (1969).
18. M. Allan and S. F. Wong, Yale University, submitted for publication.
19. D. Spence and K. T. Dolder, New Experimental Techniques in Propulsion and Energetics Research, D. Andrews and J. Suruque, Eds., Technivision Series, Slough, England, p. 423 (1970).
20. R. T. Brackmann, W. L. Fite, and W. M. Jackson. Proc. 18th Ann. Conf. of Mass Spectros. and Allier Topics, San Francisco, 1970, p. B107.
21. T. Shyn, Space Physics Department, University of Michigan, Ann Arbor, private communication (1978).

ELECTRON SCATTERING FROM ACTIVE NITROGEN: EXCITATION OF THE $3s\,^4P$ AND $2p^4\,^4P$ STATES OF ATOMIC NITROGEN

David Spence and P. D. Burrow*

There have been several recent theoretical papers[1,2] concerning electron scattering from atomic nitrogen, and in particular, the calculation of total inelastic excitation cross sections. Because of the extreme difficulty in producing targets of atomic nitrogen, apparently no experimental values of these excitation cross sections have been obtained from scattered electron measurements.

For these reasons, we have attempted, using the apparatus shown schematically in Fig. 1, to make such measurements in the energy region close to threshold. In our apparatus a beam of partially dissociated nitrogen (a few %) produced in a mullite tube by a microwave discharge is directed through a parallel plate collector in a collision chamber. A potential well is applied to the collision chamber by the parallel plates, and the apparatus is operated in the modified ac trapped electron mode.[3,4] In this mode we are able to select (i.e., energy analyze) the final energies of the scattered electrons after an inelastic collision.

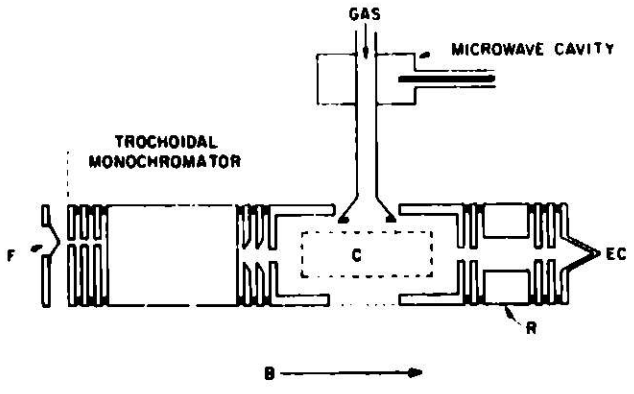

FIG. 1.--Schematic diagram of the apparatus.
(ANL Neg. 149-5977 Rev. 2)

*Consultant, Radiological and Environmental Research Division. Permanent address: Behlen Laboratory, University of Nebraska, Lincoln.

Typical spectra we obtain with the microwave discharge turned on and turned off are shown in Fig. 2. These spectra were taken at a scattered energy of about 0.080 eV. Most of the structures are due to the well-known bands of molecular nitrogen, which constitute over 95% of our target. The additional structures, which appear in Fig. 2 (top) are due to excitation of $2s^2 2p^2 (^3P) 3s\ ^4P$ and $2s2p^4\ ^4P$ states of atomic nitrogen. We were unable, under present conditions, to detect any atomic nitrogen structures outside of this energy range, probably because of the overwhelming molecular structure; nor were we able to detect any "hot bands" of the $N_2\ B^3\Pi_g$ or $E^2\Sigma_g^+$ states, indicating there was very little vibrationally excited N_2 in our beam.

By taking many spectra similar to those in Fig. 2 at different values of scattered (i.e., final) electron energies, we were able to plot the excitation cross sections shown in Fig. 3. The N $3s\ ^4P$ cross section rises very rapidly at threshold within our experimental resolution of about 0.1 eV, and then falls off rapidly. Unfortunately, in their theoretical work, Berrington et al.[2] did not include the $3s\ ^4P$ target state in their calculations, even though this is the lowest excited state configuration of N optically allowed, and is the most prominent atomic feature of our spectra. The shape of this cross section is

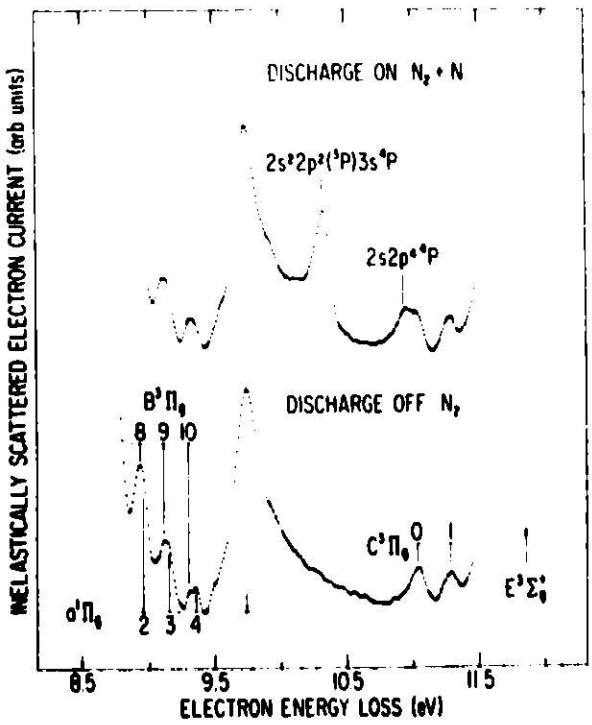

Fig. 2.--Scattered electron spectra in a mixture of N_2 + N (upper trace) and in pure N_2 (lower trace) for a scattered electron energy of about 0.08 eV. The additional structures in the upper trace are due to excitation of the $3s\ ^4P$ and $2p^4\ ^4P$ states of atomic nitrogen. (ANL Neg. 149-79-103)

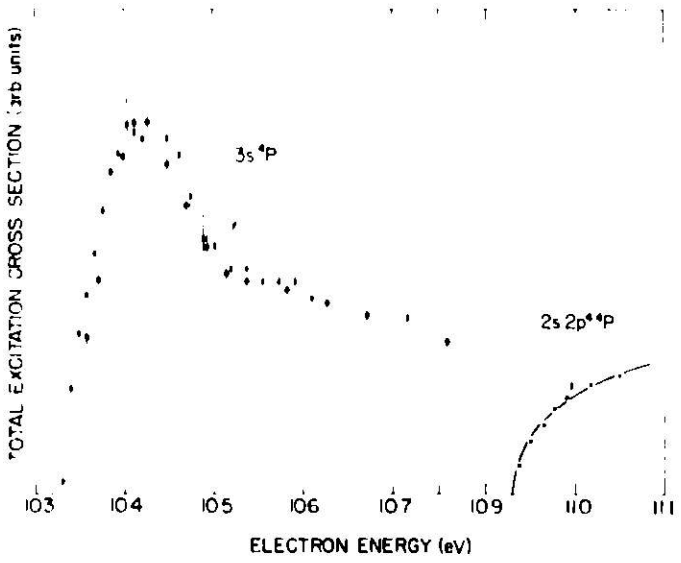

FIG. 3.--Cross sections for electron impact excitation of the $3s\,^4P$ and $2p^4\,^4P$ states of atomic nitrogen. The $3s\,^4P$ state has a characteristic resonance structure at threshold, whereas the $2p^4\,^4P$ state rises slowly from threshold in accordance with theory.

characteristic of one which has a (negative ion) resonance very close to threshold. The cross section of the $2s2p^4\,^4P$ rises slowly from threshold, in agreement with the theoretical prediction of Berrington et al.[2] Unfortunately, we were unable to plot this cross section for energies greater than about 0.1 eV above threshold because of the overwhelming influence of the $N_2\,C^3\Pi_g(v=0)$ state. Similarly, we were unable to plot the $3s\,^4P$ cross section for energies more than about 0.3 eV above threshold because this cross section is rapidly decreasing, while the underlying $N_2a^1\Pi_g$ vibrational bands are slowly increasing. In a future publication we will present additional spectra illustrating these effects.

References

1. S. Ormonde, K. Smith, B. W. Torres, and A. R. Davies, Phys. Rev. A 8, 262–295 (1973).
2. K. A. Berrington, P. G. Burke, and W. D. Robb, J. Phys. B: Atom. Molec. Phys. 8, 2500–2511 (1975).
3. F. W. E. Knoop, H. H. Brongersma, and A. J. H. Boerboom, Chem. Phys. Lett. 5, 450–452 (1970).
4. D. Spence, Phys. Rev. A 12, 2353– 2360 (1975).

RESONANCES IN THE DIFFERENTIAL ELASTIC SCATTERING OF ELECTRONS FROM MERCURY AT 180°

P. D. Burrow* and J. A. Michejda†

The lowest Feshbach resonances formed by electron scattering from Hg are observed in the total scattering cross section and in the differential elastic cross section at a scattering angle of 180°.

By means of a simple modification[1] to the standard trochoidal electron monochromator,[2] a spectrometer may be constructed for the study of electrons which are elastically scattered from a target into a small solid angle centered at 180° with respect to the direction of the incident electron beam. Observation of the differential elastic scattering cross section at this angle offers a number of advantages for the detection of resonant structure in the scattering cross section because of the formation of temporary negative ions, particularly in molecules with large dipole moments whose total scattering cross section is dominated at low energies by small angle scattering.

From an experimental point of view, this additional function may be easily incorporated into the standard electron transmission apparatus devised by Sanche and Schulz.[3] This permits the viewing of resonances both in the total cross section and in a single differential channel. In principle this provides additional information concerning the partial wave in which the resonance occurs and the phase angle of the nonresonant portion of the scattering.

An unusual example illustrating these two measurements is shown in Fig. 1. In the upper half of the drawing, we have plotted the derivative with respect to energy of the electron current transmitted through a gas cell containing mercury vapor. The lowest excited states of mercury are labeled by

*Consultant, Radiological and Environmental Research Division. Permanent address: Department of Physics and Astronomy, University of Nebraska, Lincoln, Nebraska 68588.

†Department of Engineering and Applied Science, Yale University. Present address: Bell Laboratories, Allentown, Pennsylvania 18103.

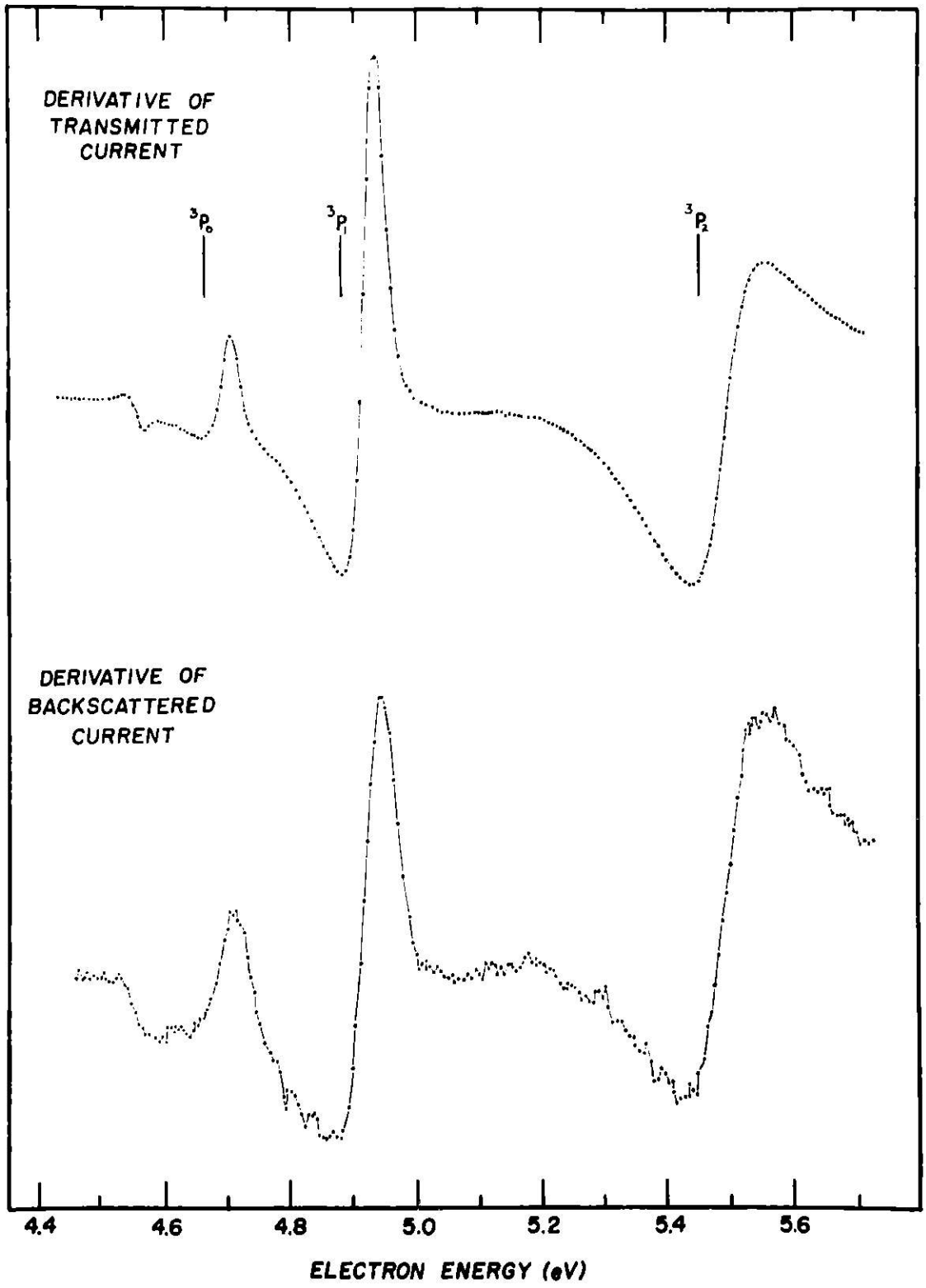

FIG. 1.--(Upper curve) The derivative of electron current transmitted through Hg vapor as a function of electron impact energy; (lower curve) the derivative of electron current elastically scattered at 180° as a function of electron impact energy. Vertical scale arbitrary.

vertical lines. The sharp structure in the transmitted current is ascribed to the Feshbach resonances associated with the excited states. At low attenuation, the plotted signal is proportional to the negative of the derivative of the total scattering cross section.

The lower curve shows the derivative with respect to energy of the electron current elastically scattered at 180°. If the energy dependence of the differential cross section in the back direction were the same as that of the total cross section, the two curves would be related "reciprocally," that is, a maximum in one would correspond to a minimum in the other. However, because of interference terms in the expression for the differential cross section which are not present in the total cross section, this clearly need not be the case. In our example these terms conspire to cause the two curves to be remarkably similar. The appearance of these resonances at other scattering angles between 30° and 150° has been discussed by Albert et al.[4]

References

1. P. D. Burrow and L. Sanche, Phys. Rev. Lett. 28, 333 (1972).
2. A. Stamatovic and G. J. Schulz, Rev. Sci. Instrum. 41, 423 (1970).
3. L. Sanche and G. J. Schulz, Phys. Rev. A 5, 1672 (1972).
4. K. Albert, C. Christian, T. Heindorff, E. Reichert, and S. Schön, J. Phys. B 10, 3733 (1977).

A NOTE ON A POSSIBLE SOURCE OF ERROR IN ELECTRON IMPACT IONIZATION CROSS SECTION MEASUREMENTS BY PARALLEL PLATE CONDENSERS

David Spence

The measurement of electron impact ionization cross sections, of crucial importance to any plasma or radiation damage mathematical model, and conceptually one of the simplest of all atomic collision measurements to make, has suffered from sources of unknown or unrecognized error. The simplest and probably most reliable method for making such measurements is the parallel plate condenser technique, which has been used for 50 years and adequately described in the literature.[1-4] This technique requires the measurement of only 3 parameters (i.e., current, pressure, and length) which can all be determined within 1 or 2% with relative ease. Despite this, such measurements among different workers often differ by 30 to 40% for the heavier rare gas atoms, diatomic and triatomic molecules (see Ref. 5 and references therein).

One possible source of error we have never seen discussed in the literature concerns the ejection of secondary electrons from the condenser plates by the impact of positive ions (although the importance of suppressing secondary electrons from the electron collector is usually stressed). In a previous publication[6] concerning the measurement of <u>negative ion</u> cross sections in a parallel plate apparatus, we noted that any measurement of positive ion cross sections ever taken probably has been afflicted to an unknown degree by the effective secondary electron coefficient, γ, due to the incidence of positive ions on the ion collector. The larger the secondary electron coefficient and the larger the escape probability of the electrons, the larger will be the apparent positive ion current, and hence the larger the calculated positive ion cross section. Since γ is not taken into account in any of the measurements of positive ion cross sections, one would expect that the lowest values of positive ion cross section obtained would be the most nearly correct values, neglecting, of course, any errors in pressure measurements and current measurements. It should be noted that γ includes not only the coefficient for electron emission by positive ions on the particular metal surface, but also the probability that

the ejected electron will actually escape.

Our reasons for arriving at the above statement was our observation[6] that many negative ion cross-section measurements by different authors were in agreement within a few percent. Strangely negative ion cross sections are often 100 times smaller than positive ion cross sections, and thus potentially more difficult to measure. Negative ion cross sections are usually determined by normalizing to a positive ion cross section determined absolutely in the same apparatus.

When determining the negative ion cross section, Q_-, by normalization to the positive ion current at a particular electron energy, one takes the ratio $M = i_-/i_+$, and then obtains the negative ion cross section, $Q_- = MQ_+$. In a given apparatus, both M and Q_+ are affected by an unknown factor $(1+\gamma)$, which cancels when one calculates Q_-. Secondary electrons do not affect the measurement of i_- because ejected electrons cannot escape from the positively biased collector. Measurements of Q_+ alone will involve this error, and is likely to be different for different surfaces and geometries. Thus we were able to explain logically the good agreement between negative ion cross sections, but poor agreement among positive ion cross sections.

It is now well known that positive ions of most gases, with energies even less than 1 eV, have a very high probability of ejecting an electron (up to 40 to 50%) from most common metals such as copper or molybdenum, materials which are often used in the construction of positive ion devices. Moreover, this ejected electron has, in general, low energy (of the order of 1 eV). Such an electron will be bent around in the applied B field used to collimate the main electron beam and strike the surface from which it was ejected. However, a 1 eV electron has an 80 to 90% chance of bouncing when it hits a metal surface, with the guilding center mutually perpendicular to the B and E fields until it hops off the end and is lost.

We have built an apparatus with collision geometry identical to that used by Tate and Smith,[2] and by Rapp and Englander-Golden.[3] We will make measurements of positive ionization cross sections under identical conditions but with different surface metals in order to test out hypothesis.

References

1. P. T. Smith, Phys. Rev. 36, 1293 (1930).
2. J. T. Tate and P. T. Smith, Phys. Rev. 39, 270 (1932).
3. D. Rapp, P. Englander-Golden, and D. D. Briglia, J. Chem. Phys. 42, 4081 (1965).
4. D. Rapp and P. Englander-Golden, J. Chem. Phys. 43, 1464 (1965).
5. L. J. Kieffer, A Compilation of Electron Collision Cross Section Data for Modeling of Gas Discharge Lasers, JILA Information Center Report 13, University of Colorado, Boulder (1973).
6. D. Spence and G. J. Schulz, Phys. Rev. 188, 280 (1969).
7. H. D. Hagstrum, in Inelastic Ion-Surface Collisions, N. H. Tolk, J. C. Tully, W. Heiland, and C. W. White, Eds., Academic Press, New York, (1977) pp. 1-25.

DIFFERENTIAL TRAPPED ELECTRON SPECTROSCOPY: A NOVEL TECHNIQUE FOR OBTAINING FRANCK-CONDON FACTORS AND IDENTIFYING THRESHOLD STRUCTURES

David Spence

In this report we introduce a simple novel technique for extracting accurate Franck-Condon factors from threshold electron spectra in which the instrumental resolution is insufficient to completely resolve vibrational energy levels. An interesting extension of our technique is its ability to identify those energy levels which have sharp maxima at threshold for excitation by electron impact, without the effort of actually measuring such a cross section. These threshold peaks are usually caused by closely neighboring negative ion resonances. These two properties of our technique are described in more detail below.

Determination of Franck-Condon Factors

Figure 1 illustrates the vibrational levels of the $B^3\Pi_g$ of N_2 obtained in the modified trapped electron apparatus as previously described.[1] This apparatus differs from the usual trapped electron apparatus[2] in that it has the facility to select the inelastically scattered electrons by energy. This is achieved by modulating the depth of the well (while keeping the incident energy independent of the modulation) and detecting the trapped electrons with a synchronous detector.[3] In this spectrum the resolution has been deliberately degraded to cause overlapping of peaks. Extraction of Franck-Condon factors from such spectra is difficult; values taken from peak height to baseline are shown in Fig. 2 and are seen to be in poor agreement with the optical data.[4] The true baseline of Fig. 1a should be a distorted bell shape indicated by the curved solid line of Fig. 1a, although from this figure there is no simple method of obtaining the true unique curve. We can circumvent this problem by modulating the energy in the collision chamber instead of the well depth. This is done simply by applying the modulation voltage to the input of the collision chamber instead of the output. This technique results in the same intensity, I, of the

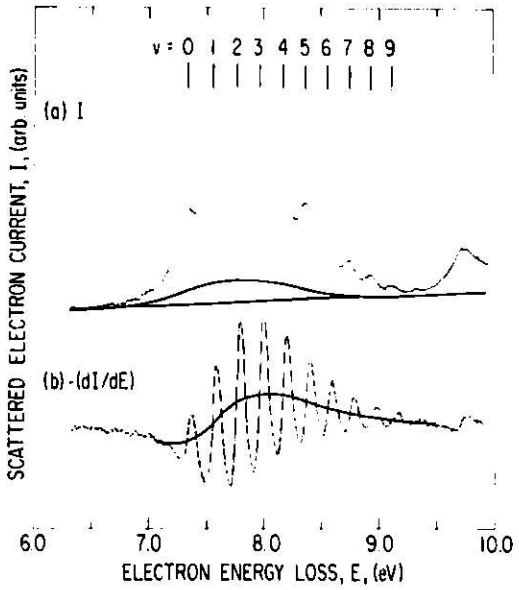

FIG. 1.--Spectra of the normal trapped electron current obtained by excitation of the $B^3\Pi_g$ state of N_2 (a) and its differential (b).

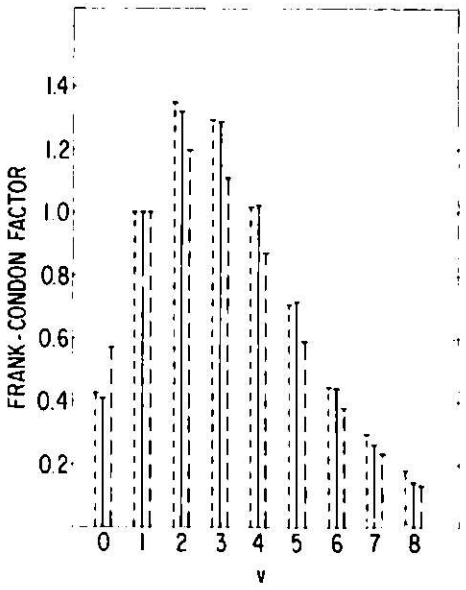

FIG. 2.--Franck-Condon factors obtained from the two spectra of Fig. 1 illustrating the good agreement between the differential data of Fig. 1 and optical values. Optical values, ——; -dI/dE, ----; I, — — —.

trapped electron current, but now because we are modulating the energy E, the detected signal will be proportional to dI/dE, i.e., the differential of the trapped electron current. Such a plot is shown in Fig. 1b, taken under exactly the same conditions as Fig. 1a. In this case, the relative height of the structures of Fig. 1a are represented by the maximum traversals of the structure of Fig. 1b. The differential of the slowly varying background of Fig. 1a is sketched in the slowly varying differential curve of Fig. 1b, and has no effect on measurements of the peak heights. Relative Franck-Condon factors obtained in this way are also indicated in Fig. 2, and show excellent agreement with optical values.[4] Normally, of course, one would have sufficient resolution to resolve these structures in N_2, but we have chosen this example merely to demonstrate the technique. One should note that this technique is not limited to the trapped electron method, but can be applied to any type of monochromator-analyzer system.

Detection of Threshold Structures

Following the usual nomenclature for the a.c. trapped electron method,[1] we have sketched the two cases—modulation of well output ΔW and modulation of accelerating voltage V_a in Fig. 3. We apply these two modes to two different types of excitation functions sketched above: (a) a cross section which rises slowly from threshold and (b) a cross section which peaks at threshold.

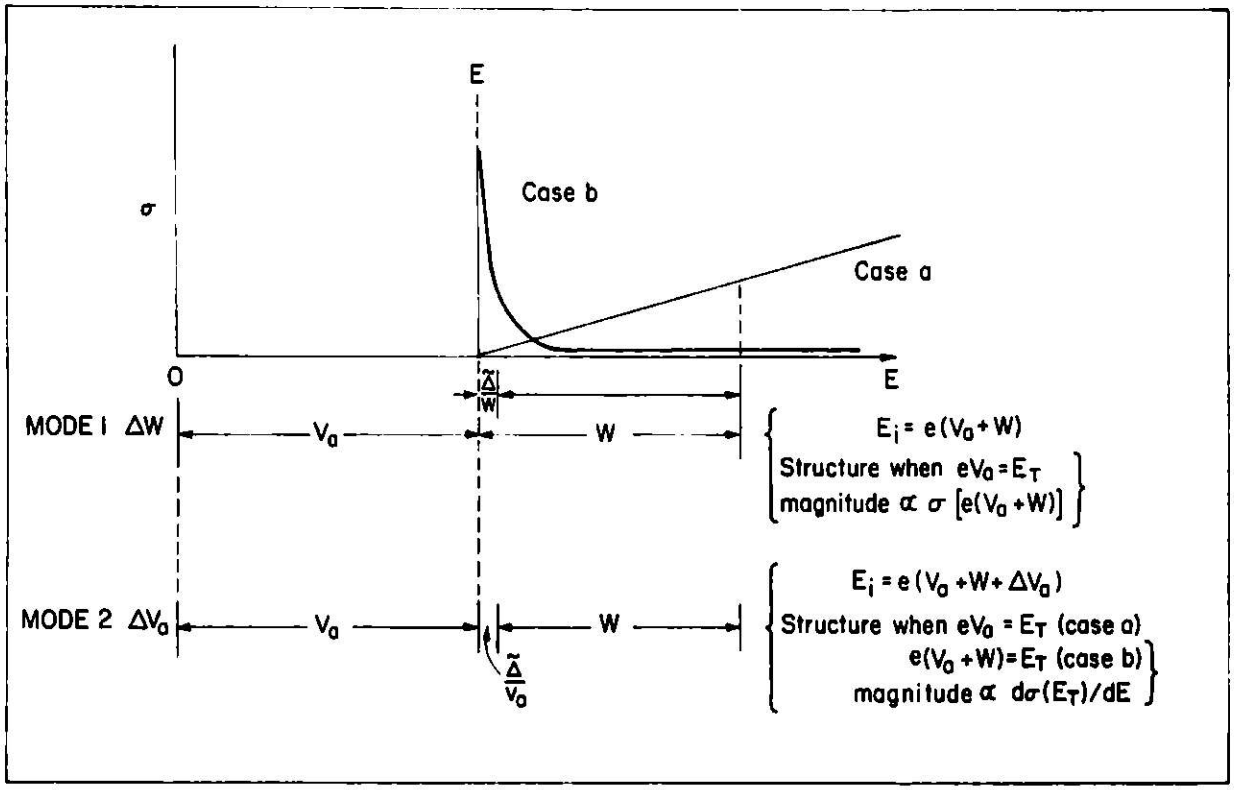

FIG. 3.--Sketch of the two modes of operation, modulation of V_a, and of W, as applied to two excitation functions, one of which peaks at threshold (case b) and one which varies slowly with energy (case a).

In mode 1 of Fig. 3, an inelastic feature will only occur when $V_a = E_T$, and the magnitude of this feature will correspond to the magnitude of the cross section at an energy $E_T + W$. In mode 2 of Fig. 3, not only is the output of the well being modulated, but also the incident energy. Suppost $V_a + W$ is initially less than E_T. As V_a is increased, then as $V_a + W$ crosses E_T there will be a large signal from case b alternately trapped and untrapped in the well, i.e.,

in case b, a signal will be detected when $V_a + W = E_T$. The slowly varying case a will result in only a small constant addition to the background when $V_a + W = E_T$, but this curve, slowly varying, will result in a large differential signal when $V_a = E_T$, as in mode 1 above. Thus, using the energy differential technique, structures appear in the spectra at $V_a + W = E_T$ for those cross sections with large peaks at threshold, and at $V_a = E_T$ for those cross sections which vary slowly with energy. Now if we take two spectra at different values of W, those structures caused by cross sections which peak at threshold will shift by an amount W relative to the other structures.

We illustrate the above effect in active nitrogen (i.e., partially dissociated nitrogen) as shown in Fig. 4 for two values of W. This is a particularly interesting example and shows three structures which are known to peak at threshold. These are (1) the v = 6 level of the a $^1\Pi_g$ state of N_2, which has been shown by Spence and Burrow[5] to peak at threshold, though the reasons for this are not completely understood; (2) the 3s ^{4}P state of atomic nitrogen;[6,7] (3) the $E\,^3\Sigma_g^+$ state of molecular nitrogen which is known to peak at < 35 meV above threshold.[8] The technique described here is readily applied to any monochromator-analyzer system and will rapidly identify those cross sections which peak near zero.

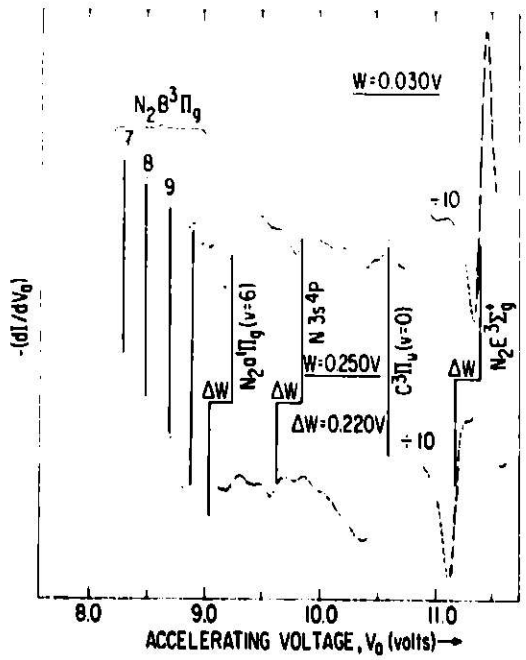

FIG. 4.--Differential trapped electron spectra taken at two different values of W in active nitrogen. The three shifted structures are caused by threshold peaks in the N_2, a $^1\Pi_g$ (v = 6) level, the N 3s ^{4}P state, and the N_2 $E\,^3\Sigma_g^+$ state.

References

1. D. Spence, Phys. Rev. A 12, 2353 (1975).
2. G. J. Schulz, Phys. Rev. 112, 150 (1958).
3. F.W.E. Knoop, H. H. Brongersma, and A.J.H. Boerboom, Chem. Phys. Lett. 5, 450 (1970).
4. W. Benesh, J. T. Vanderslice, S. G. Tilford, and P. G. Wilkinson, Astrophys. J. 143, 236 (1966).
5. D. Spence and P. D. Burrow, to appear in J. Phys. B: Atom. Molec. Phys.
6. D. Spence and P. D. Burrow, to be submitted for publication.
7. D. Spence and P. D. Burrow, Electron scattering from active nitrogen: Excitation of the $3s\ ^4P$ and $2p\ ^4P$ states of atomic nitrogen, this report.
8. J. Mazeau, F. Gresteau, R. I. Hall, and A. Huetz, J. Phys. B: Atom. Molec. Phys. 11, L557 (1978).

ELECTRON IMPACT EXCITATION CROSS SECTIONS OF THE n = 2 STATES OF HELIUM BY ELECTRON IMPACT

David Spence and Dorothy Stuit*

Because of the importance of the He n = 2 cross sections as a testing ground for new theoretical models,[1,2] we have reinvestigated the electron impact excitation of the He 2^3S, ^1S, ^3P, and ^1P cross sections from threshold to amaximum of 8 eV above threshold (in the case of the ^3S state). The only previous experimental determination of these cross sections that were performed with sufficient resolution to be meaningfully compared with present theories in this energy region were those of Brongersma et al.[3] (We exclude the data of Brunt et al.[4] from this statement because although performed with the best energy resolution to date represent a measurement of total metastable atom production which includes ^3S and ^1S contributions.)

The technique used by Brongersma et al.[3] was the then new double retarding potential difference (DRPD) method,[5] which is essentially a modified trapped electron technique with the ability to select the scattered electrons for energy. It may thus be thought of as a double electrostatic analysis system, albeit with the capability of measuring the total (rather than differential w.r.t. angle) cross section. We have used an apparatus for our measurements which is identical to that of Brongersma,[3] with the exception of the electron monochromator, in which we have replaced the RPD electron gun with a trochoidal monochromator.[6] This modification results in much higher S/N ratios for a given scanning time. As with all analyzers, there are two possible modes of operation with this technique for obtaining cross sections.

1. The first mode is to set the analyzer to accept electrons of a fixed energy loss at some threshold and sweep the incident and analyzer energy in order to plot out an excitation function. Using this mode of operation with the DRPD technique has three potentially serious defects i.e., (a) as the incident

*Undergraduate Research Participant from Le Tourneau College, Longview, Texas (1975).

energy is increased, the analyzer "slips out of tune" because of the greater depth of the well effectively "dragging down" the edges of the potential well. This defect, which produces an underestimate of the cross section at higher energies, had previously been noted by Knoop et al.,[5] but was disregarded by Brongersma et al.[3] in their cross section measurements. (b) At a higher analysis energy the instrument resolution is degraded owing to rounding of the ends of the potential well. As the cross section at a given analysis energy is proportional to the area of an "energy loss" peak, this results in an additional underestimate of the cross section at higher energy. (c) Because of the degradation in resolution at higher analysis energy, contributions from neighboring states may be included in the signal. This effect can be very large in He, for example; measurements of the ^1S can be overwhelmed by contributions from the ^3P (see Fig. 1, Ref. 3). To some degree, effects (a) and (b) are offset by effect (c), though by an unknown amount. Because of these defects, the shape of the measured cross section is dependent upon the analysis energy initially chosen to "tune" the instrument before beginning a scan. There appear to be no new criteria for producing a unique excitation function in this mode.

2. An alternative mode is to tune the analyzer to accept a fixed final energy of the scattered electrons and to sweep the incident energy. This method will produce fixed energy loss spectra whose peak areas are proportional to the cross section at a chosen value above threshold. From a series of

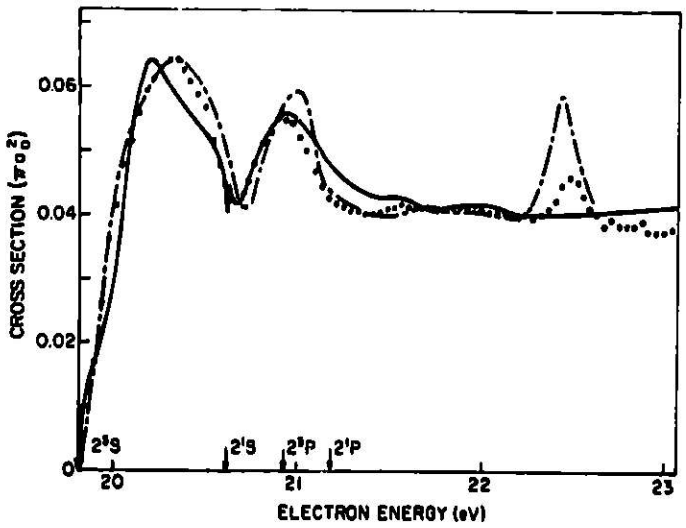

FIG. 1.--Comparison of theoretical and experimental values of the He 1s2s ^3S excitation cross section. Present experimental data (....); theoretical curve of Berrington, et al. (Ref. 2)(——); Theoretical curve of Oberoi et al. (Ref. 1)(—.—.).

such spectra one can then measure areas and plot a cross section. This technique, although much more tedious than mode 1 described above, avoids all three defects.

We have chosen, therefore, to use method 2, rather than method 1, used by previous authors. For completeness we did take spectra by method 1, which agree very well with the data of Brongersma[3] under certain non-unique tuning conditions. Although the defects of mode 1 could not be considered serious at the time of the earlier measurements,[3] the state of the theory is now so advanced that experimental refinement is essential.

In this report we will not discuss our results in detail, but merely point out general features of our data.

1. 1^1S-2^3S Cross Sections

Our data are shown in comparison with the theoretical cross sections obtained by Berrington et al.[2] and Oberoi and Nesbet (Ref. 1 in Fig. 1). Both experimental cross sections are relative, not absolute. We have chosen to normalize our data to the theoretical peak of 0.5 eV above threshold, merely for the sake of comparison. There is good general agreement among all these data. Minor differences will be discussed in a future publication.

2. 1^1S-2^1S Cross Sections

Our data, together with previous theoretical values, are shown in Fig. 2. Here the agreement among the data is somewhat poorer. Whereas the general trend in the theoretical cross section of Oberoi and Nesbet[1] is a decrease above 21.0 eV, the data of Berrington et al.[2] show a continuous rise

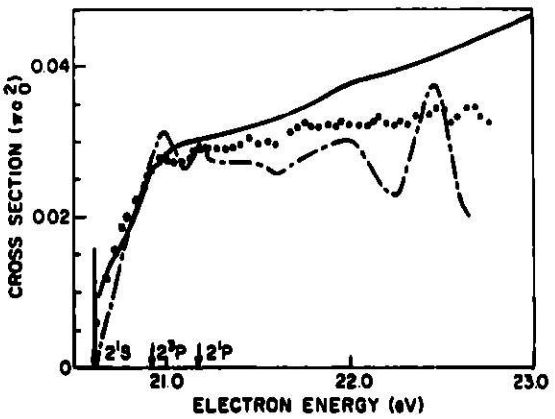

FIG. 2.--Comparison of theoretical and experimental values of He 1s2s ^1S excitation cross section. Present experimental data (....); theoretical curve of Berrington et al. (Ref. 2)(——); Theoretical curve of Oberoi et al. (Ref. 1)(—.—.).

and contain less structure. Our present data points are in somewhat closer agreement within the latter theory. We do not observe the oscillatory structure calculated by Oberoi and Nesbet,[1] although our resolution is easily sufficient to observe such structures (cf. the structures in Fig. 2). The initial general decrease in cross sections above 21.0 eV in the data of Brongersma et al.[3] is undoubtedly caused by the effect noted above, i.e., "slipping out of tune," and part of the general rise above this is due to increasing contributions to their signal from the ^3P state. A more detailed comparison between present experimental and previous experimental and theoretical data will be discussed at greater length in a future publication.

3. 1^1S-2^3P, 1^1S-2^1P Cross Sections

We have raw data for these cross sections but analysis is incomplete and will be reported later.

References

1. R. S. Oberoi and R. K. Nesbet, Phys. Rev. A 8, 2969 (1973).
2. K. A. Berrington, P. G. Burke, and A. L. Sinfailam, J. Phys. B: Atom. Molec. Phys. 8, 1459 (1975).
3. H. H. Brongersma, F.W.E. Knoop, and C. Backx, Chem. Phys. Lett. 13, 16 (1972).
4. J.N.H. Brunt, G. C. King, and F. H. Read, J. Phys. B: Atom. Molec. Phys. 10, 433 (1977).
5. F.W.E. Knoop, H. H. Brongersma, and A.J.H. Boerboom, Chem. Phys. Lett. 5, 450 (1970).
6. D. Spence, Phys. Rev. A 12, 2353 (1975).

MEASUREMENTS OF THE RATIO OF THE He $2^1s/2^3s$ ENERGY INTEGRATED TOTAL CROSS SECTIONS FROM THRESHOLD TO 0.12 eV. COMPARISON WITH THEORY

David Spence

We have used the trapped electron (TE) method to measure the ratio of the helium $2^1S/2^3S$ energy integrated total (with respect to angle) cross sections from threshold to 0.12 eV above threshold. First, we would like to dispel one seemingly common misconception regarding the ability to measure cross section ratios at energies above threshold which are less than the overall resolution of the instrument. While it is true that for energies closer to threshold than the instrumental resolution the technique is incapable of giving the correct functional dependence of an excitation cross section, it is incorrect to say that cross section ratios are resolution dependent in this energy region. In fact, we will demonstrate that such ratios are totally independent of the resolution and depend only on the chosen value of the well depth, i.e., the region of the cross section above threshold which we choose to examine. We will clarify this statement with reference to Fig. 1, where on the left-hand side we have sketched a typical trapped electron apparatus, together with the potential along the axis of the tube. For a detailed description of the operation of the trapped electron technique, one should refer to the original paper by Schulz.[1] For our purpose, one need only remember that electrons of energy eV_a enter a collision chamber which contained a potential well of depth W. The energy of the electrons in the collision chamber is thus $e(V_a + W)$. Electrons which lose an amount of energy between eV_a and $e(V_a + W)$ in an inelastic collision are trapped in the well and collected, i.e., all electrons whose final energy is $\leq eW$. Note well that there is no possible mechanism for trapping electrons of final energy $> eW$, irrespective of the energy resolution of the incident electron beam or degradation of resolution from rounding of the potential at the ends of the potential well. This is illustrated on the right-hand side of Fig. 1 (where we have sketched an arbitrary excitation function with threshold, E_T, at energy eV_a, and above is a representation of the overall instrumental resolution ΔE. If W were much greater than ΔE, then a sweep

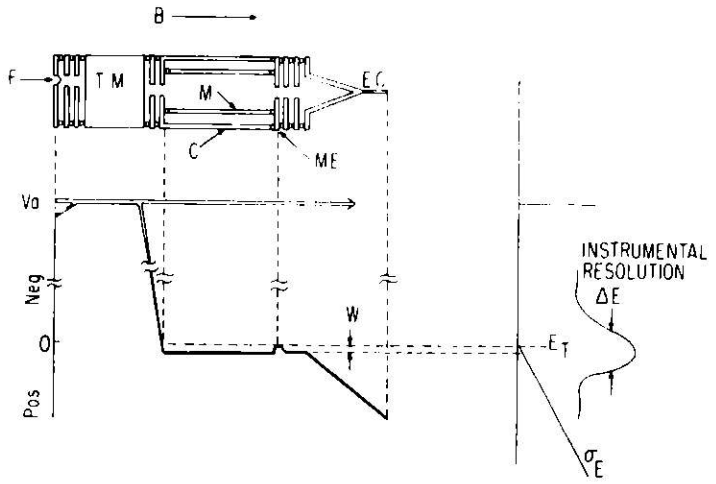

FIG. 1.--Schematic of trapped electron apparatus illustrating how, for large instrumental width ΔE, electrons of only narrow ranges of scattered electron energies eW are detected. There is no mechanism for collecting electrons of energy $>eW$ above an inelastic threshold E_T, irrespective of ΔE.

of the incident energy would plot the shape of the excitation function with a cutoff at eW above threshold. If $W \ll \Delta E$, 10 meV compared to 150 meV, and this distribution is swept over the region E_T to $E_T + W$ above threshold, then a trapped electron (TE) peak of width ΔE will be measured, but will contain electrons of energy only $\leq eW$ (i.e., ≤ 10 meV in our example). Thus, the area of the trapped electron peak will be proportional to the energy integrated cross section between E_T and $E_T + eW$. The magnitude of this peak will thus depend on ΔE. However, the ratio of two or more energy integrated cross sections will be correctly given by comparison of the areas of the trapped electron peak for any values of W, irrespective of instrumental resolution, and for $W < \Delta E$, if ΔE is the same for both peaks (which it will be); then the ratio of the magnitude of the peaks will be independent of ΔE also, and will be proportional to the ratio of the energy integrated cross section betwen E_T and $E_T + W$.

It is now well know, both theoretically[2,3] and experimentally,[1,4,5] that the ratio of the He $2^1S/2^3S$ cross section increases towards threshold. It has been claimed that the increase in this ratio can only be observed near threshold in a trapped electron apparatus by using superior resolution.[4,5] For example, Hall et al.[4] obtain a $^1S/^3S$ ratio of 1.10 with a resolution of about 80 meV, and claim this was the first measurement >1.0. In fact, Schulz,[1] in the original trapped electron paper (1950), obtained the ratio 1.05 with a resolution of about 0.2 eV. Obviously, in light of the above, what was common to both experiments[1,4] was not ΔE, but W. The only reason larger ratios have

not been obtained (or at least published)* is simply that for very small values of W the signal decreases very rapidly; or perhaps previous authors did not have sufficient control of their well (surface-potential-wise) for very small values of W. In experiments such as that of Cvejanovic and Read,[5] (which is a form of TE technique), the penetrating field, which partially determines the resolution, also determines an effective W; so as Cvejanovic and Read decrease ΔE, they are, in effect, also decreasing W, and our above comments do not apply. Using this method, they have obtained[5] a $^1S/^3S$ ratio as high as 2.6 for a resolution, and W of about 16 meV.

With the realization that the $^1S/^3S$ energy-integrated cross section ratio is independent of ΔE, we have measured the ratio from threshold to 0.12 eV. A typical spectrum corresponding to W=0.008 V is shown in Fig. 2. Though the resolution is very bad (150 meV), this ratio is seen to be 4.2. This spectrum corresponds to a data accumulation time of about 12 hours and demonstrated the stability of our surfaces over time at such low values of W. In fact, our zero W is stable to better than 3 meV over a period of a week. We determine the zero point W by observing a spectrum at a low value of W (say 5 meV), with an S/N ratio of about 10 for the ^1S peak (at which we see no ^3S signal at all), then reduce the well by 5 meV, and if no signal is obtained in 24 hours, we define that point as zero.

Fortunately, Nesbet[3] has calculated the $^1S/^3S$ energy integrated cross section ratio as a function of W (Nesbet calls it ΔE), which is suitable for direct comparison with trapped electron spectra (see Fig. 3). Also included in this plot is the single data point of Cvejanovic and Read[5] at 16 meV. Considering our maximum error of about 5 meV in W, this agreement is perfect. It is not possible to include any previous TE data in this plot because of relatively poor control of W in previous experiments. A more complete discussion and presentation of data will be submitted for publication.

---

*I had obtained $^1S/^3S$ ratios as high as 2 before 1970, as had P. D. Burrow (private communication) and G. J. Schulz, all independently. Such measurements were at that time used solely for potential well calibration purposes.

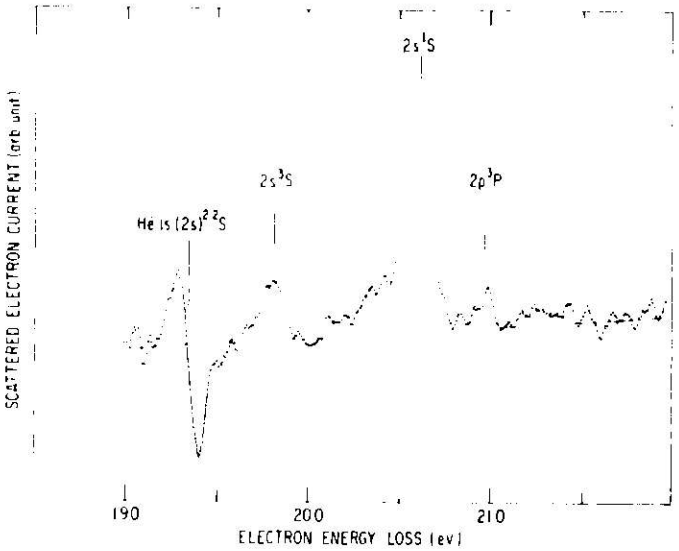

FIG. 2.--Trapped electron spectra of He for W = 0.008 V (corresponding to E = 0.008 eV), demonstrating the large $^1S/^3S$ energy integrated cross section ratios, even though the resolution ΔE is $\approx$ 150 meV.

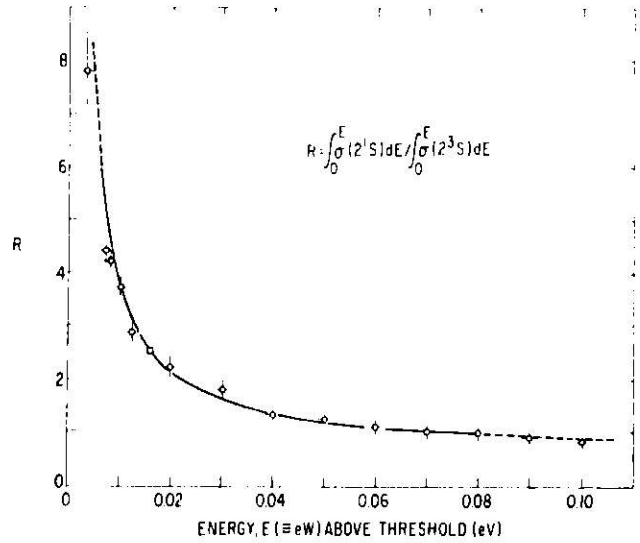

FIG. 3.--Comparison of experimental theoretical values of He $^1S/^3S$ energy integrated cross section ratios. Theory (Nesbet)[3] ——; Cvejanovic and Read,[5] □ ; present data, O.

References

1. G. J. Schulz, Phys. Rev. 112, 150 (1958).
2. K. A. Berrington, P. G. Burke, and A. L. Sinfailam, J. Phys. B: Atom. Molec. Phys. 8, 1459 (1975).
3. R. K. Nesbet, Phys. Rev. A 12, 444 (1975).
4. R. I. Hall, J. Reinhardt, G. Joyez, and J. Mazeau, J. Phys. B: Atom. Molec. Phys. 5, 66 (1972).
5. S. Cvejanovic and F. H. Read, J. Phys. B: Atom. Molec. Phys. 7, 1180 (1974).

ADDENDUM: CROSS SECTIONS AND THRESHOLD EFFECTS FOR ELECTRON IMPACT EXCITATION OF THE $(2s^2)^3P$ STATE OF HELIUM, David Spence, Phys. Rev. A 12, 2353 (1975).

David Spence

In our original article we had discussed the effects of post-collision interactions following excitation of the $(2s^2)^1S$ and $(2s2p)^3P$ autoionizing states by near-threshold electron impact from observation of structures in the spectra of scattered electrons. In light of a recent publication by Baxter et al.,[1] it appears that a reinterpretation of some of our results is necessary because of misidentification of a structure in our spectra. We point out that our raw data are correct, however. In this short report we will merely state the salient features of our reinterpretation.

Identification of Structures

In Fig. 1 of the original paper (shown as Fig. 1 here) we had concluded the two prominent structures (labeled 1 + 2 and 3) of our threshold spectra were due to He $(2s2p)^3P$ and shifted $(2s^2)^1S$ states, respectively. The lower curve of Fig., with peaks labeled 1, 2, and 3, is a threshold spectrum of Hicks et al.,[2]. Hicks et al. were not able to obtain scattered electron spectra at scattered energies other than zero, whereas our technique did have this facility. As we increased our energies above threshold, peak 3 of Fig. 1 moved closer to peak 1 + 2, and at higher energies apparently re-emerged on the low energy side. We illustrate this in Fig. 2 here (Fig. 2 of our earlier paper). However, the high resolution ejected electron spectra of Baxter et al.[1] taken as a function of excess energy, now clearly indicate that all three peaks of Fig. 1 here are oscillatory structures caused by the ^3P state alone as a result of PCI. The measurements of Baxter et al. show that the ^1S structure does indeed shift with excess energy, approximately by the amount we had measured, but that its excitation cross section is very small near threshold. The shift of peak 3 of the ^3P state is fortuitously at about the same rate as the ^1S shift, thus causing our misidentification. This misidentification has the following consequences.

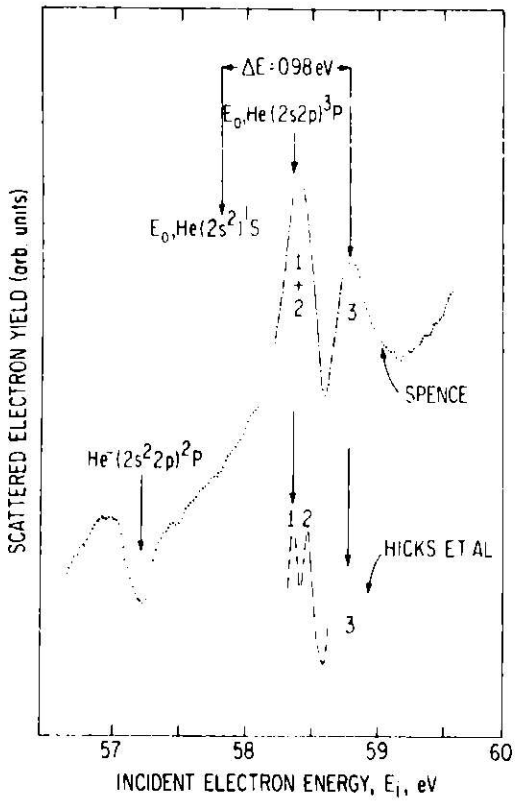

FIG. 1.--Threshold scattered electron spectra in He illustrating our labeling scheme for the observed structures. $W \approx 0$.

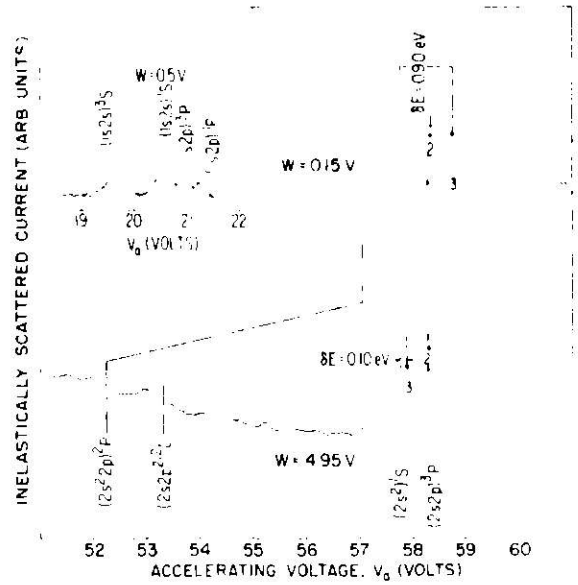

FIG. 2.--Scattered electron spectra in He for low (0.15 eV) and high (4.95 eV) energies above threshold showing how we had misinterpreted peak 3 (discussed in the text) as being due to the ^1S state which we had believed moved through the ^3P structure as the excess energy increased.

Energy Shift of the ^1S State with Excess Energy

Figure 8 of the earlier paper is shown as Fig. 3 here. Here the data points at large excess energies are taken for the real ^1S state when it appears on the low energy side of the ^3P state of Fig. 2 here. These data points are correct. The data points at low excess energies were taken for the misidentified ^1S structure which appeared on the high energy side of the first ^1P structure. These data points are incorrect. However, the slope of the real ^1S shift remains the same, and in fact, Fig. 3 here illustrates vividly the reasons for the original misidentification.

Measurement of Cross Sections and Identification of Cross-Section Structures

In Fig. 3 of Ref. 1, Baxter et al. have plotted effective excitation functions of the $(2s2p)^3P$ state of He by setting their analyzer to collect ejected

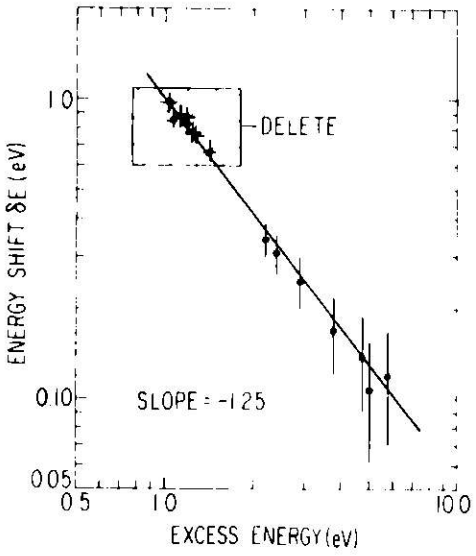

FIG. 3.--Plot of the He $(2s^2)^1S$ peak shift as a function of excess energy. The data points in the box at the upper left are due to the misidentified feature discussed in the text.

electrons of energy $33.73 + \Delta$ eV, where 33.73 is the spectroscopic energy for ejected electrons from the ^3P state, and Δ is 0.105 eV, 0.080 eV, and zero. These measurements are closely analogous to the cross section measurements shown in Fig. 9 of our earlier paper, with the exception that we were following a slightly shifted ^3P peak with excess energy. The three peaks of the excitation functions in Baxter's Fig. 3 thus shift with Δ, and we have plotted the positions of those peaks corresponding to $\Delta = 0$ and $\Delta = 0.08$ eV (which corresponds to our following the shift) by the horizontal bar above our ^3P cross section shown in Fig. 4 here (our original Fig. 9). The locations of our 3 peaks are in excellent agreement with the 3 peaks of Baxter et al.[1] However, from comparison with semiclassical theories of Baxter et al. had shown these structures to be post-collision interaction (PCI) phenomena and not caused by negative ion resonances. Hence, our interpretation of the second peak of Fig. 3 here as being due to decay of a $(2s2p^2)^2S$ resonance is incorrect.

In addition, because of our misidentification of the ^1S state close to threshold, measurements of the ^1S cross section below about 61.0 eV of Fig. 4 are incorrect, and the true cross sections probably decreases probably decrease slowly towards threshold, although we are unable to measure the true ^1S state in this energy region because of its submergence in the much larger ^3P structure.

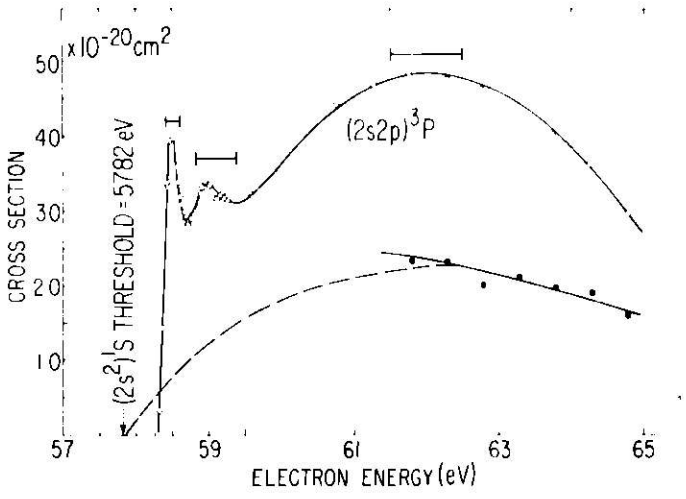

FIG. 4.--Plots of excitation cross sections of the ^1S (•) and ^3P (o) doubly-excited states of He. The horizontal bars above the ^3P cross section illustrate the energy range of the three peaks observed by Baxter et al.[1] in the excitation functions of the ^3P state obtained from excited electron spectra. These three peaks are all due to PCI phenomena and not resonances, as we originally believed. Because of the original misidentification of the ^1S state, the ^1S excitation cross section is incorrect below ≈ 61.0 eV, and probably decreases slowly toward threshold as indicated by the dashed line.

References

1. J. A. Baxter, J. Comer, P. J. Hicks, and J. W. McConkey, J. Phys. B: Atom. Molec. Phys. 12, 2031 (1979).
2. P. J. Hicks, S. C. Cvejanovic, J. Comer, F. H. Read, and J. M. Sharp, Vacuum 24, 573 (1974).

MEASUREMENT OF THE ENERGY EXCHANGE BETWEEN SCATTERED AND EJECTED ELECTRONS FOLLOWING AUTOIONIZATION OF THE $2s2p^6 3s(^1S)$ STATE OF Ne[†]

David Spence

The effects of electron correlations on the decay of short-lived autoionizing states following excitation by slow electrons has been studied experimentally at great length,[1-4] and, to a lesser degree, theoretically.[5-12] These effects have collectively become known as post-collision interaction (PCI) effects. Specifically, they result in a transfer of energy, ΔE, from the scattered to the ejected electron. If the incident electron is sufficiently slow, the ejected electron may gain more energy than the available kinetic energy of the scattered electron, which then becomes captured by the field of the positive ion to form a highly excited neutral state. Many measurements have indicated that the magnitude of ΔE is proportional to $E_1^{-1.2}$, where E_1 is the energy the scattered electron would have had in the absence of PCI. Wilden et al.[4] have determined ΔE for the $2s2p^6 3s(^1S)$ state of Ne, and the $2s^2(^1S)$, $2p^2(^1D)$, and $2s2p(^1P)$ states of He. In all cases, they find the energy exchange to be of the order $\Delta E \propto E_1^{-1.2 \pm 0.2}$, and suggest that the exponent 1.2 may have universal applicability to electron-impact induced autoionization. However, a recent quantum mechanical model of PCI, proposed by Bottcher and Schneider,[12] has indicated that in the region of E_1 close to threshold, ΔE should become proportional to $E_1^{-0.5}$. Consequently, we have extended measurements of the energy exchange, ΔE, between scattered and ejected electrons following autoionization of the $2s2p^6 3s(^1S)$ state of Ne to smaller values of E_1, which, indeed, reveal that for low values of excess energy E_1, ΔE is no longer proportional to $E_1^{-1.2}$, in accordance with the quantum mechanical model of the Bottcher and Schneider,[12] which includes dynamical screening of the ion core.

[†] Summary of a paper published in J. Phys. B: Atom. Molec. Phys. 11, L243 (1978).

References

1. P. J. Hicks, S. Cvejanovic, J. Comer, F. H. Read, and J. M. Sharp, Vacuum 24, 573–580 (1974).
2. A. J. Smith, P. J. Hicks, F. H. Read, S. Cvejanovic, G. C. King, J. Comer, and J. M. Sharp, J. Phys. B: Atom. Molec. Phys. 7, L496–L502 (1974).
3. D. Spence, Phys. Rev. A 12, 2353–2360 (1975).
4. D. G. Wilden, P. J. Hicks, and J. Comer, J. Phys. B: Atom. Molec. Phys. 10, 1477–1486 (1977).
5. R. B. Barker and H. W. Berry, Phys. Rev. 151, 14–19 (1966).
6. G. Neinhuis and H.G.M. Heideman, J. Phys. B: Atom. Molec. Phys. 8, 2225–2232 (1975).
7. R. Morgenstern, A. Niehaus, and U. Theilmann, J. Phys. B: Atom. Molec. Phys. 9, L363–L367 (1976).
8. R. Morgenstern, A. Niehaus, and U. Theilmann, J. Phys. B: Atom. Molec. Phys. 10, 1039–1058 (1977).
9. G. C. King, F. H. Read, and R. C. Bradford, J. Phys. B: Atom. Molec. Phys. 8, 2210–2224 (1975a).
10. F. H. Read, Radiat. Res. 64, 23–36 (1975).
11. F. H. Read, J. Phys. B: Atom. Molec. Phys. 10, L207–L212 (1977).
12. C. Bottcher and K. R. Schneider, J. Phys. B: Atom. Molec. Phys. 9, 911–916 (1976).

THE EFFECTS OF "POST-COLLISION INTERACTIONS" ON NEAR-THRESHOLD MEASUREMENTS OF AUTOIONIZING STATES IN Ne FROM SCATTERED ELECTRON SPECTRA*

David Spence

The spectroscopy of autoionizing states in Ne have been studied by excitation with fast[1,2] and slow[3] ions, electrons,[4] and photons,[5] with detection of scattered electrons,[2,4] ejected electrons,[1,3,6,7] photoabsorption,[5] electroionization,[8,9] and broadband photons.[10] It has been suggested[6] that some discrepancies in published energy locations of some autoionizing states is caused by the so-called "post-collision Interaction (PCI) effect" (see Ref. 6 and references therein), where energy is exchanged between the ejected and scattered electrons for very low electron-impact energies and short autoionization lifetimes. Such conditions may apply in near-threshold measurements of scattered and ejected electrons, electroionization, and broadband photons.

From measurements of scattered electron energies, we conclude that electron-impact excitation studies with no adjustable parameter other than the incident energy (including broadband photons,[10,11] electroionization,[8,9,12] and dc electron traps[13]) cannot determine true thresholds unless a state is sufficiently long-lived for PCI to be inoperable, a requirement which is usually not known a priori. We have demonstrated that recognition of the PCI mechanism is able to remove essentially all discrepancies in published data on autoionizing states of energy levels in Ne.

References

1. A. K. Edwards and M. E. Rudd, Phys. Rev. 170, 140 (1968).
2. G. Gerber and A. Niehaus, Phys. Rev. Lett. 31, 1231 (1973).
3. J. Ostgaard Olsen and N. Andersen, J. Phys. B 10, 101 (1977).
4. T. Bergmark, N. Spohr, N. Magnusson, L. O. Werme, C. Nordling, and K. Siegbahn, Institute of Physics, Uppsala University, Uppsala, Sweden, Int. Rept. #589 (1969).
5. K. Codling, R. P. Madden, and D. L. Ederer, Phys. Rev. 155, 26 (1967).

---

*Summary of a paper published in J. Chem. Phys. 68, 2980 (1978).

6. D. G. Wilden, P. J. Hicks, and J. Comer, J. Phys. B 10, 1477 (1977).
7. J. M. Sharp, J. Comer, and P. J. Hicks, J. Phys. B 8, 2512 (1975).
8. E. Bolduc, J. J. Quemener, and P. Marmet, J. Chem. Phys. 57, 1957 (1972).
9. E. Bolduc and P. Marmet, Can. J. Phys. 51, 2108 (1973).
10. P. Veillette and P. Marchand, Can. J. Phys. 54, 1208 (1976).
11. P. Veillette and P. Marchand, Can. J. Phys. 52, 930 (1974).
12. E. Bolduc, J. J. Quemener, and P. Marmet, Can. J. Phys. 51, 2108 (1973).
13. J. T. Grissom, W. R. Garrett, and R. N. Compton, Phys. Rev. Lett. 23, 1011 (1969).

MOLECULAR PHYSICS OF PRIMARY EVENTS IN RADIATION ACTION ON MATTER*

Mitio Inokuti

Let us consider an alpha particle of initial energy 5 MeV entering water vapor at one atmosphere. It has been known since the early days of the Curies that the alpha particle travels more or less along a straight line over about 3.5 cm and then stops. During the passage it collides with molecules and generates many new species in the vapor. They include about 160 thousand ions (molecules deficient in one or more electrons, thus positively charged) and an equal number of liberated electrons. The large number of ions and electrons makes it easy for us to observe them as current under modest electric fields—the principle behind a class of radiation detectors called ionization chambers. Among the new species there are tens of thousands of excited states (i.e., molecules in which one or more electrons are now put in orbits greater than those of the normal state) and a comparable number of molecular fragments such as H and OH. Some of these excited states emit light, which is also used for radiation detection—a principle for scintillation detectors. Most of the new species are chemically reactive and lead, upon thermal collisions among themselves or with normal water molecules, to new chemical products such as H_2, H_2O_2, H_3O^+, and many others, which E. J. Hart will discuss in a later paper at this sympsoium.

My report will concern the detailed analysis of how those initial species are generated. Although we have known for many decades about how fast energy is lost from the alpha particle, it is only in recent years that we have begun to answer questions such as, "Where does the alpha-particle energy go?" and "How is it used to form each of the new species?" To explain the formidable complexity involved in these questions, I need to make a few

---

*Popular version, for news release, of an invited paper presented at the Symposium on "Primary Events in Radiation Biology" at the joint meeting of the American Physical Society and the Biophysics Society, 27 March 1978, Washington, D.C.

observations. First, the alpha particle itself certainly generates ions and electrons, but some of the electrons appearing are highly energetic and they, in turn, may collide with molecules and generate more ions and electrons. Thus, molecules in water vapor are attacked by the alpha particle and by the energetic electrons, which are called secondary electrons. Of the total of 160 thousand ions, roughly half are attributable to the alpha-particle direct collisions, and roughlu half to the secondary electrons. In fact, for any kind of ionizing radiations (x rays, gamma rays, protons, and so on), much of the radiation action arises from secondary electrons. Second, the total number of collision processes involved in the whole history of the alpha-particle passage certainly must be greater than the 160 thousand, i.e., the number of ions formed. Indeed, it is more nearly half a million. Finally, one finds the variety of collision processes is enormous, as one starts looking into details. There are many kinds of excited states, some of which are well characterized, while others are not. Furthermore, ions can be in any of their alternative excited states, each having different physical and chemical properties.

Serious effort toward answering questions of the kind raised above started in the mid-1950's in the hands of pioneers, including Fano, Platzman, Spencer, and others. A major obstacle to the early work was the lack of solid information about the probabilities of the half-million collision processes. It is true that some of the probabilities are derivable from theory under certain conditions, but the knowledge of most of the probabilities must come from experiments on individual collision processes. Since the early 1960's, molecular physics of collision processes has seen a great advance, especially in detailed experimental measurements of the probabilities of diverse events.

A few examples of the development may be pointed out here. First, the relative probabilities for different values of energy transfer from a charged particle are now fairly well known from measurements on many molecular species. Also, these probabilities under certain conditions may be inferred from absorption of photons of differing energies; in this context the advent of source photons with 10 to 1000 eV in the form of synchrotron radiation and of emission from electrical discharges has been extremely important. As a result, one knows

that the average energy transfer to a water molecule per collision with a charged particle is about 37 eV, a value far exceeding the minimum energy 12.6 eV necessary for ionization. Yet, some 20% of water molecules that have received energies greater than 12.6 eV do not ionize, but decompose into neutral fragments.

Second, secondary electrons have been analyzed with respect to their energy and angle of ejection. Even for a single value of energy transfer, as realized upon photoabsorption, the energy of secondary electrons is not unique, but has a distribution that reflects different alternative states of the ions left behind.

Despite the continuing progress up to the present time, the knowledge of the probabilities of collision processes is still incomplete; there are gaps and uncertainties in the data in the literature. In order to carry out an analysis of the fate of the radiation energy, one must critically evaluate the data, make a judicious selection in the light of everything else known about the molecule, and often interpolate or extrapolate the data. Platzman started a general strategy for this purpose. Briefly, the strategy takes advantage of the fact that the probabilities of alternative events are not independent but are subject to many theoretical constraints; and it is now possible to present a reasonably trustworthy set of probabilities for water and several other basic molecules in unprecedented detail.

Once these probabilities are fixed, one starts calculations of the cumulative consequences of each collision process to the particles in the medium and to the medium molecules. Work at this stage belongs to kinetic theory, a subfield of statistical physics, and has its own challenge and charms. There are two general lines of approach. The first one is the simulation of numerous histories of events in an electronic computer, followed by a suitable summary of the results. This called the Monte-Carlo method because one decides the outcome of each collision by throwing dice, in effect, in the computer. In the second approach, one uses equations for the number of particles (e.g., electrons) having a fixed energy in the medium or for the number of new species, and solves these equations by analytical or numerical methods. Stimulated by the

advent of good probability data in several examples, work in both lines of approach has recently seen much progress.

So far our story has concerned the simplest case, in which charged particles travel through gases. In liquids and solids, atoms are packed much closer; the density of atoms is higher than in gases (at one atmosphere) by a factor of one thousand or more. The properties of ions and excited states must be different in many ways, depending upon the arrangement of atoms. In crystals, including metal and semiconductors, much of the electronic excitation energy from valence shells is quickly converted to heat and causes little permanent chemical change. In molecular substances, such as liquid water and plastics, electronic excitations do cause serious chemical changes through reactions of initial species such as ions, excited states, and molecular fragments. Full analysis of the initial species is more difficult than in gases for two major reasons. First, we have far fewer methods of characterizing or probing the initial species; any such method has to overcome the task of unraveling the properties of the initial species before they rapidly interact with neighboring molecules, possibly changing their identify. Second, because of the importance of their interactions with neighboring molecules or among themselves, it is necessary to characterize the spatial distribution of the initial species to clarify their roles in succeeding chemical changes. There have been numerous treatments of this problem so far, but much of the understanding remains far less detailed than our story about gases and quite tentative. It is hoped that the coming years will bring new techniques for probing the initial species and new theoretical approaches for describing their properties.

VARIATIONAL TREATMENT OF ELECTRON DEGRADATION AND YIELDS OF INITIAL MOLECULAR SPECIES*

A.R.P. Rau,[†] Mitio Inokuti, and Daryl A. Douthat[‡]

We present a general theory of electron degradation and of the yields of initial species such as ions and excited states that appear in matter as a result of irradiation with electrons. We give variational expressions for observable quantities such as the degradation spectrum, the mean yields, and the yield fluctuations. A systematic analysis using variational principles reveals, in greater detail than ever before, relations among major analytical methods including the Fowler method, the Spencer-Fano method, and the method of Knipp et al.[1] Each of these methods represents a different angle of approach to the same problem and leads to the same prediction for the mean yield of any initial species for a fixed set of electron cross-section data. Among our findings it is noteworthy that the knowledge of the Spencer-Fano degradation spectra for various source-electron energies enables one to calculate by quadrature not only the mean but also the statistical fluctuations of the yield of any initial species. Furthermore, when one introduces small changes in the cross-section data (because of new information or upon consideration of chemical impurities in the medium), one may express the ensuing modifications of any observable quantity in the form of a perturbation expansion. Then, every term in the perturbation series is calculable again from the Spencer-Fano degradation spectra for various source energies for the unperturbed problem. In this respect and many others, the Spencer-Fano degradation spectrum is the most basic element in the solution of the degradation problem. Finally, our mathematical analysis of various difference-integral equations (including nonlinear

---

*Abstract of a paper published in Phys. Rev. A 18, 971 (1978).

[†]Department of Physics and Astronomy, Louisiana State University, Baton Rouge, Louisiana 70803.

[‡]Consultant, Radiological and Environmental Research Division. Permanent address: Kennedy-King College, Chicago, Illinois 60621.

equations) may be of interest in areas other than electron degradation. Therefore, the present paper includes remarks on the physical meaning of adjoint operators and on other points belonging to general mathematical physics.

Reference

1. J. Knipp, T. Eguchi, M. Ohta, and S. Nagata, Prog. Theor. Phys. 10, 24 (1953).

THEORY OF THE YIELDS OF INITIAL MOLECULAR SPECIES UNDER RADIATION ACTION—GENERALIZATIONS OF THE FOWLER EQUATION

Mitio Inokuti

The standard Fowler equation concerns the mean yield of an initial species such as ions resulting from complete slowing-down of an electron of a given kinetic energy in a pure medium. Similar equations for two other cases are presented. The first applies to the proton incidence in a pure medium and the second to the electron incidence in a binary mixture.

Introduction

One of the methods for calculating the mean yield, upon complete slowing-down of electrons, of an initial species uses the Fowler equation. For the incidence and moderation of electrons in a chemically pure medium, the equation is well known, and its solutions and general properties have been extensively studied.[1,2] It is shown here that the idea of the Fowler equation can be applied to a wide range of situations, including the incidence of an ion and a medium having plural chemical components.

Proton Incidence

Suppose that a proton of kinetic energy T occurs in a pure medium composed of molecules A. Assume for simplicity that A has a single ionization threshold I. Assume further that the proton may undergo any of the following processes but no other process.

1) Elastic collisions with an energy loss E_0, characterized by cross section $\sigma_{p0}(T)$:

$$p + A \rightarrow p + A \quad . \tag{1}$$

the energy loss in an individual collision depends on the scattering angle. The above E_0 is its average, and $\sigma_{p0}(T)$ is the momentum-transfer cross section.

2) Discrete excitation with energy loss E_n, characterized by cross section $\sigma_{pn}(T)$ $(n=1,2,3,\ldots)$:

$$p + A \rightarrow p + A_n^* \quad , \tag{2}$$

where A_n^* represents any possible excitation, including electronic, vibrational,

rotational, or any combination of them. Also, A_n^* may represent any dissociation into neutral fragments, but not dissociative ionization.

3) Ionization:

$$p + A \rightarrow p + A^+ + e \quad , \tag{3}$$

where A^+ represents an ion (devoid of any internal energy, by assumption). The ionization process is characterized by the differential cross section $d\sigma_{pi}(T,E)/dE$ for a specified value E of energy transfer. Again by assumption, a secondary electron emerges with kinetic energy $E - I$. The total ionization cross section is

$$\sigma_{pi}(T) = \int_I^T \frac{d\sigma_{pi}(T,E)}{dE}\, dE \quad . \tag{4}$$

Correspondingly, assume that an electron of energy T may undergo any of the following processes, but no other process.

1) Discrete excitation with energy loss E_n, characterized by cross section $\sigma_n(T)$:

$$e + A \rightarrow e + A_n^* \quad . \tag{5}$$

It is formally straightforward to include energy losses due to elastic collisions, and to rotational or vibrational excitation. But it is usually believed that these energy losses are negligible compared to losses due to electronic excitations so long as electronic excitations are energetically possible.

2) Ionization, characterized by the differential cross section $d\sigma_i(T,E)/dE$:

$$e + A \rightarrow e + e + A^+ \quad . \tag{6}$$

The total ionization cross section is

$$\sigma_i(T) = \int_I^{\frac{1}{2}(T+I)} \frac{d\sigma_i(T,E)}{dE}\, dE \quad . \tag{7}$$

The foregoing assumptions are probably the simplest among reasonable alternatives. The assumption of the single ionization threshold is reasonable for He and possible for some other atoms, but is unrealistic for molecules; however, the removal of this restriction is straightforward as seen in the Appendix of Ref. 1. The treatment here also disregards charge transfer

processes, any process resulting in energetic H atoms, and any process by which an electron generates a proton of such a high kinetic energy that it may generate further ionization, e.g.,

$$e + H_2 \rightarrow e + e + H + p \quad , \tag{8}$$

followed by

$$p + H_2 \rightarrow p + e + H_2^+ \quad . \tag{9}$$

Within the above schematization, it is easy to write a set of equations for the mean ionization yield. For convenience, one introduces

$$P_n(T) = \sigma_{pn}(T)/\sigma_{p,tot}(T) \quad , \tag{10}$$

$$P_i(T) = \sigma_{pi}(T)/\sigma_{p,tot}(T) \quad , \tag{11}$$

$$dP_i(T,E)/dE = [d\sigma_{pi}(T,E)/dE]/\sigma_{p,tot}(T) \quad , \tag{12}$$

where

$$\sigma_{p,tot}(T) = \sum_n \sigma_{pn}(T) + \sigma_{pi}(T) \tag{13}$$

is the total collision cross section for the proton of energy T. The capital P's represent probabilities for various proton processes, and the sum of all P's is unity at any T. Similariy, for electrons, one introduces

$$p_n(T) = \sigma_n(T)/\sigma_{tot}(T) \quad , \tag{14}$$

$$p_i(T) = \sigma_i(T)/\sigma_{tot}(T) \quad , \tag{15}$$

$$dp_i(T,E)/dE = [d\sigma_i(T,E)/dE]/\sigma_{tot}(T) \quad , \tag{16}$$

with

$$\sigma_{tot}(T) = \sum_n \sigma_n(T) + \sigma_i(T) \quad . \tag{17}$$

The lower-case p's represent various electron processes, and the sum of all p's is again unity at any T.

Let M(T) be the total number of ions that a proton of energy T causes in the complete slowing-down in the medium, both directly and indirectly. Let N(T) be the total number of ions that an electron of energy T causes in its complete slowing-down. By the definition of W values, one may write

$$T/M(T) = W_{proton}(T) \quad , \tag{18}$$

$$T/N(T) = W_{electron}(T) \quad . \tag{19}$$

Then N(T) obeys the known Fowler equation[1,2]

$$N(T) = p_i(T) + \sum_n p_n(T)\, N(T-E_n) + \int_I^{\frac{1}{2}(T+I)} dE\, [dp_i(T,E)/dE]\, [N(T-E) + N(E-I)] \quad , \tag{20}$$

with the condition that

$$N(T) = 0 \qquad \text{at } T < I \quad . \tag{21}$$

In contrast, M(T) obeys a new equation

$$M(T) = P_i(T) + \sum_n P_n(T)\, M(T-E_n) + \int_I^T dE\, [dp_i(T,E)/dE]\, [M(T-E) + N(E-I)] \tag{22}$$

with the condition that

$$M(T) = 0 \qquad \text{at } T < I \quad . \tag{23}$$

Equation 20 remains the Fowler equation because an electron never generates an energetic proton within our schematization, i.e., because we have excluded processes 8 and 9, which are probably unimportant. A new point of Eq. 22 is that the last term in the integral is N(E-I) rather than M(E-I). Therefore, one must solve Eq. 20 and obtain N(T) first, and then study Eq. 22 for M(T). In other words, the electron problem is an essential component of the proton problem and must be solved first. This remark always applies to irradiation with any particle other than electrons.

The special role of electrons arises from basic physics, viz., from their small mass and from their universal presence in ordinary matter. Mathematically speaking, as soon as we include processes in which an electron generates an energetic proton that may cause further ionization, we have a set of coupled equations in which N(T) and M(T) appear symmetrically. For certain purposes, such a symmetric treatment may be preferable. However, we shall study only Eq. 22 in the following.

Suppose N(T) is known either numerically or approximately, either from theory or experiment, and let us concentrate on Eq. 22. It is useful to recast it in the form

$$M(T) = \hat{P}_i(T) + \sum_n P_n(T)\, M(T-E_n) + \int_I^T dE\, [dP_i(T,E)/dE]\, M(T-E) \quad , \qquad (24)$$

where

$$\hat{P}_i(T) = P_i(T) + \int_I^T dE\, [dP_i(T,E)/dE]\, N(E-I) \qquad (25)$$

is calculable from N(E-I). The integral in Eq. 25 represents the contributions of all secondary electrons that ensue from an ionizing collision of the proton at energy T.

To solve Eq. 24, one may try a continuous-slow-down approximation (CSDA), which is reasonable for protons at high T. In other words, one assumes that all E_n and E are much smaller than T. The integral in Eq. 24 covers all E up to T, and thus the CSDA cannot be completely right. The essence of the assumption here is to say that the product $[dP_i(E,T)/dE]\, M(T-E)$ is negligibly small for $E \approx T$. Under the CSDA, one uses the Taylor expansion $M(T-E_n)$ and M(T-E) around M(T) in Eq. 24. Then one obtains

$$\hat{P}_i(T) - \mu^{(1)}(T)\, d\, M(T)/dT + \tfrac{1}{2}\, \mu^{(2)}\, d^2 M(T)/dT^2 + \ldots = 0 \quad , \qquad (26)$$

where

$$\mu^{(m)}(T) = \sum_n E_n^m\, P_n(T) + \int_I^T dE\, E^m\, dP_i(T,E)/dE \qquad (27)$$

is the mth moment of the collision probabilities (or collision spectrum). Obviously, $\mu^{(1)}(T)$ is the ratio of the stopping cross section to the total collision cross section, and $\mu^{(2)}(T)$ is related to the energy straggling. In Eq. 26, one sees only the derivatives of M(T), but not M(T) itself, which has dropped off in the CSDA procedure.

The simplest approximation now is to ignore $d^2M(T)/dT^2$ and higher derivatives in Eq. 26. Then one has

$$dM(T)/dT \cong \hat{P}_i(T)/\mu^{(1)}(T) \quad .$$

Integration, with the use of Eq. 25, leads to

$$M(T) \cong \int_I^T dT' [s(T')]^{-1} [\sigma_{pi}(T') + \int_I^{T'} dE\, d\sigma_{pi}(T', E) N(E-I)] \quad , \tag{28}$$

where s(T) is the stopping cross section for a proton of energy T. This result, i.e., Eqs. 27 and 28, is formally identical to the intuitive expressions of Jacobi and Stolterfoht[3] and Bichsel and Inokuti.[4]

A second approximation is obtained by inserting Eq. 27 into the third term of Eq. 26. Then one obtains

$$dM(T)/dT \cong \hat{P}_i(T)/\mu^{(1)}(T) + \tfrac{1}{2}\mu^{(2)}(T)\, d/dR [\hat{P}_i(T)/\mu^{(1)}(T)] \quad . \tag{29}$$

Alternatively, it is possible to solve Eq. 26 exactly, once all derivatives higher than $d^2M(T)/dT^2$ are ignored.

Finally, the method[2] of the adjoint operator may be applied to Eq. 24. The function adjoint to M(T) is in essence the degradation spectrum for protons in the medium. A full analysis of this topic is in progress.

Electron Incidence in a Binary Mixture

Let there be two chemical components 1 and 2 with number densities $\nu^{(1)}$ and $\nu^{(2)}$. A molecule of component 1 has discrete excitation energies $E_n^{(1)}$ $(n = 1, 2, 3, \ldots)$, corresponding excitation cross sections $\sigma_n^{(1)}(T)$, the differential ionization cross section $d\sigma_i^{(1)}(T,E)/dE$, and the total ionization section

$$\sigma_i^{(1)}(T) = \int_{I^{(1)}}^{\frac{1}{2}(T+I^{(1)})} [d\sigma_i^{(1)}(T,E)/dE]dE \quad , \tag{30}$$

all for an electron of energy T. Again, it is assumed that the molecule has a single ionization threshold $I^{(1)}$. Let the total inelastic collision cross section be $\sigma_{tot}^{(1)}(T)$. A molecule of component 2 may be characterized by corresponding quantities all with superscript (2).

Then, the mean number N(T) of initial ions that an electron of energy T generates during complete slowing-down in the medium is written as

$$[\nu^{(1)}\sigma_{tot}^{(1)}(T) + \nu^{(2)}\sigma_{tot}^{(2)}(T)]\,N(T) = \nu^{(1)}\{\sigma_i^{(1)}(T) + \sum_n \sigma_n^{(1)}(T)\,N(T-E_n^{(1)})$$

$$+ \int_{I^{(1)}}^{\frac{1}{2}(T+I^{(1)})} [d\sigma_i^{(1)}(T,E)/dE]\,[N(T-E) + N(E-I^{(1)})]\}$$

$$+ \nu^{(2)}\{\sigma_i^{(2)}(T) + \sum_n \sigma_n^{(2)}(T)\,N(T-E_n^{(2)})$$

$$+ \int_{I^{(2)}}^{\frac{1}{2}(T+I^{(2)})} [d\sigma_i^{(2)}(T,E)/dE]\,[N(T-E) + N(E-I^{(2)})]\}\ , \qquad (31)$$

subject to the condition that

$$N(T) = 0 \qquad \text{at } T < \text{Min}\{I^{(1)}, I^{(2)}\}\ . \qquad (32)$$

Among many conceivable analyses of Eq. 31, the simplest procedure is to use the linear approximation[1]

$$N(T) \cong (T-U)/W_a\ , \qquad (33)$$

where U and W_a are parameters of the energy dimension to be determined. The use of the argument of Ref. 1 leads to

$$U + \nu^{(1)}I^{(1)} + \nu^{(2)}I^{(2)} = \frac{\nu^{(1)}E_{i1}^{(1)}\sigma_{i1}^{(1)} + \nu^{(2)}E_{i1}^{(2)}\sigma_{i1}^{(2)}}{\nu^{(1)}\sigma_{i1}^{(1)} + \nu^{(2)}\sigma_{i2}^{(2)}} \qquad (34)$$

and

$$W_a = \frac{\nu^{(1)}\sum_n E_n^{(1)}\sigma_n^{(1)} + \nu^{(2)}\sum_n E_n^{(2)}\sigma_n^{(2)}}{\nu^{(1)}\sigma_i^{(1)} + \nu^{(2)}\sigma_i^{(2)}}$$

$$+ \frac{\nu^{(1)}E_{i1}^{(1)}\sigma_{i1}^{(1)} + \nu^{(2)}E_{i1}^{(2)}\sigma_{i1}^{(2)}}{\nu^{(1)}\sigma_{i1}^{(1)} + \nu^{(2)}\sigma_{i1}^{(2)}}\ , \qquad (35)$$

where

$$\sigma_{i1}^{(\ell)} = \int_I^{2I} dE\, d\sigma_i^{(\ell)}(T,E)/dE\ , \qquad (36)$$

$$E_{i1}^{(\ell)}\sigma_{i1}^{(\ell)} = \int_I^{2I} dE\, E d\sigma_i^{(\ell)}(T,E)/dE\ , \qquad (37)$$

with $\ell = 1$ or 2 are to be evaluated at high values of T. The parameter W_a, which should then come out largely independent of T, represents the asymptotic W value at high electron energies.

The dependence of W_a on the composition $\nu^{(1)}/\nu^{(2)}$ should be noted. In Eq. 35 there are two terms, each of which is a linear fraction in $\nu^{(1)}/\nu^{(2)}$. If one rewrites Eq. 35 into the form of a single fraction, then both the denominator and the numerator will be quadratic in $\nu^{(1)}/\nu^{(2)}$. This dependence is to be contrasted with the linear-fraction formula[5-7] used for a long time for empirical analysis of data on binary mixtures. Further work is needed to clarify whether Eq. 35 may indeed describe data better.

The use of the method[2] of the adjoint operator is now being studied. Studies of the electron degradation spectrum, which will be the function adjoint to N(T), is especially important because most of the practially significant applications in radiation chemistry and biology concern mixtures. The central goal in this effort will be to elucidate the dependence of the electron degradation spectrum upon chemical composition.

References

1. M. Inokuti, Radiat. Res. 64, 6 (1975).
2. A.R.P. Rau, M. Inokuti, and D. A. Douthat, Phys. Rev. A 18, 971 (1978).
3. W. Jacobi and N. Stolterfoht, Proc. Third Symp. on Microdosimetry, H. G. Ebert et al., Eds., Commission of the European Communities, Luxemburg, EUR-4810 d-f-e, p. 109 (1972).
4. H. Bichsel and M. Inokuti, Radiat. Res. 67, 613 (1976); Argonne National Laboratory Radiological and Environmental Research Division Annual Report, July 1975–September 1976, ANL-76-88, Part I, p. 167.
5. T. E. Bortner and G. S. Hurst, Phys. Rev. 93, 1236 (1954).
6. H. J. Moe, T. E. Bortner, and G. S. Hurst, J. Chem. Phys. 61, 422 (1957).
7. G. S. Hurst, T. E. Bortner, and R. E. Glick, J. Chem. Phys. 42, 713 (1965).

GENERAL USE OF THE LAGRANGE MULTIPLIER IN NONLINEAR MATHEMATICAL PHYSICS*

Toshio Mura,† Hideki Sekine,‡ and Mitio Inokuti

In the traditional calculus of variations, one begins with a functional of an unknown function, seeks for a stationary value of that functional, and thereby derives an (Euler) equation for that unknown function. Spruch, Gerjuoy, and co-workers[1-4] developed a method that follows an inverse process, for application chiefly in quantum mechaniss. In this method, one begins with an equation, either linear or nonlinear, and seeks a variational principle for any quantity given as a functional of the solution of that equation. The equation may involve algebraic, differential, integral, or finite-difference operators, or even any combination of them. The method is, in effect, an extension of the Newton method of finding a root of an algebraic equation to an analogous problem in a functional space. Alternatively, one may view the method as a generalization of the use of the Lagrange multiplier. The notion of an adjoint equation, satisfied by the generalized Lagrange multiplier, plays a key role. The power of the method, especially noticeable in nonlinear problems, has been demonstrated in many branches of mathematical physics, including electron-transport theory.[5] Here we discuss several examples including large nonlinear deflection of a beam due to a load, and the limit analysis for obtaining the safety factor as treated earlier by Mura and Lee.[6]

References

1. E. Gerjuoy, A.R.P. Rau, and L. Spruch, J. Math. Phys. 13, 1797 (1972).

*Summary of a paper presented at the Symposium on Variational Methods in Mechanics, Evanston, Illinois, September 1978. A full text will appear in the forthcoming proceedings.

†Department of Civil Engineering, Northwestern University, Evanston, Illinois 60201.

‡Department of Mechanical Engineering, Tohoku University, Sendai 980, Japan.

2. E. Gerjuoy, A.R.P. Rau, and L. Spruch, Phys. Rev. A 8, 662 (1973).
3. E. Gerjuoy, A.R.P. Rau, L. Rosenberg, and L. Spruch, Phys. Rev. A 9, 108 (1974).
4. E. Gerjuoy, A.R.P. Rau, L. Rosenberg, and L. Spruch, J. Math. Phys. 16, 1104 (1975).
5. A.R.P. Rau, M. Inokuti, and D. A. Douthat, Phys. Rev. A 18, 971 (1978).
6. T. Mura and S. L. Lee, J. Appl. Math. 21, 243 (1963).

MEAN EXCITATION ENERGIES FOR STOPPING POWER AS DERIVED FROM OSCILLATOR-STRENGTH DISTRIBUTIONS*

Mitio Inokuti and James E. Turner†

The mean excitation energy I is the most important of the material properties that enter into the Bethe formula for stopping power of fast charged particles. For a pure gas consisting of molecules with an oscillator-strength density df/dE at excitation energy E measured from the ground state, the mean excitation energy I is defined by

$$\ln I = \int dE\, df/dE\, \ln E / \int dE\, df/dE \,. \qquad (1)$$

For condensed matter, I is defined by an expression similar to Eq. 1, but with df/dE replaced by E Im $[1/\epsilon(E)]$, where $\epsilon(E)$ is the complex dielectric response function at photon energy E.

As a part of the critical survey of stopping-power data for the International Commission on Radiation Units and Measurements we have undertaken a review of I values in the literature. Trustworthy determination of the I values from df/dE, is crucial for better understanding of other properties in the stopping-power formula, such as inner-shell corrections, z^3- and z^4-terms (which represent departures from the first Born approximation), and the Fermi density correction. In addition, comparison of the I values for free atoms, molecules, solids, and liquids sheds considerable light on the effects of atomic aggregation and binding on stopping power. In this respect, the recent progress in the mapping of df/dE for many materials over wide ranges of E, both experimental and theoretical, proves to be extremely valuable.

---

*Summary of an invited lecture at the VIth Symposium on Microdosimetry, Brussels, Belgium, 22-26 May 1978. A full text appears in the Proceedings, J. Booz and H. G. Ebert, Eds., Harwood Academic Publishers, Ltd., London, pp. 657–687 (1978).

†Oak Ridge National Laboratory, Oak Ridge, Tennessee 37830.

STOPPING POWER OF PARTIALLY STRIPPED IONS*

Yong-Ki Kim

The Bethe formula for the stopping power[1] is valid for fast and bare incident ions. The formula has been generalized to partially stripped ions by applying a sum-rule method for ion-atom collisions.[2] The formula retains the same form as that for the bare ions except for effective charge ζ and the effective ionization energy J. Both parameters are defined rigorously in terms of the properties of the incident ion and the target atom or molecule:

$$-dE/dx = N_0 4\pi a_0^2 \alpha^2 R\beta^{-2} \zeta^2 \{ \ln[4\beta^2 R/J\alpha^2(1-\beta^2)] - \beta^2 \} \quad ,$$

where N_0 = density of target particles, $a_0 = 0.529$ Å, $\alpha = 1/137$, $R = 13.6$ eV, and $\beta = v_{ion}/c$. For a bare ion, expressions for ζ and J reduce to the well-known result $\zeta^2 = 2Z^2$ and J = mean excitation energy, I_0.

References

1. H. Bethe, Z. Physik 76, 293 (1932).
2. G. H. Gillespie, Phys. Rev. A 15, 563 (1977).

---

*Abstract of a paper to be presented at the 6th International Congress of Radiation Research, Tokyo, May 13–19, 1979.

QUANTUM DEFECTS FOR HIGHLY STRIPPED IONS*

W. R. Johnson† and K. T. Cheng‡

A version of quantum defect theory appropriate to the analysis of the spectra of highly ionized atoms is obtained from the single-electron Dirac equation. Quantum defect μ_n are defined as the principal quantum number n increases along a Rydberg series using Sommerfeld's relativistic one-electron energy level formula. Considering the analytic properties of solutions to the Dirac equation, we establish that μ_n can be extended smoothly away from the bound state energies just as in the nonrelativistic theory. Moreover, the relativistic $\mu(\epsilon)$ can be analytically continued beyond the threshold $\epsilon = mc^2$ and related to the non-Coulomb scattering phase shift $\delta(\epsilon)$. At the threshold, we establish the result $\delta(mc^2) = \pi\mu(mc^2)$, well known in the nonrelativistic quantum defect theory. Several examples of the relativistic quantum defect theory are given for highly stripped Na-like and Li-like ions.

*Abstract of a paper published in J. Phys. B 12, 863 (1979).

†Physics Department, University of Notre Dame, Notre Dame, Indiana 46556.

‡Postdoctoral appointee from the University of Notre Dame.

RESONANCE TRANSITIONS $2p^6$-$2p^5 3s$ IN Ne-LIKE IONS

K. T. Cheng* and Yong-Ki Kim

The electric dipole transitions $(2p^6)\,^1S-(2p^5 3s)\,^1P^o$ in Ne-like ions are studied using the multiconfiguration Dirac-Fock method. Effects of spin-orbit interaction and interchannel couplings on oscillator strengths are discussed.

The electric dipole transitions between the $(2p^6)\,^1S$ ground state and the two $(2p^5 3s)J^\pi = 1^-$ excited states are studied using the multiconfiguration Dirac-Fock (MCDF) scheme.[1] Nonrelativistically, the upper $(2p^5 3s)1^-$ state is a $^1P^o$ state, while the lower one is $^3P^o$. For convenience, we shall refer to these two excited states by their LS designations, although in the present intermediate coupling calculations, they are actually linear combinations of the two LS components:

$$\Psi = a\Psi(^1P^o) + b\Psi(^3P^o) \quad . \tag{1}$$

While we expect that the LS coupling scheme is a good approximation for light atoms, we find that it breaks down as the nuclear charge Z increases along the isoelectronic sequence. In Fig. 1, we have plotted the two mixing coefficients a and b for the upper $^1P^o$ state as a function of the nuclear charge Z. As one can see, for low Z Ne-like ions, it is indeed very close to a pure $^1P^o$ state. However, the coupling scheme changes very rapidly, and for Fe^{16+} (Z = 26), this state is actually closer to a pure $(2p_{\frac{1}{2}}^{-1} 3s_{\frac{1}{2}})$ jj state than a $^1P^o$ LS one.

This finding shows that the effect of spin-orbit interactions is strong in Ne-like ions. An interesting consequence is that the spin-forbidden transition ^1S-$^3P^o$ is never highly suppressed because of the mixing with the allowed channel ^1S-$^1P^o$. In fact, the absorption oscillator strength $f(^3P^o)$ of the forbidden transition is actually larger than $f(^1P^o)$ of the allowed one for Z > 22, as we can see in Fig. 2. This is rather surprising in view of the fact that for

*Postdoctoral appointee from the University of Notre Dame.

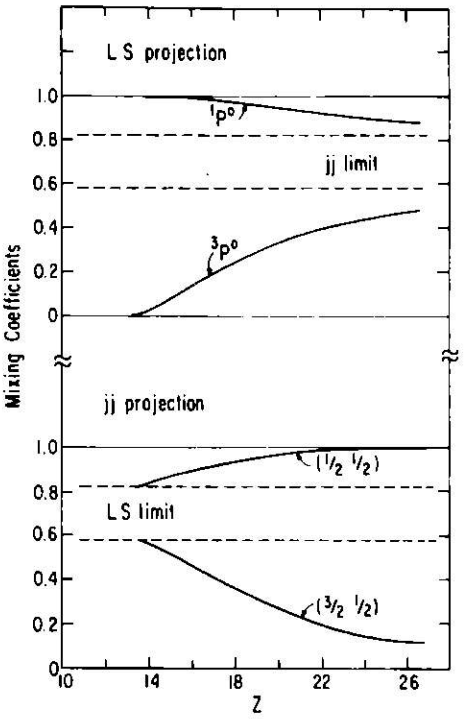

FIG. 1.--The projections of the upper $(2p^5 3s)J^\pi = 1^-$ eigenstate onto the LS and jj basis.

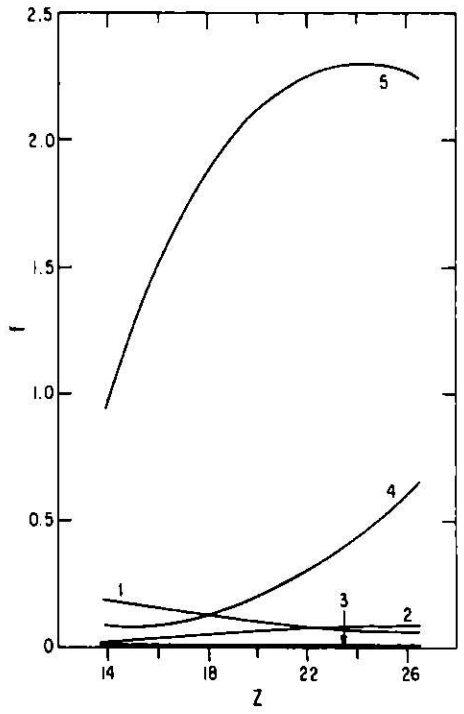

FIG. 2.--Oscillator strengths of the transitions from the ground state to the five $J^\pi = 1^-$ states. The numbers 1–5 refer to the final states of that particular transition in order of increasing energies from the ground state, i.e., 1–2 for $(2p^5 3s)1^-$ lower and upper states, and 3–5 for $(2p^5 3d)1^-$ lower, middle, and upper states.

Be-like[2] and Mg-like[3] ions, $f(^3P^o)$ of the forbidden transition $(ns^2)^1S$-$(nsnp)$ $^3P^o$ never becomes larger than $f(^1P^o)$ of the allowed one, $(ns^2)^1S$–$(nsnp)^1P^o$, even up to Z = 92.

Another interesting feature of the f-values of these two transitions is that they are strongly perturbed by the resonance transitions $(2p^6)^1S$-$(2p^5 3d)J^\pi = 1^-$. Nonrelativistically, the three $(2p^5 3d)1^-$ states are, in order of increasing energies with respect to the ground state, $^3D^o$, $^3P^o$, and $^1P^o$. By coupling the $2p^5 3s$ and $2p^5 3d$ configurations together in MCDF calculations, we find that the values of $f(^1P^o)$ and $f(^3P^o)$ for the $2p^6$-$2p^5 3s$ transitions increase by as much as 20% from the uncoupled ones. Such a large change can be explained

Table 1. Oscillator strengths of $(2p^6)\ ^1S - (2p^5 3s)\ 1^-$ transitions for Ne-like ions.

Ion	MP[a]	HF[b]	$(2p^5 3s)$[c]	$(2p^5 3s) + 2p^5 3d)$[d]	RRPA[e]	Experiment
			Upper 1^- state			
Si^{4+}	0.161	0.19	0.188	0.227		
P^{5+}	0.150	0.18	0.174	0.215		
S^{6+}	0.137	0.17	0.159	0.200	0.201	0.194 ± 0.052[f]
Cl^{7+}	0.122	0.15	0.144	0.185	0.187	0.156 ± 0.030[f] 0.2 ± 0.05[g]
Ar^{8+}	0.111	0.14	0.130	0.169	0.172	0.17 ± 0.05[g]
K^{9+}	0.099	0.12	0.117	0.155		
Ca^{10+}	0.090	0.11	0.106	0.143		
Fe^{16+}	0.056	0.07	0.068	0.099		
			Lower 1^- state			
Si^{4+}	0.018	0.021	0.0216	0.0278		
P^{5+}	0.024	0.028	0.0291	0.0380		
S^{6+}	0.031	0.036	0.0377	0.0498	0.0430	0.0488 ± 0.0133[f]
Cl^{7+}	0.038	0.044	0.0467	0.0619	0.0554	0.0463 ± 0.0161[f] 0.052 ± 0.009[g]
Ar^{8+}	0.045	0.052	0.0554	0.0760	0.0679	0.056 ± 0.012[g]
K^{9+}	0.051	0.060	0.0632	0.0871		
Ca^{10+}	0.056	0.066	0.0697	0.0965		
Fe^{16+}	0.067	0.082	0.0881	0.1237	0.123	

a. Crance, Ref. 5.
b. Kastner et al., Ref. 4.
c. This work, 2-channel results.
d. This work, 5-channel results.
e. Shorer, Ref. 6.
f. Cumutte and Cocke, from Ref. 7.
g. Berry et al., Ref. 7.

as a redistribution of oscillator strengths. In Fig. 2, we have plotted the f-values of the transitions from the ground state to the five $J^{\pi} = 1^{-}$ excited states as functions of Z. These results are obtained from calculations including intermediate couplings but not mixings between $2p^5 3s$ and $2p^5 3d$ configurations. As one can see, the f values of the $2p^6$-$2p^5 3d$ channels are much larger than those of the $2p^6$-$2p^5 3s$ ones (with the exception of the ^1S-$^3D^o$ channel, which is forbidden by both the spin and the orbital angular momentum selection rules). As a result, even small mixings among these channels cause redistributions of oscillator strengths and thus relatively large increases in the f values of the $2p^6$-$2p^5 3s$ channels.

In Table 1 we compare our results on the oscillator strengths of the two $2p^6$-$2p^5 3s$ transitions with other theories and with experimental measurements. We find that our two-channel results are in good agreement with the Hartree-Fock (HF) calculations of Kastner et al.,[4] and are higher than the model potential (MP) values of Crance.[5] Our five-channel results are about 20% higher than the two-channel ones, and are in good agreement with recent relativistic random phase approximation (RRPA) studies of Shorer.[6] The experimental data[7] at Cl^{7+} and Ar^{8+} ions are consistent with theoretical values though the large error bars in these data prohibit a clear preference towards various theoretical predictions. Detailed discussions of these comparisons are given in Ref. 7.

References

1. J. P. Desclaux, Comput. Phys. Commun. 9, 31 (1975).
2. Yong-Ki Kim and J. P. Desclaux, Phys. Rev. Lett. 36, 139 (1976).
3. K. T. Cheng and W. R. Johnson, Phys. Rev. A 16, 263 (1977).
4. S. O. Kastner, K. Omidvar, and J. H. Underwood, Astrophys. J. 148, 269 (1967).
5. M. Crance, Atom. Data 5, 186 (1973).
6. P. Shorter, Center for Astrophysics, Harvard University, to be published.
7. H. G. Berry, J. Desesquelles, K. T. Cheng, and R. M. Schectman, Phys. Rev. A 18, 546 (1978).

EXCITATION ENERGIES AND OSCILLATOR STRENGTHS IN THE SILVER ISOELECTRONIC SEQUENCE*

K. T. Cheng† and Y.-K. Kim

Excitation energies and oscillator strengths for electric dipole transitions between low-lying states in the silver isoelectronic sequence are studied using relativistic Hartree-Fock wavefunctions. For $Z \geq 61$, our calculation shows that the ground state of Ag-like ions is $4f^2F_{\frac{5}{2}}$ rather than $5s^2S_{\frac{1}{2}}$. We found a diminishing role of the spin-orbit effect on transitions between levels with high angular momenta. Effects of anti-crossings between $4d^9 4f^2$ and $4d^{10} 5\ell$ ($\ell = 0, 2, 4$) states at high Z are discussed.

*Abstract of a paper published in J. Opt. Soc. Am. 69, 125 (1979).

†Postdoctoral appointee from the University of Notre Dame, Notre Dame, IN.

ATOMIC CROSS SECTIONS FOR FAST Xe AND U IONS COLLIDING WITH ATOMS AND MOLECULES*

G. H. Gillespie,† K. T. Cheng,‡ and Y.-K. Kim

Cross sections for total inelastic scattering of Xe^{n+} (n = 1 to 6, 8, 18, 36, 44, 50, 52, 53) and U^{n+} (n = 1, 2, 4, 6, 8, 10, 20, 52, 82) ions by atoms and molecules (H_2, Li, C, N, O, Ne, Ar, Kr) have been calculated from a sum rule method[1] for the Born cross sections. Necessary form factors were calculated from relativistic Hartree-Fock wavefunctions. These cross sections are needed for estimating the stripping of projectile ions by buffer gases in the fusion reactor.

For charge states of $n \leq 10$, the cross sections for the stripping of projectile ions range from $\sim 10^{-17}$ cm^2/β^2 for Ne and N_2 (computed as twice the cross section for N) to $\sim 10^{-18}$ cm^2/β^2 for Li and H_2, where $\beta = v_{ion}/c$. Ionization of buffer gases by the projectile, however, has cross sections one order of magnitude larger, i.e., $\sim 10^{-16}$ cm^2/β^2 for Ne and N_2 and $\sim 10^{-17}$ cm^2/β^2 for Li and H_2.

Reference

1. G. H. Gillespie, Y.-K. Kim, and K. T. Cheng, Phys. Rev. A 17, 1284 (1978).

---

*Abstract of a paper presented at the Workshop on Heavy Ion Inertial Fusion, Argonne National Laboratory, September 19–26, 1978.

†Physical Dynamics, Inc., La Jolla, California.

‡Postdoctoral appointee from the University of Notre Dame, Notre Dame, IN.

LOW-LYING STATES OF $(Cs_2)^*$

Gurupada Das,[†] R. C. Raffenetti,[†] and Y.-K. Kim

Using an MCSCF/CI method, we generated wavefunctions for the ground state $^1\Sigma_g^+$ and the excited states of the symmetries $^1\Sigma_g^+$, $^1\Pi_g$, and $^1\Delta_g$ of the $(Cs_2)^{++}$ ion which asymptotically correspond to the single atomic excitation and/or single electron transfer between the two Cs^+ ions in their ground state. These molecular wavefunctions are needed in the calculation of charge transfer cross sections between the Cs^+ ions. There are no curve crossings between the ground and excited states for internuclear separation of ~4 bohrs or more. We infer, therefore, that the charge transfer cross section is unlikely to exceed geometrical cross sections at low collision energies.

*Abstract of a paper presented at the Workshop on Heavy Ion Inertial Fusion, Argonne National Laboratory, September 19–26, 1978.

†Chemistry Division, Argonne National Laboratory.

CHARGE EXCHANGE CROSS SECTIONS FOR THE REACTION $Xe^{+8} + Xe^{+8} \rightarrow Xe^{+9} + Xe^{+7}$

Joseph Macek*

We have estimated the charge changing cross section for collisions of Xe^{+8} ions with Xe^{+8} ions in the 0 to 150 keV energy range using the Fano-Lichten[1] electron promotion model. The charge transfer takes place via a crossing of the $6g\sigma$ and $5s\sigma$ independent-particle molecular energy curves. Using appropriately scaled H_2^+ energies of Bates and Reid,[2] we find that the crossing occurs at an internuclear distance of 0.4 atomic units. The corresponding charge exchange cross section is then estimated to be of the order of $\pi(0.4 \text{ a.u.})^2 \approx 10^{-17} \text{ cm}^2$. This value is likely to be an upper estimate since it assumes equal probability for direct excitation of Xe^{+8} as for charge exchange to Xe^{+7}, whereas direct excitation should be more likely.

References

1. U. Fano and W. Lichten, Phys. Rev. Lett. 14, 627 (1965).
2. D. R. Bates and R. H. G. Reid, Advances in Atomic and Molecular Physics 4, 13 (1968).

*Consultant, Radiological and Environmental Research Division. Permanent address: Department of Physics and Astronomy, The University of Nebraska, Lincoln, Nebraska 68588.

FINE STRUCTURES IN THE $1s2p^2\ ^4P$ and $1s2s2p\ ^4P^o$ STATES OF Li-LIKE IONS*

K. T. Cheng,† J. P. Desclaux,‡ and Y.-K. Kim

The fine structure intervals in the $1s2p^2\ ^4P$ and $1s2s2p\ ^4P^o$ states of Li-like ions ($Z \leq 26$) have been calculated from relativistic multiconfiguration Hartree-Fock wavefunctions.[1] It is found that the Breit interaction plays a crucial role in attaining good agreement with recent experimental data on C^{3+}, N^{4+}, and O^{5+} by Livingston and Berry.[2]

References

1. J. P. Desclaux, Comput. Phys. Commun. 9, 31 (1975).
2. A. E. Livingston and H. G. Berry, Phys. Rev. A 17, 1966 (1978).

---

*Abstract of a paper published in J. Phys. B 11, L359 (1978).

†Postdoctoral appointee from the University of Notre Dame, Notre Dame, IN.

‡Centre d'Etudes Nucleaires de Grenoble, 38041 Grenoble, France.

PUBLICATIONS BY THE STAFF OF THE FUNDAMENTAL MOLECULAR PHYSICS AND CHEMISTRY SECTION FOR THE PERIOD OCTOBER 1977–SEPTEMBER 1978

MAJOR PAPERS

H. G. Berry, J. Desequelles, K. T. Cheng, and R. M. Schectman, Ne I-like lines and Na I-like satellites in argon and chlorine, Phys. Rev. A 18 (2), 546–551 (August 1978).

F. T. Chan, C. H. Chang, M. Lieber, and Y.-K. Kim, Comparison of the Born and Glauber generalized oscillator strengths for the 2s→3p transition of atomic hydrogen, Phys. Rev. A 17(6), 1869–1873 (June 1978).

K. T. Cheng and Y.-K. Kim, Spectroscopic data for Cu-like ions, ANL/FPP/TM-109, Fusion Power Program Technical Report (April 1978).

K. T. Cheng, J. P. Desclaux, and Y.-K. Kim, Fine structure in the $1s2p^2\ ^4P$ and $1s2s2p\ ^4P^o$ states of Li-like ions, J. Phys. B: Atom. Molec. Phys. 11(12), L359–L362 (June 1978).

J. L. Dehmer and Dan Dill, Photoion angular distributions in dissociative photoionization of H_2 at 304 Å, Phys. Rev. A 18(1), 164–171 (July 1978).

J. L. Dehmer, Angular distributions of photoelectrons and non-thermal photo-ions from atoms and molecules. J. Physique, Colloque C4 (Suppl. 7) 39, C4–42–C4–C50 (July 1978).

P. M. Dehmer and J. L. Dehmer, Photoelectron spectrum of Xe_2 and potential energy curves for Xe_2^+, J. Chem. Phys. 68(8), 3462–3470 (1978).

P. M. Dehmer and J. L. Dehmer, Photoelectron spectra of Ar_2 and Kr_2 and dissociation energies of rare gas dimer ions, J. Chem. Phys. 69(1), 125–133 (July 1978).

I n Dill and J. L. Dehmer, Total elastic electron scattering cross section for N_2 between 0 and 1000 eV, Phys. Rev. A 16, 1423–1431 (1977).

M. A. Dillon, Generalized differential oscillator strengths for the electron impact ionization of helium determined for large and intermediate momentum transfers at 300 to 500 eV incident energies, J. Chem. Phys. 68, 2037–2040 (March 1978).

George H. Gillespie, Yong-Ki Kim, and Kwok-tsang Cheng, Born cross sections for ion-atom collisions, Phys. Rev. A 17(4), 1284–1295 (April 1978).

Mitio Inokuti, On the Compton profile, Butsuri (Proc. Phys. Soc. Japan) 32, 970–974 (December 1977)(in Japanese).

Mitio Inokuti, Yukikazu Itikawa, and James E. Turner, Addenda: Inelastic collision of fast charged particles with atoms and molecules—The Bethe theory revisited [Rev. Mod. Phys. 43, 297 (1971)] Rev. Mod. Phys. 50(1), 23–35 (January 1978).

Mitio Inokuti, T. Baer, and J. L. Dehmer, Addendum: Systematics of moments of dipole oscillator-strength distributions for atoms in the first and second row, Phys. Rev. A 17(3), 1229–1231 (March 1978).

M. Inokuti and J. E. Turner, Mean excitation energies for stopping power as derived from oscillator-strength distributions, Proc. Sixth Symp. on Microdosimetry, Brussels, 22–26 May 1978, Eds., J. Booz and H. G. Ebert, Harwood Academic Publishers, Ltd., London, pp. 675–687 (1978).

W. R. Johnson and K. T. Cheng, Relativistic effects on low-energy $5s \rightarrow \epsilon p$ photoionization for xenon, Phys. Rev. Lett. 40, 1167–1170 (May 1978).

Yong-Ki Kim and Kwok-tsang Cheng, Transition probabilities for the resonance transitions of Na-like ions, J. Opt. Soc. Am. 68, 836–842 (June 1978).

Yong-Ki Kim and Kwok-tsang Cheng, Bethe cross sections for the sodium isoelectronic sequence, Phys. Rev. A 18, 36–47 (July 1978).

A.R.P. Rau, Mitio Inokuti, and D. A. Douthat, Variational treatment of electron degradation yields of initial molecular species, Phys. Rev. A 18, 971–988 (September 1978).

Jon Siegel, Dan Dill, and J. L. Dehmer, Differential elastic electron scattering cross sections for N_2, Phys. Rev. A 17, 2106–2109 (June 1978).

D. Spence, The effects of "post-collision interactions" on near-threshold measurements of autoionizing states in Ne from scattered electron spectra, J. Chem. Phys. 68, 2980–2981 (1978).

D. Spence, Measurement of the energy exchange between scattered and ejected electrons following autoionization of the $2s2p^6\ 3s(^1S)$ state of Ne, J. Phys. B: Atom. Molec. Phys. 11, L243–L247 (1978).

L. H. Toburen, Steven T. Manson, and Yong-Ki Kim, Energy distributions of secondary electrons. III. Projectile energy dependence for ionization of He, Ne, and Ar by protons, Phys. Rev. A 17, 148–159 (January 1978).

Scott Wallace, Dan Dill, and J. L. Dehmer, Fixed-molecule photoelectron angular distributions: K-shell cross sections of CO at fixed detection angles, Phys. Rev. B 17, 2004–2010 (February 1978).

CONFERENCE PAPERS AND ABSTRACTS

30th Annual Gaseous Electronic Conference, Palo Alto, California, 18–21 October 1977, abstracts published in Bull. Am. Phys. Soc. 23(2) (1978).

P. M. Dehmer and J. L. Dehmer, Photoelectron spectrum of the Xe_2 Dimer, p. 134.

D. Spence, R. H. Huebner, and P. D. Burrow, Excitation of molecular nitrogen by low-energy electron impact in the region of the dissociation threshold, p. 143.

D. Spence and R. H. Huebner, Excitation of Rydberg states in the energy region of the Schumann-Runge continuum of O_2 by low-energy electron impact, p. 143.

D. Spence, A new technique to differentiate between resonance (negative ion) and doubly-excited autoionizing states in the ionization continuum of the rare gases, p. 145.

D. Spence, Measurement of doubly-excited states in Ne from scattered electron spectra, p. 145.

9th Annual Meeting of the Division of Electron and Atomic Physics, Knoxville, Tennessee, 5–7 December 1977, abstracts published in Bull. Am. Phys. Soc. 22(11) (December 1977).

K. T. Cheng and Y.-K. Kim, Oscillator strengths in Ag-isoelectronic sequence, p. 1332.

J. L. Dehmer and P. M. Dehmer, Photoelectron spectra of Ar_2 and Kr_2 potential energy curves for rare gas dimer ions, p. 1325.

S. T. Manson, J. L. Dehmer, and M. Inokuti, Inner-shell properties of atomic ions, 1. 1332.

Symposium on Primary Events in Radiation Biology, Joint Meeting of the American Physical Society and Biophysics Society, 27 March 1978, Washington, D.C., abstract published in Bull. Am. Phys. Soc. 23 (1978).

M. Inokuti, Molecular physics of primary events in radiation action in matter, p. 221.

Distribution for ANL-78-65 Part I

Internal:

W. E. Massey
M. V. Nevitt
R. V. Laney
W. K. Sinclair
R. H. Huebner
R. J. Royston
P. D. Vashishta
P. R. Fields
P. M. Failla
P. F. Gustafson
S. Wexler
S. Gordon
J. Berkowitz
T. Gilbert
M. C. Sauer
T. Dunning
K-T. Lu
G. T. Garvey
F. Clark
J. Dehmer
P. M. Dehmer
M. A. Dillon
P. Frenzen
Y.-K. Kim
P. Nicole
J. C. Person
R. E. Rowland
R. Schlenker
D. Spence
A. F. Stehney
O. J. Steingraber
C. Yack
G. Berry
J. Eland
M. Peshkin
D. S. Gemmell
D. Grahn
D. Y. Smith
J. Siegel
K. Cheng
C. C. Baker
R. C. Arnold
R. L. Martin
J. B. Hamilton
RER Division (100)
A. B. Krisciunas (15)
E. N. Pettitt
M. Fieldhouse
ANL Contract File
ANL Libraries (5)
TIS Files (4)

External:

DOE-TIC, for distribution per UC-48 (177)
Manager, Chicago Operations and Regional Office, DOE
Chief, Office of Patent Counsel, DOE-CORO
President, Argonne Universities Association
Radiological and Environmental Research Division Review Committee:
- W. J. Bair, Pacific Northwest Labs.
- A. K. Blackadar, Pennsylvania State U.
- R. S. Caldecott, U. Minnesota
- A. W. Castleman, Jr., U. Colorado
- H. L. Friedell, Case Western Reserve U. Hospitals
- E. D. Goldberg, Scripps Inst. Oceanography
- D. Kleppner, Massachusetts Inst. Technology
- D. W. Schindler, U. Manitoba
- W. H. Smith, Yale U.

AUA Biology Representatives:
- W. C. Ashby, Southern Illinois U., Carbondale
- R. M. Bock, U. Wisconsin-Madison
- R. C. Bockrath, Jr., Indiana U.
- W. Chavin, Wayne State U.
- J. Courtright, Marquette U.
- W. F. Danforth, Illinois Inst. Technology
- H. S. Ducoff, U. Illinois, Urbana
- A. Eisenstark, U. Missouri, Columbia
- D. Feir, St. Louis U.
- R. W. Greene, U. Notre Dame
- D. L. Hartl, Purdue U.
- R. W. Hoshaw, U. Arizona
- J. O. Hutchens, U. Chicago
- B. H. Judd, U. Texas at Austin
- G. M. Maggiora, U. Kansas

H. J. McDonald, Loyola U. Medical Center
M. C. Miller, U. Cincinnati
W. C. Myser, Ohio State U.
R. R. Novales, Northwestern U.
J. W Osborne, U. Iowa
R. J. Robel, Kansas State U.
R. C. Rustad, Case Western Reserve U.
S. Silver, Washington U.
A. S. Sussman, U. Michigan
P. W. Todd, Pennsylvania State U.
M. J. Ulmer, Iowa State U.
I. Ungar, Ohio U.
J. J. Wolken, Mellon Institute
L. Wolterink, Michigan State U.
W. Adams, Div. Basic Energy Sciences, USDOE
W. J. Argersinger, Jr., U. Kansas
Arkansas, U. of, Library for Medical Sciences, Little Rock
L. Armstrong, Jr., Johns Hopkins U.
P. Ausloos, National Bureau of Standards
J. A. Auxier, Oak Ridge National Lab.
J. N. Bardsley, U. Pittsburgh
N. F. Barr, Office of Energy Research, USDOE
E. C. Beaty, U. Colorado
B. Bederson, New York U.
M. Berger, National Bureau of Standards
C. C. Bhalla, Kansas State U.
H. Bichsel, U. Washington
R. D. Birkhoff, Oak Ridge National Lab.
W. H. Blahd, Veterans Administration Ctr., Los Angeles
R. P. Blaunstein, Office of Environment, USDOE
M. J. W. Boness, Avco Everett Research Corp., Everett, Mass.
R. A. Bonham, Indiana U.
J. W. Boring, U. Virginia
W. Brandt, New York U.
A. B. Brill, Vanderbilt U.
B. H. Bruckner, National Ctr. for Radiological Health, USHEW, Rockville, Md.
S. R. Bull, U. Missouri
R. A. Burnstein, Illinois Inst. Technology
W. W. Burr, Jr., Office of Environment, USDOE
P. D. Burrow, U. Nebraska
L. K. Bustad, Washington State U.
T. A. Carlson, Oak Ridge National Lab.
R. S. Caswell, National Bureau of Standards
R. J. Celotta, National Bureau of Standards
C. Y. Chen, U. California, San Diego
J. E. Christian, Purdue U.
L. G. Christophorou, Oak Ridge National Lab.
W. A. Chupka, Yale U.
R. G. Cochran, Texas A&M U.
S. H. Cohn, Brookhaven National Lab.
Colorado, U. of, Joint Inst. for Laboratory Astrophysics (JILA)
R. N. Compton, Oak Ridge National Lab.
F. J. Congel, Macalester College
J. W. Cooper, National Bureau of Standards

Cornell University, Library, Geneva, N. Y.
J. A. Cummings, Wisconsin State U.
A. Dalgarno, Harvard College Observatory and Smithsonian Astrophysical Observ.
D. Dill, Boston U.
D. A. Douthat, Kennedy-King College, Chicago
M. P. Durso, Health and Safety Lab., USDOE, New York
D. L. Ederer, National Bureau of Standards
C. E. Edmund, Milwaukee, Wis.
R. D. Evans, Scottsdale, Arizona
U. Fano, U. Chicago
M. R. Flannery, Georgia Inst. Technology
W. R. Garrett, Oak Ridge National Lab.
R. Geballe, U. Washington
S. Geltman, U. Colorado
G. H. Gillespie, Physical Dynamics, Inc., La Jolla
W. A. Glass, Battelle Northwest Lab.
M. Goldman, U. California, Davis
E. S. Green, U. Florida
T. A. Green, Sandia Labs.
R. Grunewald, U. Wisconsin, Milwaukee
A. J. Haverfield, Battelle Northwest Lab.
R. J. W. Henry, Louisiana State U.
G. R. Holeman, Yale U.
Houston, U. of, Libraries
F. P. Hudson, Office of Environment, USDOE
G. S. Hurst, Oak Ridge National Lab.
Illinois, U. of, Library, Chicago
K. H. Johnson, Massachusetts Inst. Technology
W. R. Johnson, U. Notre Dame
R. J. Kandell, Office of Basic Energy Sciences USDOE
W. V. Kessler, Purdue U.
E. W. Klappenbach, USEPA, Chicago
W. M. Kosman, Valparaiso U.
M. O. Krause, Oak Ridge National Lab.
A. Kupperman, California Inst. Technology
C. E. Kuyatt, National Bureau of Standards
P. Lambropoulos, U. Southern California
N. F. Lane, Rice U.
E. N. Lassettre, Carnegie-Mellon U.
S. H. Levine, Pennsylvania State U.
W. C. Lineberger, U. Colorado
S. Lipsky, U. Minnesota
L. Lohr, Jr., U. Michigan
C. D. Lorents, Stanford Research Inst.
H. Maccabee, Lawrence Berkeley Lab.
J. H. Macek, U. Nebraska
R. P. Madden, National Bureau of Standards
J. L. Magee, Lawrence Berkeley Lab.
C. J. Maletskos, Gloucester, Mass.
S. T. Manson, Georgia State U.
E. A. Martell, NCAR, Boulder
J. V. Martinez, Office of Basic Energy Sciences, USDOE
Mayo Clinic Library, Rochester
S. P. McGlynn, Louisiana State U.

D. H. McKelvie, U. Arizona
V. McKoy, California Inst. Technology
J. E. McLaughlin, Health and Safety Lab., USDOE, New York
R. Meer, Massachusett General Hospital
G. G. Meisels, U. Nebraska
J. Mentall, NASA Goddard Space Flight Center
E. Merzbacher, U. North Carolina at Chapel Hill
Michigan Technological U. Library, Houghton
D. W. Moeller, Kresge Center for Environmental Health, Boston
R. D. Moseley, Jr., U. New Mexico Medical School
G. Murphy, Iowa State U.
W. G. Myers, Ohio State U. Hospital
D. P. Naismith, U. North Dakota
R. K. Nesbet, IBM Research Labs., San Jose
W. R. Ney, National Council on Radiation Protection and Measurements, Bethesda
G. Nichols, Jr., Boston, Mass.
D. W. Norcross, U. Colorado
O. F. Nygaard, Case Western Reserve U.
M. J. Ohanian, U. Florida
A. L. Orvis, Mayo Clinic
J. Ovadia, Michael Reese Hospital, Chicago
J. Pan, Purdue U., Calumet Campus
A. V. Phelps, U. Colorado
M. L. Pool, Western Illinois U.
M. Pope, New York U.
C. Powell, National Bureau of Standards
R. H. Pratt, U. Pittsburgh
A. R. P. Rau, Louisiana State U.
W. P. Reinhardt, U. Colorado
J. S. Risley, North Carolina State U. at Raleigh
R. H. Ritchie, Oak Ridge National Lab.
J. S. Robertson, Mayo Clinic
W. C. Roesch, Battelle Northwest Lab.
C. C. J. Roothaan, U. Chicago
H. H. Rossi, Columbia U.
M. E. Rudd, U. Nebraska
J. H. Rust, U. Chicago
E. L. Saenger, Cincinnati General Hosp.
E. Salmon, McLean, Va.
J. A. R. Samson, U. Nebraska
R. P. Saxon, Stanford Research Inst.
R. H. Schuler, U. Notre Dame
Searle Diagnostics Inc., Des Plaines, Ill.
D. A. Shirley, U. California, Berkeley
T. W. Shyn, U. Michigan
J. B. Smathers, Texas A&M U.
F. T. Smith, Stanford Research Inst.
L. V. Spencer, National Bureau of Standards
A. F. Starace, U. Nebraska
R. F. Stebbings, Rice U.
R. L. Stockbauer, National Bu. Standards, Washington
P. M. Stone, Div. Magnetic Fusion Energy, USDOE
S. Tani, Marquette U.
H. S. Taylor, U. Southern California

L. S. Taylor, Bethesda, Md.
P. E. Thiess, Catholic U. of America
J. Thomas, Ebasco Services, Inc., New York
J. K. Thomas, U. Notre Dame
C. A. Tobias, Donner Lab , U. California, Berkeley
L. H. Toburen, Battelle Northwest Lab.
S. Trajmer, Jet Propulsion Lab.
M. Truppa, Waldie & Briggs, Chicago
J. E. Turner, Oak Ridge National Lab.
A. C. Upton, SUNY at Stony Brook
D. Varney, Eastern Kentucky U.
S. D. Vesselinovitch, U. Chicago
D. A. Vroom, Gulf Energy & Environmental Systems, San Diego
S. Wallace, Massachusetts Inst. Technology
W. L. Wiese, National Bu. Standards, Washington
R. H. Williams, U. Michigan
W. E. Wilson, Battelle Northwest Lab.
W. F. Witzig, Pennsylvania State U.
R. W. Wood, Office of Environment, USDOE
K. F. Wylie, U. Mississippi
R. N. Zare, Stanford U.
Biblioteca sede Central, Buenos Aires, Argentina
Comision Nacional de Energia Atomica, Library, Buenos Aires, Argentina
Cancer Institute Library, Melbourne, Australia
C. A. Dudley, IAEA, Vienna, Austria
J. M. Debois, St. Norbertus Hospital, Duffel, Belgium
A. Heyndrickx, U. Ghent, Belgium
N. Brearley, U. British Columbia, Vancouver, Canada
C. E. Brion, U. British Columbia, Vancouver, Canada
Canadian Forces Base, Halifax, Canada
J. D. Carette, Universite Laval, Quebec, Canada
G. Cowper, Atomic Energy of Canada Ltd., Chalk River
Defence Scientific Information Service, Ottawa, Canada
J. W. McConkey, U. Windsor, Canada
J. W. McGowan, U. Western Ontario, London, Canada
Radiation Protection Bu., Health and Welfare Canada, Ottawa
A. G. Szabo, National Research Council of Canada, Ottawa
Toronto, U. of, Library, Canada
C. Willis, National Research Council of Canada, Ottawa
C. M. Lee, Academia Sinica, Peking, Peoples' Republic of China
C. H. Cheng, Tsing Hua U., Republic of China
V. Cermak, Czechoslovak Academy of Sciences, Prague
Czechoslovak Atomic Energy Commission
H. H. Andersen, U. Aarhus, Denmark
M. Faber, Finsen Inst. Copenhagen, Denmark
P. Sigmund, U. Odense, Denmark
J. W. Boag, Sutton, Surrey, England
P. R. J. Burch, U. Leeds, England
K. Codling, U. Reading, England
J. A. Dennis, National Radiological Protection Board, Harwell, England
K. T. Dolder, The University, Newcastle-upon-Tyne, England
J. A. Edgington, Queen Mary College, London, England
J. F. Fowler, Mt. Vernon Hospital, Northwood, England
S. J. Harris, U. Surrey, Guildford, England
C. R. Hill, Inst. of Cancer Research, Belmont, England

G. V. Marr, U. Reading, England
W. V. Mayneord, Tadworth, Surrey, England
M. R. C. McDowell, Royal Holoway College, Surrey, England
MRC Radiobiology Unit, Librarian, Harwell, England
National Radiological Protection Board, Library, Harwell, England
D. H. Peirson, U. K. AERE, Harwell, England
E. E. Pochin, National Radiological Protection Board, Harwell, England
F. H. Read, U. Manchester, England
K. J. Ross, U. Southampton, England
M. J. Seaton, U. College London, England
A. J. Swallow, Christie Hospital & Holt Radium Inst., Manchester, England
J. B. West, Daresbury Lab., Daresbury, England
R. Åberg, Helsinki U. of Technology, Otaniemi, Finland
Institute of Radiation Protection, Library, Helsinki, Finland
M. Barat, U. de Paris, Orsay, France
J-P. Briand, Lab. de Physique Atomique et Nucleaire, Paris, France
J. Coursaget, CEA, Saclay, France
J.-P. Desclaux, CEN/G DRF-CPN, Grenoble, France
J. Durup, U. de Paris, Orsay, France
P. M. Guyon, U. Paris, Orsay, France
R. I. Hall, U. de Paris, Paris, France
M. Tronc, Lab. de Collisions Electroniques, Orsay, France
R. Voltz, Centre de Recherches Nucleaires, Strasbourg-Cronenbourg, France
F. Wuilleumier, U. Paris, Orsay, France
J. S. Briggs, U. Freiburg, Germany
R. J. Buenker, U. Bonn, Germany
G. Drexler, Institute für Strahlenschutz, Munich
H. Ehrhardt, Trier-Kaiserslautern U., Germany
J. Geiger, Trier-Kaiserslautern U., Germany
Gesellschaft für Strahlenforschung m.b.H., Frankfurt, Germany
R. Haensel, U. Kiel, Germany
D. Harder, U. Göttingen, Germany
I. V. Hertel, Freie U., Berlin, Germany
H. Hotop, U. Kiel, Germany
A. Kaul, Klinikum Steglitz der F. U. Berlin, Germany
W. Mehlhorn, U. Freiburg, Germany
H. Muth, U. Saarlandes, Homburg, Germany
A. Niehaus, U. Freiburg, Germany
E. Oberhausen, U. Saarlandes, Homburg, Germany
H. G. Pretzke, Institute für Strahlenschutz, Munich, Germany
S. D. Peyerimhoff, U. Bonn, Germany
B. Sonntag, Deutsches Elektronen Synchrotron, Hamburg, Germany
K. J. Vogt, Kernforschungsanlage, Jülich, Germany
R. K. Hukkoo, Bhabha Atomic Research Centre, Bombay, India
I. B. Berlman, Hebrew U., Jerusalem, Israel
Y. Feige, Israel AEC, Yavne, Israel
A. Benco, CCR Euratom, Ispra, Italy
E. Casnati, CNEN, Rome, Italy
A. Cigna, CNEN, Rome, Italy
G. F. Clemente, CNEN, Rome, Italy
F. A. Gianturco, U. degli Studi, Bari, Italy
O. Rimondi, Istituto di Fisica, Bologna, Italy
Y. Hatano, Tokyo Inst. Tech., Tokyo, Japan
T. Higashimura, Kyoto U., Japan

H. Inokuchi, Inst. for Molecular Science, Okazaki, Japan
Y. Itakawa, Nagoya U., Japan
S. Kaneko, U. Tokyo, Japan
Y. Kaneko, Tokyo Metropolitan U., Japan
M. Matsuzawa, U. of Electro-Communications, Tokyo, Japan
M. Nakamura, Tsukuba U., Ibaraki-ken, Japan
N. Oda, Tokyo Inst. of Technology, Tokyo, Japan
T. Sasaki, U. Tokyo, Japan
H. Suzuki, Sophia U., Tokyo, Japan
T. Takahashi, Inst. of Physical and Chemical Res., Saitama-ken, Japan
K. Takayanagi, U. Tokyo, Japan
H. Tanaka, Sophia U., Tokyo, Japan
K. Tanaka, Inst. for Molecular Science, Okazaki, Japan
T. Watanabe, U. Tokyo, Japan
Sang-Soo Lee, The Korea Advanced Inst. of Science, Seoul, Korea
Korean Atomic Energy Research Inst., Seoul, Korea
H. H. Brongersma, Philips Research Laboratories, Eindhoven, The Netherlands
F. J. de Heer, FOM Inst. for Atomic and Molecular Physics, Amsterdam, The Netherlands
J. Kistemaker, FOM Inst. for Atomic and Molecular Physics, Amsterdam, The Netherlands
M. van der Wiel, FOM Inst. for Atomic and Molecular Physics, Amsterdam, The Netherlands
P. G. Burke, Queen's U., Belfast, Northern Ireland
J. F. Williams, Queen's U., Belfast, Northern Ireland
M. U. Shaikh, Pakistan Atomic Energy Commission, Rawalpindi
R. D. Cherry, U. Cape Town, South Africa
K. Liden, Radiation Phys. Dept., Lasarettet, Lund, Sweden
National Institute of Radiation Protection, Stockholm, Sweden
G. Wendin, Inst. of Theoretical Physics, Göteborg, Sweden
A. Donath, Service Cantonal de Controle des Irradiations, Geneva, Switzerland
A. Gunther, CERN, Geneva, Switzerland
H. Willax, Schweizerisches Inst. fur Nuklearforschung, Zurich, Switzerland
G. D. Alkhazov, Academy of Sciences of the U.S.S.R., Leningrad
M. Ya. Amusia, Academy of Sciences of the U.S.S.R., Leningrad
E. Komarov, Central Res. Inst. of Roentgenology and Radiology, Leningrad, U.S.S.R.
V. Tal'roze, Academy of Sciences of the U.S.S.R., Moscow
D. Srdoc, Rudjer Boskovic Inst., Zagreb, Yugoslavia